

Review article

Impact of cholesterol on disease progression

Chun-Jung Lin^{a,b,†}, Cheng-Kuo Lai^{a,b,†}, Min-Chuan Kao^{b,†}, Lii-Tzu Wu^b, U-Ging Lo^a, Li-Chiung Lin^{a,c}, Yu-An Chen^b, Ho Lin^{c,*}, Jer-Tsong Hsieh^{a,d,**}, Chih-Ho Lai^{b,e,f,***}, Chia-Der Lin^{b,g,****}

^aDepartment of Urology, University of Texas Southwestern Medical Center, Dallas, Texas 75235, USA

^bGraduate Institute of Clinical and Basic Medical Science, School of Medicine, China Medical University, Taichung 404, Taiwan

^cDepartment of Life Sciences, National Chung Hsing University, Taichung 402, Taiwan

^dGraduate Institute of Cancer Biology, China Medical University, Taichung 404, Taiwan

^eDepartment of Microbiology and Immunology, Chang Gung University, Taoyuan 333, Taiwan

^fDepartment of Nursing, Asia University, Taichung 413, Taiwan

^gDepartment of Otolaryngology-Head and Neck Surgery, China Medical University Hospital, Taichung 404, Taiwan

Received 9th of April 2015 Accepted 30th of April 2015

© Author(s) 2015. This article is published with open access by China Medical University

Keywords:

Cancer development;

Cholesterol;

HMG-CoA reductase;

Infectious disease;

Lipid rafts

ABSTRACT

Cholesterol-rich microdomains (also called lipid rafts), where platforms for signaling are provided and thought to be associated with microbe-induced pathogenesis and lead to cancer progression. After treatment of cells with cholesterol disrupting or usurping agents, raft-associated proteins and lipids can be dissociated, and this renders the cell structure nonfunctional and therefore mitigates disease severity. This review focuses on the role of cholesterol in disease progression including cancer development and infectious diseases. Understanding the molecular mechanisms of cholesterol in these diseases may provide insight into the development of novel strategies for controlling these diseases in clinical scenarios.

1. Metabolism of cholesterol**1.1. Biosynthesis of cholesterol**

Cholesterol is an extremely important biological molecule as it is a precursor for the synthesis of steroid hormones, bile acids, and vitamin D [1]. The human body manufactures around 1 g of cholesterol each day and approximately 20-25% of total daily cholesterol production occurs in the liver [2]. Synthesis of cholesterol is a series process and starts with acetyl CoA and acetoacetyl-CoA, which are hydrated to form 3-hydroxy-3-methylglutaryl CoA (HMG-CoA). This molecule is subsequently reduced to mevalonate by the enzyme HMG-CoA reductase [3]. This is the regulated, rate-limiting, and irreversible step in cholesterol biosynthesis and is the target of action for statin drugs (HMG-CoA reductase competitive inhibitors) [4].

1.2. Association of abnormal cholesterol levels with diseases

Both dietary cholesterol and synthesized *de novo* are transported

by lipoprotein particles through the circulatory system. The four major types of lipoproteins are chylomicron, very low-density lipoprotein (VLDL), low-density lipoprotein (LDL), and high-density lipoprotein (HDL). Chylomicrons and VLDL deliver triacylglycerol to cells in the body, whereas LDL delivers cholesterol to cells in the body. Meanwhile, HDL is involved in reverse cholesterol transport. The synthesis and utilization of cholesterol must be tightly regulated in order to prevent over-accumulation and abnormal depositing within the body. There are two manifestations of cholesterol disorders, hyperlipidemia and hypolipidemia. The reasons for cholesterol disorders include dietary issues, genetic disorders, and other diseases [5-7]. For example, due to a genetic disorder caused by a defect on chromosome 19, cholesterol continues to be produced despite there already being an excess of cholesterol in the blood (lack of uptake by LDL receptor), and this may cause familial hypercholesterolemia [8]. In contrast, hypo-cholesterol level may result from liver disease, hypothyroidism, and genetic disorders such as familial hypobetalipoproteinemia and Smith-Lemli-Opitz syndrome (7-dehydrocholesterol reductase deficiency) [9].

* Corresponding author. Department of Life Sciences, National Chung Hsing University, Taichung 402, Taiwan.

** Corresponding author, Department of Urology, University of Texas Southwestern Medical Center, Dallas, Texas 75235, USA.

*** School of Medicine, China Medical University, Taichung 404, Taiwan.

**** Corresponding author, Department of Otolaryngology-Head and Neck Surgery, China Medical University and Hospital, Taichung 404, Taiwan.

† Equal contribution to this work.

E-mail addresses: hlin@dragon.nchu.edu.tw (H. Lin), JT.Hsieh@UTSouthwestern.edu (J.-T. Hsieh), chl@mail.cmu.edu.tw (C.-H. Lai), d6355@mail.cmuh.org.tw (C.-D. Lin).

Table 1 – Diseases associated with abnormal cholesterol levels.

Diseases associated with high cholesterol level	References
Atherosclerosis	[11]
Stroke	[12]
Cardiovascular disease (i.e. coronary heart disease and heart attacks)	[13]
Xanthomas (familial hypercholesterolemia)	[14, 15]
Tangier disease (familial HDL deficiency)	[16]
Diseases associated with low cholesterol level	
Huntington disease	[17, 8]
Increase in deaths from trauma and hemorrhagic stroke	[19, 20]
Increase risk of neuropsychiatric disorders (i.e. depression , suicide, anxiety, impulsivity, and aggression)	[21-24]

Table 2 – The relationship between cancers and cholesterol.

Cancer	Positive related	Negative related
Bladder cancer	[47]	[48]
Breast cancer	[37-40, 49]	[48, 50, 51]
Colon cancer	[44, 45, 52, 53]	–
Female reproductive organ cancer	[46]	[54]
Kidney cancer	[47]	–
Liver cancer	[55]	[53]
Lung cancer	[46, 47]	[53]
Melanoma	[46]	[56, 57]
Non-Hodgkin's lymphomas	[47]	–
Oral cancer	[41]	[58-60]
Pancreas cancer	[47]	–
Prostate cancer	[61-63]	[47, 48]
Stomach cancer	[47]	[53]

The level of cholesterol in the body being too high or too low may cause various symptoms, syndromes, or diseases. Excessive cholesterol is associated with several cardiovascular diseases and such levels are easily attained with an unhealthy diet. In fact, it should be noted that it is not essential for cholesterol to be obtained from one's diet as it is easily synthesized in the body. Whereas, low cholesterol is associated with mental disorders, neuropsychiatric diseases, and mortality in elderly [10]. Some critical diseases related to cholesterol levels are listed in Table 1.

1.3. The cholesterol lowering agents

The most important drugs for the treatment of dyslipidemia are statins which have been shown in multiple clinical trials to reduce cardiovascular events and mortality [25]. Statins can inhibit HMG-CoA reductase and design to subsequently inhibit enzyme activity in the liver [26]. Inhibition of cholesterol synthesis further decreases circulating LDL, which reduces levels of cholesterol in the hepatocyte and therefore lead to up-regulated expressions of LDL receptors. Some other drugs have been developed to treat dyslipidemia in specific subsets of patients. For instance, fibrates, which bind to the nuclear receptor PPAR-alpha, can increase HDL levels and decrease triglyceride levels [27]. Fibrates were originally used to address the primary problem of high levels of triglycerides. Another example is niacin (nicotinic acid), which increases HDL levels and decreases triglyceride and LDL levels

at high doses (much higher than required for its role as a vitamin) [28, 29]. And there is ezetimibe, which inhibits cholesterol absorption in the small intestine and effectively lowers LDL cholesterol [30].

2. Role of cholesterol in cancer progression

2.1. Cholesterol and cancer development

Cholesterol is known as a main component of lipid rafts and has been documented to regulate cell membrane proteins, receptor trafficking, signal transduction, as well as influence cell membrane fluidity [31]. Moreover, cholesterol and other lipid-components participate in the production of hormones [32] and energy [33]. However, when large concentrations of cholesterol accumulate in the human body, especially in the organs and blood stream, the risk of various diseases increases (Table 2). Notably, studies have revealed that an increased cholesterol level participates in cancer cell malignancy, and the dysfunction of cholesterol metabolism may also influence cancer progression [34-36]. For example, mevalonate, a cholesterol synthesis precursor, promotes breast cancer cell proliferation *in vivo* and *in vitro* [37, 38]. Additionally, 27-hydroxycholesterol, which is a metabolite from cholesterol, is expressed much higher in the estrogen receptor-positive breast cancer patient site, when compared with both normal breast tissue

Table 3 – Functions of cholesterol-rich microdomains in pathogen infection.

Pathogen	Function	References
<i>Aggregatibacter actinomycetemcomitans</i>	CDT holotoxin entry into host cells	[71,72]
<i>Anaplasma phagocytophilum</i>	<i>A. phagocytophilum</i> infection	[73]
<i>Campylobacter jejuni</i>	CDT holotoxin entry into host cells	[74, 75]
<i>Haemophilus ducreyi</i>	CDT holotoxin entry into host cells	[76]
<i>Helicobacter pylori</i>	CagA translocation and VacA function	[77-80]
HIV	Facilitate HIV infection	[81]
Prion	Promote the conversion of PrP ^c into the isoform PrP ^{Sc}	[82]

and a patient's cancer-free region control [39, 40]. In oral cancer, cholesterol was found to be significantly increased in tumor tissue compared to normal tissue [41]. Moreover, previous studies have reported that elevated cholesterol in the circulatory system promotes Akt signaling, decreases apoptosis activity in LNCap prostate cell line, and enhances tumor aggressiveness in a xenograft animal model [42, 43]. Further, it has been reported that serum cholesterol is a positive factor in colon cancer development [44, 45]. Other cancers, including female reproductive organ cancers, lung cancer, and melanoma are also documented to correlate with high levels of cholesterol [46].

2.2. Reducing cholesterol inhibits cancer progression

In addition to the correlation between cholesterol and cancer progression, disruption of cell membrane lipid rafts or cholesterol components and interference of cholesterol synthesis are considered as treating prospects toward cancer treatment [64, 65]. Therefore, clinical use of cholesterol-controlling medicines has been implied to possess chemoprotective effects [66]. Statins, HMG-CoA reductase inhibitors, are cholesterol-lowering agents [67], and the total consumption of statins has been increasing in recent years [46]. Statins are documented to decrease the proliferation of cancer cells [49, 63], reduce the risk of cancer incidence rate [61], and even influence the mortality rate in cancer patients [68]. However, the findings of statins use in the treatment of cancer have revealed inconsistencies. Some reports have even claimed that the use of statin may increase the risk of cancer [51, 57], or have no correlation in the treatment of cancer [50, 69]. Therefore, the benefits of the cholesterol-controlling aspect in the treatments of lipid rafts-related cancers, animal models, and the details of their underlying mechanisms may need further investigations.

Despite arising number of reports that support the claim that the use of statin significantly reduces the incidence of cancer, not all of the statistical results are consistent with such a claim [48, 70]. Research into cholesterol-related cancer progression and the use of cholesterol-lowering drugs are mostly of the database analysis variety. However, the results may differ according to participant sample selection, sample size, and related confounding factors. Therefore, additional studies with cellular or animal models, long-term vs. short-term statin users follow-up, and even studies consisting of large sample sizes with multiple confounders would help further elucidate this issue.

3. Association of cholesterol with pathogen infections

Cholesterol is the most important component of lipid rafts in eukaryotic cells. Lipid rafts are also considered a critical factor in host-pathogen interaction and colonization of hosts by several pathogens including bacteria, viruses, as well as prions. Most of the studies we refer to here describe a few examples of the role of cholesterol in promoting pathogenic infections (Table 3).

3.1. Lipid rafts serve as platforms for bacterial pathogens

In order to promote their internalization into host, bacterial pathogens may utilize host cells to enhance their own adherence and survival abilities [83, 84]. Adhesion to host cells by pathogens is the first step in their invasion process and may be associated with lipid rafts. The most commonly described cellular target of intestinal pathogens is *Campylobacter jejuni*, which attach to host epithelial cells via membrane cholesterol [85-87]. In addition, the major virulence factor expressed by *C. jejuni* is cytolethal distending toxin (CDT) [74], which also can be produced by various common Gram-negative bacteria, including *Aggregatibacter actinomycetemcomitans* [88], *Escherichia coli* [89], *Haemophilus ducreyi* [76], *Helicobacter hepaticus* [90], and *Shigella dysenteriae* [91]. It has been reported that *C. jejuni* CDT-induced pathogenesis of host cells is dependent on membrane cholesterol levels. By using cholesterol-depleting agents such as methyl- β -cyclodextrin (M β CD) which markedly decreased the intoxication of cells [74, 92]. Further evidence of the role of lipid rafts in both *C. jejuni* and *A. actinomycetemcomitans* CDT-induced genotoxicity of host cells have been demonstrated through the cholesterol recognition/interaction amino acid consensus (CRAC) region of the CdtC subunit [71, 75]. These findings indicate that membrane cholesterol provides an essential component for CDT binding to the cell membrane and also serves as a portal for CdtB delivery into host cells for the induction of cell intoxication. Moreover, in this case, the virulence protein cytotoxin-associated gene A (CagA) of *Helicobacter pylori*, is delivered into the target cells by the type IV secretion system [93] and utilizes membrane cholesterol to lead to the activation of pro-inflammatory signaling pathways within gastric cells [75, 78, 94, 95]. Furthermore, a dramatic demonstration of the dissociation of infectivity and pathology is *H. pylori* within encoding glucosyltransferase, which is indispensable for cholesterol glucosylation and promotes *H. pylori*-induced phagocytosis escape and subsequent immune responses [77, 96]. Similar to *C. jejuni* and *H. pylori*, the recent description of the combination of apoE-deficiency and a high cholesterol diet in mice facilitated *Anaplasma phagocytophilum* infection *in vivo* and induced proinflammatory responses [73]. However, not all pathogens require lipid rafts to gain entry into host cells. Recently, it has been shown that cholesterol-mediated

invasions and intracellular replication are not required for *Chlamydia trachomatis* and *Salmonella enterica* serovar Typhimurium infection of mice embryonic fibroblasts (MEFs) [97]. Together, these examples illustrate that lipid rafts provide several advantages for bacteria, including virulence factors in modulating internalization and transport of extracellular proteins as well as signaling platforms.

3.2. Conversion of prions is associated with lipid rafts

Neurodegenerative disorders caused by prions have been linked to the variant Creutzfeldt-Jakob Disease (vCJD) in humans [98]. The cellular prion protein (PrP^C) is called a normal cell surface glycoprotein by means of a glycosylphosphatidylinositol (GPI)-anchor. GPI-anchored PrP^C is presented in lipid rafts where are microdomains enriched in cholesterol [99]. It is widely known that PrP^C is found in membrane cholesterol and plays a crucial role in the development of prion-related diseases by changing its conformation to a pathological isoform (PrP^{Sc}) [82]. PrP^{Sc} is an essential part of the prion, causing fatal and transmissible neurodegenerative prion diseases [82]. Several lines of evidence suggest that lipid rafts are highly essential for the transport of PrP^C and the toxicity of PrP^{Sc} in neuronal cells [100, 101]. Altogether, these studies indicate the critical role of lipid rafts, which maintain the cell surface localization of GPI-anchor attachment of PrP^C and are involved in prion conversion and neurotoxicity.

3.3. Lipid rafts facilitate virus infection

Human immunodeficiency virus (HIV) is the retrovirus that is well known to cause acquired immunodeficiency syndrome (AIDS) [102]. Previous clinical evidence indicated that the level of cholesterol may be a potential factor for controlling the spread or fusion of many viruses [103, 104] which are involved in HIV production and infectivity [81]. It has been reported that the negative effector (Nef) protein from HIV can enhance cholesterol uptake and biosynthesis by activating the transcription of the sterol-responsive element binding factor 2 (SREBF-2) and SREBF-2-regulated genes [105]. In addition, the Nef inhibits the activity of the cellular cholesterol transporter ATP-binding cassette A1 (ABCA1) [106], which in response binds to cholesterol and delivers it to the lipid rafts. Conversely, reduction of cellular cholesterol by ABCA1 activation has been shown to potently inhibit HIV replication [107, 108]. Taken together, these results reveal that HIV requires cholesterol for its egress from and entry into cells.

4. Conclusions and perspectives

Cholesterol-enriched microdomains, which provide platforms for signaling, are thought to be associated with the development of various types of cancers. It has also been clear that the role of cholesterol in pathogen-host interactions contributes to further ensure the pathogens' survival and virulence delivery into host. These findings indicate that an adequate regulation of cholesterol may prevent cancer progression as well as mitigate microbe-induced the pathogenesis of hosts. Fully unveiling the role of cholesterol in diseases' manifestations may shed light on the possibility to develop a novel approach to the retardation or possible prevention of cancer development and the treatment of infectious diseases.

Acknowledgments

The authors would like to thank Dr. Ming-Chei Maa and Chang-Mei Lin for their valuable suggestions and editorial assistance. This work was funded by the Ministry of Science and Technology (103-2633-B-039-001 and 103-2991-I-005-507), China Medical University (CMU103-S-15 and CMU103-S-18), and the Tomorrow Medicine Foundation.

Declaration of interest

The authors declare no conflicts of interest for this work.

Open Access This article is distributed under terms of the *Creative Commons Attribution License* which permits any use, distribution, and reproduction in any medium, provided original author(s) and source are credited.

REFERENCES

- [1] Russell DW, Setchell KD. Bile acid biosynthesis. *Biochemistry* 1992; 31: 4737-49.
- [2] Lewis GF. Determinants of plasma HDL concentrations and reverse cholesterol transport. *Curr Opin Cardiol* 2006; 21: 345-52.
- [3] Hampton R, Dimster-Denk D, Rine J. The biology of HMG-CoA reductase: the pros of contra-regulation. *Trends Biochem Sci* 1996; 21: 140-5.
- [4] Barrios-Gonzalez J, Miranda RU. Biotechnological production and applications of statins. *Appl Microbiol Biotechnol* 2010; 85: 869-83.
- [5] Porter FD, Herman GE. Malformation syndromes caused by disorders of cholesterol synthesis. *J Lipid Res* 2011; 52: 6-34.
- [6] Khosla P, Hayes KC. Dietary palmitic acid raises plasma LDL cholesterol relative to oleic acid only at a high intake of cholesterol. *Biochim Biophys Acta* 1993; 1210: 13-22.
- [7] Pollin TI, Quartuccio M. What We Know About Diet, Genes, and Dyslipidemia: Is There Potential for Translation? *Curr Nutr Rep* 2013; 2: 236-42.
- [8] Varghese MJ. Familial hypercholesterolemia: a review. *Ann Pediatr Cardiol* 2014; 7: 107-17.
- [9] Jira P. Cholesterol metabolism deficiency. *Handb Clin Neurol* 2013; 113: 1845-50.
- [10] Martinez-Carpio PA, Barba J, Bedoya-Del Campillo A. Relation between cholesterol levels and neuropsychiatric disorders. *Rev Neurol* 2009; 48: 261-4.
- [11] Feig JE, Hewing B, Smith JD, Hazen SL, Fisher EA. High-density lipoprotein and atherosclerosis regression: evidence from preclinical and clinical studies. *Circ Res* 2014; 114: 205-13.
- [12] Lisak M, Demarin V, Trkanjec Z, Basic-Kes V. Hypertriglyceridemia as a possible independent risk factor for stroke. *Acta Clin Croat* 2013; 52: 458-63.
- [13] Kratzer A, Giral H, Landmesser U. High-density lipoproteins as modulators of endothelial cell functions: alterations in patients with coronary artery disease. *Cardiovasc Res* 2014.
- [14] Sibley C, Stone NJ. Familial hypercholesterolemia: a challenge of diagnosis and therapy. *Cleve Clin J Med* 2006; 73: 57-64.

- [15] Moghadasian MH, Salen G, Frohlich JJ, Scudamore CH. Cerebro-tendinous xanthomatosis: a rare disease with diverse manifestations. *Arch Neurol* 2002; 59: 527-29.
- [16] Puntoni M, Sbrana F, Bigazzi F, Sampietro T. Tangier disease: epidemiology, pathophysiology, and management. *Am J Cardiovasc Drugs* 2012; 12: 303-11.
- [17] Valenza M, Rigamonti D, Goffredo D, Zuccato C, Fenu S, Jamot L, *et al.* Dysfunction of the cholesterol biosynthetic pathway in Huntington's disease. *J Neurosci* 2005; 25: 9932-39.
- [18] Block RC, Dorsey ER, Beck CA, Brenna JT, Shoulson I. Altered cholesterol and fatty acid metabolism in Huntington disease. *J Clin Lipidol* 2010; 4: 17-23.
- [19] Rodriguez-Luna D, Rubiera M, Ribo M, Coscojuela P, Pagola J, Pineiro S, *et al.* Serum low-density lipoprotein cholesterol level predicts hematoma growth and clinical outcome after acute intracerebral hemorrhage. *Stroke* 2011; 42: 2447-52.
- [20] Wang X, Dong Y, Qi X, Huang C, Hou L. Cholesterol levels and risk of hemorrhagic stroke: a systematic review and meta-analysis. *Stroke* 2013; 44: 1833-9.
- [21] Ancelin ML, Carriere I, Boulenger JP, Malafosse A, Stewart R, Cristol JP, *et al.* Gender and genotype modulation of the association between lipid levels and depressive symptomatology in community-dwelling elderly (the ESPRIT study). *Biol Psychiatry* 2010; 68: 125-32.
- [22] Lester D. Serum cholesterol levels and suicide: a meta-analysis. *Suicide Life Threat Behav* 2002; 32: 333-46.
- [23] Fawcett J, Busch KA, Jacobs D, *et al.* Suicide: a four-pathway clinical-biochemical model. *Ann N Y Acad Sci* 1997; 836: 288-301.
- [24] Duits N, Bos FM. Psychiatric disorders with use of simvastatin. *Ned Tijdschr Geneesk* 1993; 137: 1312-5.
- [25] Koba S. Statin therapy for atherogenic hypertriglyceridemia. *Nihon Rinsho* 2013; 71: 1655-60.
- [26] Sirtori CR. The pharmacology of statins. *Pharmacol Res* 2014.
- [27] Remaley AT, Norata GD, Catapano AL. Novel concepts in HDL pharmacology. *Cardiovasc Res* 2014.
- [28] Ginsberg HN, Reyes-Soffer G. Niacin: a long history, but a questionable future. *Curr Opin Lipidol* 2013; 24: 475-9.
- [29] Song WL, FitzGerald GA. Niacin, an old drug with a new twist. *J Lipid Res* 2013; 54: 2586-94.
- [30] Sano M. An inhibitor of intestinal cholesterol transporter. *Nihon Rinsho* 2013; 71: 1661-6.
- [31] Silvius JR. Role of cholesterol in lipid raft formation: lessons from lipid model systems. *Biochim Biophys Acta* 2003; 1610: 174-83.
- [32] Miller WL. Molecular biology of steroid hormone synthesis. *Endocr Rev* 1988; 9: 295-318.
- [33] Rui L. Energy metabolism in the liver. *Compr Physiol* 2014; 4: 177-97.
- [34] Li HY, Appelbaum FR, Willman CL, Zager RA, Banker DE. Cholesterol-modulating agents kill acute myeloid leukemia cells and sensitize them to therapeutics by blocking adaptive cholesterol responses. *Blood* 2003; 101: 3628-3634.
- [35] Cruz PM, Mo H, McConathy WJ, Sabnis N, Lacko AG. The role of cholesterol metabolism and cholesterol transport in carcinogenesis: a review of scientific findings, relevant to future cancer therapeutics. *Front Pharmacol* 2013; 4: 119.
- [36] Liu HH, Tsai YS, Lai CL, Tang CH, Lai CH, Wu HC, *et al.* Evolving personalized therapy for castration-resistant prostate cancer. *Bio-Medicine* 2013; 4: 7-15.
- [37] Duncan RE, El-Soheemy A, Archer MC. Mevalonate promotes the growth of tumors derived from human cancer cells *in vivo* and stimulates proliferation *in vitro* with enhanced cyclin-dependent kinase-2 activity. *J Biol Chem* 2004; 279: 33079-84.
- [38] dos Santos CR, Domingues G, Matias I, Matos J, Fonseca I, de Almeida JM, *et al.* LDL-cholesterol signaling induces breast cancer proliferation and invasion. *Lipids Health Dis* 2014; 13: 16.
- [39] Nelson ER, Wardell SE, Jasper JS, Park S, Suchindran S, Howe MK, *et al.* 27-Hydroxycholesterol links hypercholesterolemia and breast cancer pathophysiology. *Science* 2013; 342: 1094-8.
- [40] Wu Q, Ishikawa T, Sirianni R, Tang H, McDonald JG, Yuhanna IS, *et al.* 27-Hydroxycholesterol promotes cell-autonomous, ER-positive breast cancer growth. *Cell Rep* 2013; 5: 637-45.
- [41] Kolanjiappan K, Ramachandran CR, Manoharan S. Biochemical changes in tumor tissues of oral cancer patients. *Clin Biochem* 2003; 36: 61-5.
- [42] Zhuang L, Kim J, Adam RM, Solomon KR, Freeman MR. Cholesterol targeting alters lipid raft composition and cell survival in prostate cancer cells and xenografts. *J Clin Invest* 2005; 115: 959-68.
- [43] Freeman MR, Solomon KR. Cholesterol and prostate cancer. *J Cell Biochem* 2004; 91: 54-69.
- [44] van Duijnhoven FJ, Bueno-De-Mesquita HB, Calligaro M, Jenab M, Pischon T, Jansen EH, *et al.* Blood lipid and lipoprotein concentrations and colorectal cancer risk in the European Prospective Investigation into Cancer and Nutrition. *Gut* 2011; 60: 1094-102.
- [45] Jacobs RJ, Voorneveld PW, Kodach LL, Hardwick JC. Cholesterol metabolism and colorectal cancers. *Curr Opin Pharmacol* 2012; 12: 690-5.
- [46] Boudreau DM, Yu O, Johnson J. Statin use and cancer risk: a comprehensive review. *Expert Opin Drug Saf* 2010; 9: 603-21.
- [47] Hu J, La Vecchia C, de Groh M, Negri E, Morrison H, Mery L. Dietary cholesterol intake and cancer. *Ann Oncol* 2012; 23: 491-500.
- [48] Goldstein MR, Mascitelli L, Pezzetta F. Do statins prevent or promote cancer? *Curr Oncol* 2008; 15: 76-7.
- [49] Campbell MJ, Esserman LJ, Zhou Y, Shoemaker M, Lobo M, Borman E, *et al.* Breast cancer growth prevention by statins. *Cancer Res* 2006; 66: 8707-14.
- [50] Desai P, Chlebowski R, Cauley JA, Manson JE, Wu C, Martin LW, *et al.* Prospective analysis of association between statin use and breast cancer risk in the women's health initiative. *Cancer Epidemiol Biomarkers Prev* 2013; 22: 1868-76.
- [51] McDougall JA, Malone KE, Daling JR, Cushing-Haugen KL, Porter PL, Li CI. Long-term statin use and risk of ductal and lobular breast cancer among women 55 to 74 years of age. *Cancer Epidemiol Biomarkers Prev* 2013; 22: 1529-37.
- [52] Agnoli C, Grioni S, Sieri S, *et al.* Colorectal cancer risk and dyslipidemia: a case-cohort study nested in an Italian multicentre cohort. *Cancer Epidemiol* 2014; 38: 144-51.
- [53] Kitahara CM, Berrington de Gonzalez A, Freedman ND, Huxley R, Mok Y, Jee SH, *et al.* Total cholesterol and cancer risk in a large prospective study in Korea. *J Clin Oncol* 2011; 29: 1592-8.
- [54] Melvin JC, Seth D, Holmberg L, Garmo H, Hammar N, Jungner I, *et al.* Lipid profiles and risk of breast and ovarian cancer in the Swedish AMORIS study. *Cancer Epidemiol Biomarkers Prev* 2012; 21: 1381-4.
- [55] Saito N, Sairenchi T, Irie F, Iso H, Iimura K, Watanabe H, *et al.* Low

- serum LDL cholesterol levels are associated with elevated mortality from liver cancer in Japan: the Ibaraki Prefectural health study. *Tohoku J Exp Med* 2013; 229: 203-11.
- [56] Jagtap D, Rosenberg CA, Martin LW, Pettinger M, Khandekar J, Lane D, *et al.* Prospective analysis of association between use of statins and melanoma risk in the Women's Health Initiative. *Cancer* 2012; 118: 5124-31.
- [57] Mascitelli L, Pezzetta F, Goldstein MR. The epidemic of nonmelanoma skin cancer and the widespread use of statins: Is there a connection? *Dermatoendocrinol* 2010; 2: 37-8.
- [58] Chawda JG, Jain SS, Patel HR, Chaduvula N, Patel K. The relationship between serum lipid levels and the risk of oral cancer. *Indian J Med Paediatr Oncol* 2011; 32: 34-37.
- [59] Lohe VK, Degwekar SS, Bhowate RR, Kadu RP, Dangore SB. Evaluation of correlation of serum lipid profile in patients with oral cancer and precancer and its association with tobacco abuse. *J Oral Pathol Med* 2010; 39: 141-8.
- [60] Srinivas GV, Namala S, Ananthaneni A, Puneeth HK, Devi BS. Evaluation and correlation of serum lipid profile in oral and gastrointestinal cancer patients. *J Int Oral Health* 2013; 5: 72-7.
- [61] Jacobs EJ, Rodriguez C, Bain EB, Wang Y, Thun MJ, Calle EE. Cholesterol-lowering drugs and advanced prostate cancer incidence in a large U.S. cohort. *Cancer Epidemiol Biomarkers Prev* 2007; 16: 2213-7.
- [62] Pelton K, Freeman MR, Solomon KR. Cholesterol and prostate cancer. *Curr Opin Pharmacol* 2012; 12: 751-9.
- [63] Yokomizo A, Shiota M, Kashiwagi E, Kuroiwa K, Tatsugami K, Inokuchi J, *et al.* Statins reduce the androgen sensitivity and cell proliferation by decreasing the androgen receptor protein in prostate cancer cells. *Prostate* 2011; 71: 298-304.
- [64] Silvente-Poirot S, Poirot M. Cholesterol metabolism and cancer: the good, the bad and the ugly. *Curr Opin Pharmacol* 2012; 12: 673-6.
- [65] Buchwald H. Cholesterol inhibition, cancer, and chemotherapy. *Lancet* 1992; 339: 1154-6.
- [66] Demierre MF, Higgins PD, Gruber SB, *et al.* Statins and cancer prevention. *Nat Rev Cancer* 2005; 5: 930-42.
- [67] Clendening JW, Penn LZ. Targeting tumor cell metabolism with statins. *Oncogene* 2012; 31: 4967-78.
- [68] Nielsen SF, Nordestgaard BG, Bojesen SE. Statin use and reduced cancer-related mortality. *N Engl J Med* 2012; 367: 1792-802.
- [69] Baigent C, Blackwell L, Emberson J, Holland LE, Reith C, Bhalra N, *et al.* Efficacy and safety of more intensive lowering of LDL cholesterol: a meta-analysis of data from 170,000 participants in 26 randomised trials. *Lancet* 2010; 376: 1670-81.
- [70] Jacobs EJ, Newton CC, Thun MJ, Gapstur SM. Long-term use of cholesterol-lowering drugs and cancer incidence in a large United States cohort. *Cancer Res* 2011; 71: 1763-71.
- [71] Boesze-Battaglia K, Besack D, McKay T, *et al.* Cholesterol-rich membrane microdomains mediate cell cycle arrest induced by *Actinobacillus actinomycetemcomitans* cytolethal-distending toxin. *Cell Microbiol* 2006; 8: 823-36.
- [72] Boesze-Battaglia K, Brown A, Walker L, Besack D, Zekavat A, Wrenn S, *et al.* Cytolethal distending toxin-induced cell cycle arrest of lymphocytes is dependent upon recognition and binding to cholesterol. *J Biol Chem* 2009; 284: 10650-8.
- [73] Xiong Q, Wang X, Rikihisa Y. High-cholesterol diet facilitates *Anaplasma phagocytophilum* infection and up-regulates macrophage inflammatory protein-2 and CXCR2 expression in apolipoprotein E-deficient mice. *J Infect Dis* 2007; 195: 1497-503.
- [74] Lin CD, Lai CK, Lin YH, Hsieh JT, Sing YT, Chang YC, *et al.* Cholesterol depletion reduces entry of *Campylobacter jejuni* cytolethal distending toxin and attenuates intoxication of host cells. *Infect Immun* 2011; 79: 3563-75.
- [75] Lai CH, Lai CK, Lin YJ, Hung CL, Chu CH, Feng CL, *et al.* Characterization of putative cholesterol recognition/interaction amino acid consensus-like motif of *Campylobacter jejuni* cytolethal distending Toxin C. *PLoS One* 2013; 8: e66202.
- [76] Cope LD, Lumbley S, Latimer JL, Klesney-Tait J, Stevens MK, Johnson LS, *et al.* A diffusible cytotoxin of *Haemophilus ducreyi*. *Proc Natl Acad Sci U S A* 1997; 94: 4056-61.
- [77] Wunder C, Churin Y, Winau F, Warnecke D, Vieth M, Lindner B, *et al.* Cholesterol glucosylation promotes immune evasion by *Helicobacter pylori*. *Nat Med* 2006; 12: 1030-8.
- [78] Lai CH, Chang YC, Du SY, Wang HJ, Kuo CH, Fang SH, *et al.* Cholesterol depletion reduces *Helicobacter pylori* CagA translocation and CagA-induced responses in AGS cells. *Infect Immun* 2008; 76: 3293-303.
- [79] Lai CH, Hsu YM, Wang HJ, Wang WC. Manipulation of host cholesterol by *Helicobacter pylori* for their beneficial ecological niche. *BioMedicine* 2013; 3: 27-33.
- [80] Ricci V, Galmiche A, Doye A, Necchi V, Solcia E, Boquet P. High cell sensitivity to *Helicobacter pylori* VacA toxin depends on a GPI-anchored protein and is not blocked by inhibition of the clathrin-mediated pathway of endocytosis. *Mol Biol Cell* 2000; 11: 3897-909.
- [81] Cui HL, Grant A, Mukhamedova N, Pushkarsky T, Jennelle L, Dubrovsky L, *et al.* HIV-1 Nef mobilizes lipid rafts in macrophages through a pathway that competes with ABCA1-dependent cholesterol efflux. *J Lipid Res* 2012; 53: 696-708.
- [82] Prusiner SB. Prions. *Proceedings of the National Academy of Sciences of the United States of America* 1998; 95: 13363-83.
- [83] Bhavsar AP, Guttman JA, Finlay BB. Manipulation of host-cell pathways by bacterial pathogens. *Nature* 2007; 449: 827-34.
- [84] Duncan MJ, Shin JS, Abraham SN. Microbial entry through caveolae: variations on a theme. *Cellular Microbiology* 2002; 4: 783-91.
- [85] Wooldridge KG, Williams PH, Ketley JM. Host signal transduction and endocytosis of *Campylobacter jejuni*. *Microb Pathog* 1996; 21: 299-305.
- [86] Elmi A, Watson E, Sandu P, Gundogdu O, Mills DC, Inglis NF, *et al.* *Campylobacter jejuni* outer membrane vesicles play an important role in bacterial interactions with human intestinal epithelial cells. *Infect Immun* 2012; 80: 4089-98.
- [87] Hu L, McDaniel JP, Kopecko DJ. Signal transduction events involved in human epithelial cell invasion by *Campylobacter jejuni* 81-176. *Microb Pathog* 2006; 40: 91-100.
- [88] Sugai M, Kawamoto T, Peres SY, Ueno Y, Komatsuzawa H, Fujiwara T, *et al.* The cell cycle-specific growth-inhibitory factor produced by *Actinobacillus actinomycetemcomitans* is a cytolethal distending toxin. *Infect Immun* 1998; 66: 5008-19.
- [89] Peres SY, Marches O, Daigle F, Nougayrede JP, Haurault F, Tasca C, *et al.* A new cytolethal distending toxin (CDT) from *Escherichia coli* producing CNF2 blocks HeLa cell division in G2/M phase. *Mol Microbiol* 1997; 24: 1095-107.
- [90] Young VB, Knox KA, Schauer DB. Cytolethal distending toxin

sequence and activity in the enterohepatic pathogen *Helicobacter hepaticus*. *Infect Immun* 2000; 68: 184-91.

- [91] Okuda J, Kurazono H, Takeda Y. Distribution of the cytolethal distending toxin A gene (cdtA) among species of *Shigella* and *Vibrio*, and cloning and sequencing of the cdt gene from *Shigella dysenteriae*. *Microb Pathog* 1995; 18: 167-72.
- [92] Lai CK, Su JC, Lin YH, Chang CS, Feng CL, Lin HJ, *et al*. Involvement of cholesterol in *Campylobacter jejuni* cytolethal distending toxin-induced pathogenesis. *Future Microbiol* 2015; 10: 489-501.
- [93] Ramarao N, Gray-Owen SD, Backert S, Meyer TF. *Helicobacter pylori* inhibits phagocytosis by professional phagocytes involving type IV secretion components. *Mol Microbiol* 2000; 37: 1389-404.
- [94] Lai CH, Wang HJ, Chang YC, Hsieh WC, Lin HJ, Tang CH, *et al*. *Helicobacter pylori* CagA-mediated IL-8 induction in gastric epithelial cells is cholesterol-dependent and requires the C-terminal tyrosine phosphorylation-containing domain. *FEMS Microbiol Lett* 2011; 323: 155-63.
- [95] Lu DY, Chen HC, Yang MS, Hsu YM, Lin HJ, Tang CH, *et al*. Ceramide and Toll-like receptor 4 are mobilized into membrane rafts in response to *Helicobacter pylori* infection in gastric epithelial cells. *Infect Immun* 2012; 80: 1823-33.
- [96] Du SY, Wang HJ, Cheng HH, Chen SD, Wang LH, Wang WC. Cholesterol glucosylation by *Helicobacter pylori* delays internalization and arrests phagosome maturation in macrophages. *J Microbiol Immunol Infect* 2014.
- [97] Gilk SD, Cockrell DC, Luterbach C, Hansen B, Knodler LA, Ibarra JA, *et al*. Bacterial colonization of host cells in the absence of cholesterol. *PLoS Pathog* 2013; 9: e1003107.
- [98] Biasini E, Turnbaugh JA, Unterberger U, Harris DA. Prion protein at the crossroads of physiology and disease. *Trends in Neurosciences* 2012; 35: 92-103.
- [99] Gilch S, Kehler C, Schatzl HM. The prion protein requires cholesterol for cell surface localization. *Molecular and Cellular Neuroscience* 2006; 31: 346-53.
- [100] Gilch S, Kehler C, Schatzl HM. The prion protein requires cholesterol for cell surface localization. *Mol Cell Neurosci* 2006; 31: 346-53.
- [101] Botto L, Cunati D, Coco S, Sesana S, Bulbarelli A, Biasini E, *et al*. Role of lipid rafts and GM1 in the segregation and processing of prion protein. *PLoS One* 2014; 9: e98344.
- [102] Douek DC, Roederer M, Koup RA. Emerging concepts in the immunopathogenesis of AIDS. *Annu Rev Med* 2009; 60: 471-84.
- [103] Daya M, Cervin M, Anderson R. Cholesterol enhances mouse hepatitis virus-mediated cell fusion. *Virology* 1988; 163: 276-83.
- [104] Danthi P, Chow M. Cholesterol removal by methyl-beta-cyclodextrin inhibits poliovirus entry. *Journal of Virology* 2004; 78: 33-41.
- [105] van't Wout AB, Swain JV, Schindler M, Rao U, Pathmajeyan MS, Mullins JI, *et al*. Nef induces multiple genes involved in cholesterol synthesis and uptake in human immunodeficiency virus type 1-infected T cells. *Journal of Virology* 2005; 79: 10053-8.
- [106] Mujawar Z, Rose H, Morrow MP, Pushkarsky T, Dubrovsky L, Mukhamedova N, *et al*. Human immunodeficiency virus impairs reverse cholesterol transport from macrophages. *PLoS Biol* 2006; 4: e365.
- [107] Dubrovsky L, Van Duyn R, Senina S, Guendel I, Pushkarsky T, Sviridov D, *et al*. Liver X receptor agonist inhibits HIV-1 replication and prevents HIV-induced reduction of plasma HDL in humanized mouse model of HIV infection. *Biochem Biophys Res Commun* 2012; 419: 95-98.
- [108] Jiang H, Badralmaa Y, Yang J, Lempicki R, Hazen A, Natarajan V. Retinoic acid and liver X receptor agonist synergistically inhibit HIV infection in CD4+ T cells by up-regulating ABCA1-mediated cholesterol efflux. *Lipids Health Dis* 2012; 11: 69.

Original article

Associations of EDNRA and EDN1 polymorphisms with carotid intima media thickness through interactions with gender, regular exercise, and obesity in subjects in Taiwan: Taichung Community Health Study (TCHS)

Tsai-Chung Li^{a,b,#}, Chia-Ing Li^{c,d,#}, Li-Na Liao^c, Chiu-Shong Liu^{c,d,f}, Chuan-Wei Yang^{c,g}, Chih-Hsueh Lin^{d,f}, Jen-Hao Hsiao^h, Chih-Yi Hsiao^c, Wen-Yuan Lin^{d,f}, Fang-Yang Wu^c, Cheng-Chieh Lin^{c,d,f,*}

^aGraduate Institute of Biostatistics, College of Public Health, China Medical University, Taichung 404, Taiwan

^bDepartment of Healthcare Administration, College of Health Science, Asia University, Taichung 413, Taiwan

^cDepartment of Medical Research, China Medical University Hospital, Taichung 404, Taiwan

^dSchool of Medicine, College of Medicine, China Medical University, Taichung 404, Taiwan

^eDepartment of Public Health, College of Public Health, China Medical University, Taichung 404, Taiwan

^fDepartment of Family Medicine, China Medical University Hospital, Taichung 404, Taiwan

^gPh.D. Program for Aging, College of Medicine, China Medical University, Taichung 404, Taiwan

^hBioinformatics and Biostatistics Core, Center of Genomic Medicine, National Taiwan University Taipei 106, Taiwan

Received 7th of April 2015 Accepted 28th of April 2015

© Author(s) 2015. This article is published with open access by China Medical University

Keywords:

EDNRA;

EDN1;

Polymorphisms;

Intima media thickness

ABSTRACT

The aim of this study was to evaluate the interacted association between EDNRA and EDN1 polymorphisms and gender, regular exercise, and obesity status on carotid intima media thickness (IMT) in community-dwelling subjects of the Taichung Community Health Study. Five single-nucleotide polymorphisms (SNPs rs1395821, rs1878406, rs5333, rs1800541, and rs5370) of the EDNRA and EDN1 gene were examined in 480 participants from 160 families. The IMT protocol involves scanning the common carotid arteries (CCAs), the carotid bifurcations (bulb), and the origins (first 1 cm) of the internal carotid arteries (ICAs). Generalized linear models with a generalized estimating equation were employed to consider the dependence among family members. After multivariate adjustment, the effects of interactions between EDNRA and EDN1 gene with gender, obesity, and exercise were observed. For gene-gender interaction on CCA IMT, the adjusted mean for men carrying the GA/GG genotype of EDNRA SNP rs1878406 was 1.18 times higher than that for men carrying the AA genotype (95% CI: 1.01, 1.37). As for bulb and ICA IMT, the adjusted mean values for women carrying the AC/AA genotype of EDN1 rs5370 was lower than those carrying the CC genotype: 0.89, [0.82, 0.98]; and 0.90 [0.83, 0.99], respectively. We did observe significant effects of EDNRA SNPs rs1395821 and rs5333 in individuals who regularly exercised. A significantly lower adjusted mean in CCA IMT for non-obese individuals carrying EDNRA SNP rs5333 was observed (0.92 [0.86, 0.99]) compared with non-obese individuals carrying the AA genotype. This study first reported significant interactions of EDNRA and EDN1 polymorphisms with gender, regular exercise, and obesity on carotid IMT in Han Chinese participants.

1. Introduction

Cardiovascular disease (CVD), including coronary heart disease (CHD), stroke, and peripheral arterial disease, is responsible for a lot of morbidity and premature mortality. The pathogenesis of CVD appears to be multi-factorial. Genetics and environments are two major determinants that result in the development of

metabolic syndrome, a cluster of CVD risk factors. These CVD risk factors include high blood pressure, high (pro)-insulin concentrations, excess body weight with central obesity, an altered lipid profile (dyslipidaemia), and inflammation which increases the likelihood of developing atherosclerosis.

Carotid intima-media thickness (IMT) is a quantitative measure of subclinical atherosclerosis [1]. During the progression of

* Corresponding author. School of Medicine, College of Medicine, China Medical University, No. 91, Hsueh-Shih Road, Taichung 404, Taiwan.

Equal contribution as the first author.
E-mail address: cclin@mail.cmuh.org.tw (C.-C. Lin).

atherosclerosis, there are arterial wall vessels changes characterized by a gradual increase in carotid IMT. Carotid IMT is one of the best established and most commonly used early surrogate markers of atherosclerosis [2] as well as a strong predictor of myocardial infarction [3]. Subclinical measurements of carotid IMT have been proposed to be good quantitative phenotypes for the evaluation of its genetic determinants [4]. It has been reported that there is an estimated heritability of 32%-59% in carotid IMT across different populations, indicating genetic factors play an important role in carotid IMT [5-7].

Endothelin-1 (ET-1), encoded by the *EDN1* gene located in chromosome 6p21-24, is a potent vasoconstrictor in the body. ET-1 is expressed in several tissues, including endothelial cells and cardiomyocytes [8], and acts as a modulator of vasomotor tone and vascular remodeling [9, 10]. ET-1 is present in atherosclerotic lesions, and mediates endothelial dysfunction by increasing fibroblast and macrophage activity [11]. ET-1 itself has been considered as a preclinical risk factor for cardiovascular disease [12, 13]. In addition, ET-1 levels are associated with insulin resistance and impairment of glucose transport [14-16], and the one common polymorphism in the *EDN1* gene (rs5390 - Lys198Asn) has been reported to be associated to blood pressure in interaction with body mass index in European [17] and Japanese [18, 19] populations. One important single-nucleotide polymorphism (SNP) [-1394TNG (rs1800541)] in the promoter region of *EDN1* gene has been associated with a risk of developing myocardial infarction, rheumatoid arthritis, and asthma [20-24].

Endothelin type A receptor (EDNRA) is a receptor for ET-1, a potent vasoconstrictor. EDNRA is expressed in vascular smooth-muscle cells [25]. Two studies have investigated the association between single nucleotide polymorphisms (SNPs) in EDNRA and carotid IMT [26, 27], but they showed conflicting results. One study identified that rs6841473 in the EDNRA gene modified the association between smoking and left carotid IMT in Africa Americans [26], whereas the other study did not find the association between rs1878406 in the EDNRA gene and carotid IMT in patients with rheumatoid arthritis [27].

The effects of the genetic loci of the *EDN1* and *EDNRA* genes in Han Chinese populations remain unclear. The paucity of research in this area highlights a need for additional study of the relation between endothelial system genes and carotid IMT. Furthermore, very few studies have focused on the interaction between these genes and environmental factors. Therefore, in our study we examined the associations of five SNPs in *EDN1* and *EDNRA* genes with carotid IMT in a Han Chinese sample from the Taichung Community Health Study (TCHS), and evaluated their interaction effects by gender, regular exercise, and obesity status.

2. Methods

A community-based family study of subclinical atherosclerosis was conducted. All index subjects were identified from our cohort of Taichung Health Study (TCHS), conducted in 2004. TCHS consisted of 2,359 adults aged ≥ 40 years who were randomly selected from among Taichung's general population. This cohort was longitudinally followed from October 2006 to 2009. A total of 1,666 residents were followed and the overall follow-up rate was 73.3%. Carotid IMT was measured at the second wave of the survey. This study was approved by the Human Research Committee of China Medical University Hospital. Informed consent

was obtained from each participant.

All study subjects and their relatives were contacted individually by letter and phone and invited to participate in the study. Data were collected for these study subjects, their spouses, and their all first-degree blood relatives (parents, biological siblings, and offspring) who were 20 years of age or older. A total of 160 index subjects who could provide information on their spouse, and one first-degree blood relative of each index participant were included for this genetic study, for a total of 480 people. The inclusion criterion for study subjects was that they must have more than one first-degree relatives.

3. Measurements

3.1. Anthropometric measurement

Anthropometric measurements and blood samples were obtained from the complete physical examination. Weight and height were measured on an autoanthropometer (super-view, HW-666), with the subjects shoeless and wearing light clothing. Body mass index (BMI) was derived from the formula of weight (kg) \div (height)² (m)². Obesity was defined as a BMI greater than or equal to 27 kg/m².

3.2. Extracranial carotid artery ultrasound measurement

After resting for at least 10 min in the supine position with the neck in slight hyperextension, all study subjects underwent a carotid ultrasound examination using a 7.5-MHz probe to scan the near and far wall of their arterial segments bilaterally in order to get the longitudinal (anterior oblique, lateral, and posterior oblique) and transverse views (GE L7000, GE, Milwaukee, Wis., U.S.A.). The protocol involved scanning the common carotid arteries (CCAs), the carotid bifurcations (bulb), and the origins (the first 1 cm) of the internal carotid arteries (ICAs). The near and far walls of these arterial segments were scanned longitudinally and transversally. The CCA image was taken just before the carotid artery bulb (≈ 5 mm) (CCA IMT). The carotid artery bulb was measured at the level of the proximal ICA sinus (bulb IMT), typically centered on the flow divider. The ICA measurement was made in the ICA where the walls were again parallel (ICA IMT).

3.3. Genetic analysis

Genomic DNA was isolated from the blood samples using the QIAamp DNA Blood Kit (Qiagen, Chatsworth, CA, USA). The concentration of the purified DNA was quantified using a ND-2000c spectrophotometer (NanoDrop Technologies, Wilmington, DE, USA). We selected the rs1395821, rs1878406, and rs5333 SNPs of the EDNRA gene, and the rs1800541 and rs5370 of the EDN1 gene based on the findings for the CHB population in the International HapMap Project. The SNP genotyping was performed using an Illumina VeraCode GoldenGate genotyping assay (Illumina, San Diego, CA, USA).

3.4. Sociodemographic factors and life style behaviors

Data on sociodemographic characteristics, including gender, age, educational attainment, marital status, household income, smoking, drinking, physical activity, occupational activity, menopausal status, dietary habits, family history of cardiovascular-related diseases, physician-diagnosed diseases, and medication history were

Table 1 – Characteristics of study subjects.

	Total (n = 480)	Men (n = 251, 52.3%)	Women (n = 229, 47.7%)
Age (years)	51.39 ± 15.08	51.49 ± 16.28	51.28 ± 13.67
BMI (kg/m ²)	23.93 ± 3.38	24.73 ± 3.41	23.05 ± 3.14
Obesity	77 (16.4)	53 (21.12)	24 (10.48)
Health behavior			
Regular exercise	306 (63.75)	165 (65.74)	141 (61.57)
Smoking	84 (17.5)	79(31.47)	5 (2.18)
Drinking	93 (19.38)	76 (30.28)	17 (7.42)
Betel nut chewing	13 (2.71)	13 (5.18)	0 (0)
Disease History			
Hypertension	121 (25.21)	77 (30.68)	44 (19.21)
Hyperglycemia	50 (10.44)	33 (13.15)	17 (7.46)
Hyperlipidemia	162 (33.89)	87 (34.8)	75 (32.89)
CVA	6 (1.25)	4 (1.59)	2 (0.87)
Cancer	18 (3.76)	6 (2.39)	12 (5.26)
IMT measurements			
IMT-CCA- distance (mm)	0.86 ± 0.29	0.91 ± 0.34	0.8 ± 0.22
IMT-Bulb- proximal (mm)	1.25 ± 0.70	1.31 ± 0.73	1.18 ± 0.66
IMT-ICA- proximal (mm)	0.86 ± 0.46	0.93 ± 0.51	0.79 ± 0.37

Data were presented as mean ± SD for continuous variables or n (%) for categorical variables.
BMI: body mass index; CVA: cerebral vascular accident.

collected when the participants underwent a complete physical exam. Participants who engaged in regular exercise were defined as those who currently participated in regular leisure-time activities for at least 30 min per week for at least 6 months.

3.5. Statistical analysis

Simple descriptive analyses, such as mean, standard deviation, and proportion were presented. Generalized linear models (GLM) with generalized estimating equation(s) (GEE) were employed to compare differences in demographic factors, lifestyle behaviors, and disease history, including hypertension, hyperglycemia, hyperlipidemia, cardiovascular disease, and cancer among genotypes of SNPs in the EDNRA and EDN1 genes by considering the dependence among family members. Five SNPs were tested for deviation from HWE using PLINK software. Gene-environment interactions including gene-gender, gene-exercise, and gene-obesity interactions on carotid IMT were assessed by GLM with GEE adjusted for age, gender, obesity, regular exercise, smoking habits, alcohol drinking, and betel nut chewing. The gene-environment interactions were examined by entering the product terms of each environmental factor and individual SNP with either major allele as the reference group. In addition, three dummy variables measured the main effect of individual SNPs, the main effect of each environmental factor, and the combined effect of individual SNPs with each environmental factor. The values of carotid IMT for CCA, bulb, and ICA were natural log-transformed due to their skewed distributions. Adjusted mean ratio and 95% confidence intervals (CIs) of carotid IMT values were presented. Furthermore, the haplotypes in this sample were analyzed separately for each gene at a frequency > 5%. The significance level was set at a two-sided $P < 0.05$. All analyses used Statistical Analysis Sys-

tem software (v9.4, SAS Institute Inc., Cary, NC, USA), PLINK (v1.07) (<http://pngu.mgh.harvard.edu/purcell/plink>) [28], and Haploview (v4.2) [29].

4. Results

The characteristics of all study subjects and stratified by gender are shown in Table 1. The mean age of the community-dwelling men and women was 51.49 years (SD = 16.28 years) and 51.28 years (13.67 years), respectively. Among the study subjects, 52.3% were men. The prevalence of obesity, regular exercise, smoking, drinking, and betel nut chewing were 16.4%, 63.75%, 17.5%, 19.38%, and 2.71%, respectively. The self-reported diagnosed diseases included hypertension (25.21%), hyperglycemia (10.44%), hyperlipidemia (33.89%), CVA (1.25%), and cancer (3.76%). The mean values of CCA IMT, bulb IMT, and ICA IMT in men were 0.91 (0.34), 1.31 (0.73), and 0.93 (0.51), respectively; and in women were 0.8 (0.22), 1.18 (0.66), and 0.79 (0.37), respectively.

All five of the SNPs studied in the two genes were within the HWE ($P > 0.05$) and the allele and genotype distributions for all polymorphisms are shown in Table 2. The associations of the EDNRA and EDN1 polymorphisms with CCA IMT, bulb IMT, and ICA IMT were examined. The mean values of CCA IMT, bulb IMT, and ICA IMT were not significantly different among genotypes of these 5 SNPs (data not shown). Multiple linear regression analyses were performed on haplotypes in the EDN1 and EDNRA genes. The haplotypes with a frequency of >5% were retained for analysis and we identified four haplotypes of the EDNRA gene for analysis. Two haplotypes of the EDNRA gene were prevalent (A-G-A: 45% and G-G-A: 26.7%), and the other

Table 2 – Genotype distributions of study subjects and IMT distributions according to genotype status.

Gene	SNP	Genotype or allele	n (%)	CCA IMT [#]	BULB IMT [#]	ICA IMT [#]
EDNRA	rs1395821	A A	184 (38.33)	0.84 ± 1.35	1.13 ± 1.63	0.82 ± 1.52
		A G	229 (47.71)	0.82 ± 1.33	1.11 ± 1.62	0.78 ± 1.45
		G G	64 (13.33)	0.78 ± 1.29	1.02 ± 1.57	0.74 ± 1.41
		G*	357 (0.37)			
EDNRA	rs1878406	A A	22 (4.58)	0.84 ± 1.37	1.2 ± 1.7	0.89 ± 1.52
		A G	158 (32.92)	0.83 ± 1.33	1.15 ± 1.63	0.8 ± 1.48
		G G	298 (62.08)	0.81 ± 1.33	1.08 ± 1.61	0.78 ± 1.47
		A*	202 (0.27)			
EDNRA	rs5333	A A	300 (62.5)	0.82 ± 1.34	1.09 ± 1.62	0.78 ± 1.47
		A G	161 (33.54)	0.83 ± 1.32	1.14 ± 1.63	0.79 ± 1.48
		G G	18 (3.75)	0.8 ± 1.27	1 ± 1.47	0.85 ± 1.5
		G*	197 (0.21)			
EDN1	rs1800541	A A	313 (65.21)	0.81 ± 1.31	1.09 ± 1.61	0.78 ± 1.48
		A C	148 (30.83)	0.84 ± 1.36	1.14 ± 1.65	0.81 ± 1.46
		C C	18 (3.75)	0.8 ± 1.36	1.06 ± 1.42	0.73 ± 1.43
		C*	184 (0.19)			
EDN1	rs5370	A A	34 (7.08)	0.82 ± 1.32	1.11 ± 1.62	0.78 ± 1.47
		A C	191 (39.79)	0.83 ± 1.34	1.11 ± 1.63	0.8 ± 1.47
		C C	250 (52.08)	0.8 ± 1.37	1.04 ± 1.56	0.81 ± 1.5
		A*	259 (0.37)			

Data were presented as n (%) for genotypes and alleles or mean ± SD for IMT.

#: Geometric mean was presented.

*: Minor allele.

Table 3 – Significant gene-environment interactions on CCA-distance, BULB-proximal, and ICA-proximal.

Environment	Gene	SNP	P for interaction		
			CCA IMT	BULB IMT	ICA IMT
Gender	EDNRA	rs1395821	0.03 ^d		0.026 ^d
	EDNRA	rs1878406	0.017 ^r		
	EDNRA	rs5333	0.036 ^r		
	EDN1	rs1800541		0.024 ^d	
	EDN1	rs5370		0.019 ^d	0.033 ^r
Regular exercise	EDNRA	rs1395821		0.02 ^r	0.031 ^r
	EDNRA	rs5333		0.002 ^r	
Obesity	EDNRA	rs5333	0.027 ^r		

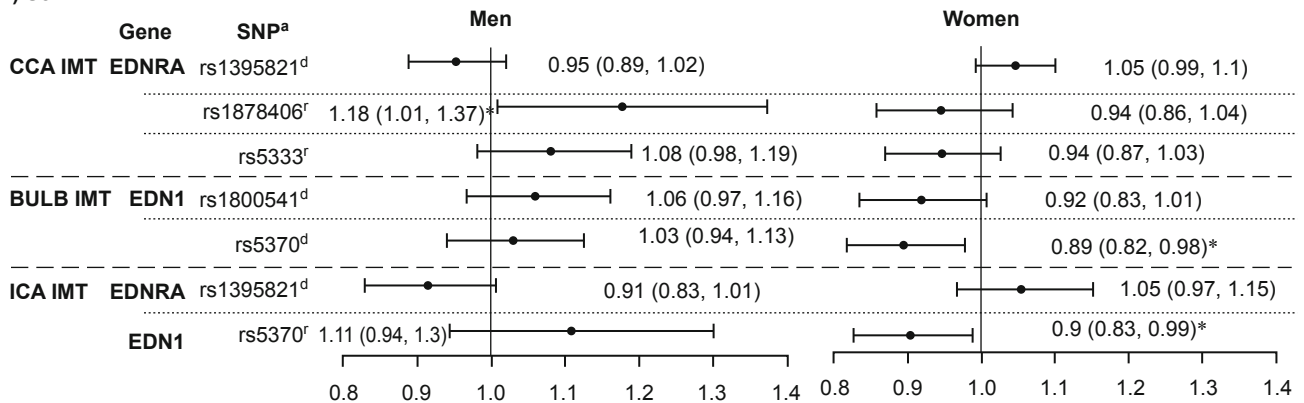
d: interaction term was assessed by a dominant model; r: interaction term was assessed by a recessive model.

two haplotypes were less common with estimated frequencies of 8.34% and 5.02%. Individuals who carried the G-G-A EDNRA haplotype displayed significantly thinner ICA IMT without adjustment ($\beta = -0.07$ [95% CI: -0.13, -0.01]; $P < 0.05$). After multivariate adjustment, this effect became borderline significant.

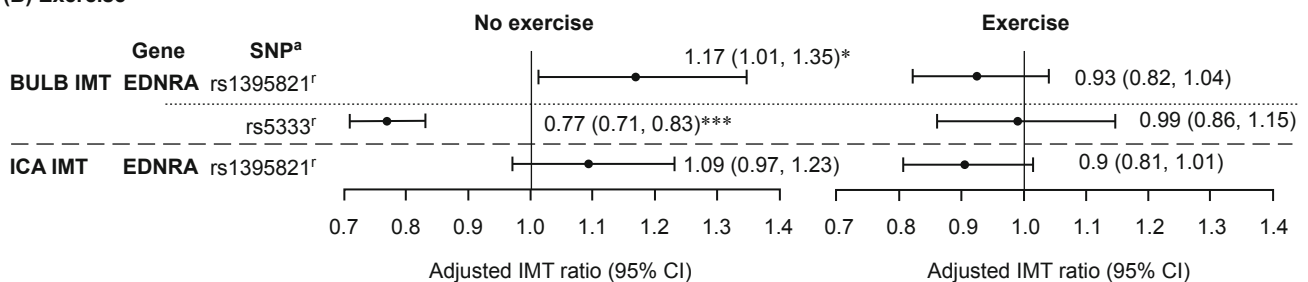
The gene-gender, gene-exercise, and gene-obesity interactions for EDNRA and EDN1 SNPs on carotid IMT were explored (Table 3). After multivariate adjustment, the effects of interactions

between EDNRA SNPs rs1395821, rs1878406, and rs5333 with gender as well as EDNRA SNP rs5333 with obesity on CCA IMT were observed. We also observed significant interactions of EDN1 SNPs rs1800541 and rs5370 with gender as well as EDNRA SNPs rs1395821 and rs5333 with regular exercise on bulb IMT. As for ICA IMT, the interactions of EDNRA SNP rs1395821 and EDN1 SNP rs5370 with gender, as well as EDNRA SNP rs1395821 with regular exercise were significant.

(A) Sex



(B) Exercise



(C) Obesity

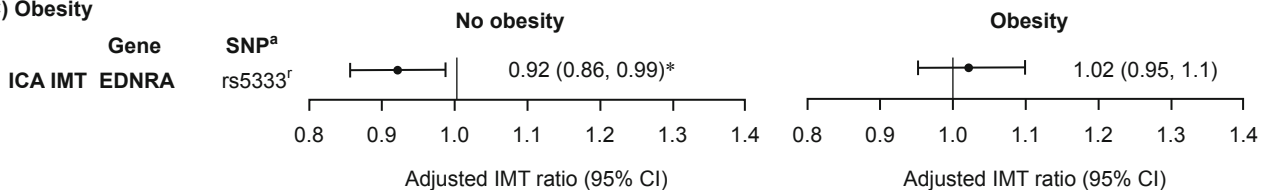


Fig. 1 - Stratified analysis by gender (A), exercise (B), and obesity (C) for significant interaction of *EDNRA* rs1395821, rs1878406, and rs5333, as well as *EDN1* rs1800541, and rs5370 with gender, exercise, and obesity on CCA, bulb, and ICA IMTs are shown. The adjusted mean ratios were obtained from the models with consideration of SNP, age, gender, obesity, smoking, alcohol drinking, and betel nut chewing. * $P < 0.05$. r: recessive model; d: dominant model.

To explore the significant interactions identified above, we estimated the adjusted mean ratio in carotid IMT measurements for either *EDNRA* or *EDN1* minor—major/minor—minor genotypes in comparison with the major—major genotype stratified by gender, regular exercise, and obesity (Figure 1). For gene-gender interaction on CCA IMT, the adjusted mean for men carrying the GA/GG genotype of *EDNRA* SNP rs1878406 was 1.18 times higher than that for men carrying the AA genotype (95% CI: 1.01, 1.37). On the other hand, we did not observe significant effects for *EDNRA* SNP rs1878406 in women. As for bulb and ICA IMT, the adjusted mean values for women carrying the AC/AA genotype of *EDN1* rs5370 was lower than those carrying the CC genotype (0.89, [0.82, 0.98]; and 0.9 [0.83, 0.99], respectively). But the effects of *EDN1* rs5370 on bulb and ICA IMT were not significant in men (Figure 1A). For gene-exercise interaction, we observed that individuals carrying the GA/GG genotype of *EDNRA* SNP rs1395821 had higher mean values of bulb IMT than those carrying the AA genotype among individuals who did not regularly exercise. Whereas individuals carrying the GA/GG genotype of *EDNRA* SNP rs5333 had higher mean values of bulb IMT than those carrying the AA genotype among the subjects who did not

regularly exercise. On the other hand, we did not observe significant effects of *EDNRA* SNPs rs1395821 and rs5333 in individuals who regularly exercised (Figure 1B). A significantly lower adjusted mean in CCA IMT for non-obese individuals carrying *EDNRA* SNP rs5333 was observed (0.92 [0.86, 0.99]) compared with non-obese individuals carrying the AA genotype (Figure 1C). In contrast, it was found that *EDNRA* SNP rs5333 had no effect on CCA IMT in obese individuals.

5. Discussion

ET-1 is a potent vasoconstrictor in the body and is involved with the biology of the vascular endothelium. In the present study, we examined the evidence for gene-gender, gene-exercise, and gene-obesity interaction between the two SNPs in the *EDN1* gene and three SNPs in the *EDNRA* gene in relation to carotid IMT in Han Chinese subjects of Taiwan. We found gender, regular exercise, and obesity significantly interacted with SNPs in the *EDNRA* gene, and gender interacted with SNPs in the *EDN1* gene to influence carotid IMTs in the Han Chinese participants of the TCHS

study. Stratified analysis indicated that EDNRA SNP rs1878406 was associated with CCA IMT in male participants, while EDN1 SNP rs5333 was associated with bulb and ICA IMT in women. For EDNRA SNP rs1878406, the minor allele (A) was associated with higher CCA IMT levels in men whereas the minor allele (G) of EDN1 SNP rs5333 was associated with lower bulb and ICA IMT levels in women. Furthermore, the minor allele (G) of EDNRA SNP rs5333 decreased bulb and CCA IMT levels in individuals without regular exercise or obesity whereas the minor allele (G) of EDNRA SNP rs1395821 increased bulb IMT level in individuals without regular exercise. These findings could provide valuable information towards delineating the genetic mechanisms underlying carotid IMTs.

Previous epidemiological genetic studies of ET-1 have principally focused on hypertensive properties [17-19, 30], as have genetic studies of EDNRA [31]. Few studies thus far have explored their associations with IMT [26, 27, 30, 32]. One prior study explored the interaction of smoking with SNP rs6841473 in EDNRA on left carotid IMT in Africa Americans. The minor allele (T) of rs6841473 increased the left carotid IMT level in non-smoking Africa Americans, but had little effect in black smokers [26]. Another study examined the association between mean carotid intima media thickness and EDN1 SNP rs5370 in a general population sample of Western Australia and they found the minor allele was marginally associated with increased mean IMT levels [30]. Another study explored the potential relationship between EDNRA rs1878406 polymorphisms and carotid IMT in patients with rheumatoid arthritis, and no statistically significant differences were found when this polymorphism was assessed according to carotid IMT values [27]. A study conducted in Japanese patients with essential hypertension investigated the relationship between 11 SNPs of ET-1 family genes (including three in EDN1, one in EDNRA) and atherosclerotic changes and found a significant correlation between mean carotid IMT and EDNRArs5333 in male, but not female, hypertensive patients [32]. In the present study, we did not observe main effects of rs1395821, rs1878406, and rs5333 of the EDNRA gene, and rs1800541, and rs5370 of the EDN1 gene on carotid IMT levels. Instead, we identified a significant interaction of gender with these three SNPs in the EDNRA gene and with these two SNPs in the EDN1 gene, regular exercise with rs1395821 and rs5333 in the EDNRA gene, and obesity with rs5333 in the EDNRA gene in Han Chinese subjects. When we stratified our study sample by gender, we observed no significant evidence for associations between some SNPs and carotid IMT in each of the two strata due to a limited sample size in each stratum.

EDNRA encodes the receptor for ET-1, which plays an important role in potent and long-lasting vasoconstriction [26, 33]. Endothelium dysfunction is accompanied in atherosclerosis [26, 33]. Previous bench research found that endothelin receptor antagonists are effective in attenuating vascular abnormality in atherosclerosis [26, 33]. As for EDN1, it encodes preproendothelin that is processed to form endothelin 1, a potent vasoconstrictor. SNP rs1800541 is located in the EDN1 promoter region with potential regulatory effects on gene expression and rs5370 is one common non-synonymous SNP that is located in the CT-pro-ET-1 part of the ET-1 coding gene. Previous studies have reported rs5370 to be associated with idiopathic pulmonary arterial hypertension [34] and risk for hypertension [10]. The potential physiological functions of these two genes, along with the significant associations in our study and the previous studies [26, 30], implicate them as strong candidate genes for atherosclerosis. Never-

theless, future functional studies in humans may be necessary.

One limitation of the present study is that the sample size of our study was relatively small, particularly in the evaluation of gene-gender interactions. Therefore, we may have missed important polymorphisms that are associated with carotid IMT due to a low statistical power for stratified analysis. Future studies with a larger number of participants are needed.

Our study had important strengths. First, we assessed for the first time the potential association between the 5 polymorphisms in EDNRA and EDN1 genes and subclinical atherosclerosis as well as the interactions between these 5 variants with gender, regular exercise, and obesity in Han Chinese. Second, our study subjects were from a representative sample of Taiwan's Chinese population. Therefore, the generalization of our results to other Han Chinese populations is applicable. Third, the measurement of both carotid IMT and genotypes had stringent quality controls.

In conclusion, the current study identified three variants (rs1395821, rs1878406, rs5333) in the EDNRA gene and two variants (rs1800541 and rs5370) in the EDN1 gene that interacted with gender; two in the EDNRA gene (rs1395821 and rs5333) interacted with regular exercise; and one in the EDNRA gene (rs5333) interacted with obesity on carotid IMT in Han Chinese participants from the TCHS. These findings help delineate the genomic mechanisms underlying carotid IMT. Still, further studies will be necessary to genotype other important variants underlying the EDNRA and EDN1 signals, and to elucidate the mechanisms with which gender, regular exercise, and obesity modify the effects of these polymorphisms on carotid IMT in Han Chinese.

Acknowledgments

This study is supported in part by the Ministry of Science and Technology of Taiwan (National Science Council) (NSC 99-2628-B-039-007-MY3 & NSC 94-2314-B-039-019), the Taiwan Ministry of Health and Welfare Clinical Trial and Research Center of Excellence (MOHW104-TDU-B-212-113002), and the China Medical University (CMU102-BC-11).

Declaration of Interest

Authors declare no conflicts of interest for this work.

Open Access This article is distributed under terms of the Creative Commons Attribution License which permits any use, distribution, and reproduction in any medium, provided original author(s) and source are credited.

REFERENCES

- [1] Annett JL, Sing CF, Biron P, Mongeau JG. Familial aggregation of blood pressure and weight in adoptive families. II. Estimation of the relative contributions of genetic and common environmental factors to blood pressure correlations between family members. *Am J Epidemiol* 1979; 110: 492-503.
- [2] O'Leary DH, Polak JF. Intima-media thickness: a tool for athero-

- sclerosis imaging and event prediction. *Am J Cardiol* 2002; 90: 181-211.
- [3] van der Meer IM, Bots ML, Hofman A, del Sol AI, van der Kuip DA, Witteman JC. Predictive value of noninvasive measures of atherosclerosis for incident myocardial infarction: the Rotterdam Study. *Circulation* 2004; 109: 1089-94.
- [4] Arnett DK, Baird AE, Barkley RA, Basson CT, Boerwinkle E, Ganesh SK, *et al.* Relevance of genetics and genomics for prevention and treatment of cardiovascular disease: a scientific statement from the American Heart Association Council on Epidemiology and Prevention, the Stroke Council, and the Functional Genomics and Translational Biology Interdisciplinary Working Group. *Circulation* 2007; 115: 2878-901.
- [5] Xiang AH, Azen SP, Buchanan TA, Raffel LJ, Tan S, Cheng LS, *et al.* Heritability of subclinical atherosclerosis in Latino families ascertained through a hypertensive parent. *Arterioscler Thromb Vasc Biol* 2002; 22: 843-8.
- [6] Zhao J, Cheema FA, Bremner JD, Goldberg J, Su S, Snieder H, *et al.* Heritability of carotid intima-media thickness: a twin study. *Atherosclerosis* 2008; 197: 814-20.
- [7] Medda E, Fagnani C, Schillaci G, Tarnoki AD, Tarnoki DL, Baracchini C, *et al.* Heritability of arterial stiffness and carotid intima-media thickness: an Italian twin study. *Nutr Metab Cardiovasc Dis* 2014; 24: 511-7.
- [8] Brunner F, Bras-Silva C, Cerdeira AS, Leite-Moreira AF. Cardiovascular endothelins: essential regulators of cardiovascular homeostasis. *Pharmacol Ther* 2006; 111: 508-31.
- [9] Hickey KA, Rubanyi G, Paul RJ, Highsmith RF. Characterization of a coronary vasoconstrictor produced by cultured endothelial cells. *Am J Physiol* 1985; 248 (5 Pt 1): C550-6.
- [10] Rankinen T, Church T, Rice T, Markward N, Leon AS, Rao DC, *et al.* Effect of endothelin 1 genotype on blood pressure is dependent on physical activity or fitness levels. *Hypertension* 2007; 50: 1120-5.
- [11] Luscher TF, Barton M. Endothelins and endothelin receptor antagonists: therapeutic considerations for a novel class of cardiovascular drugs. *Circulation* 2000; 102: 2434-40.
- [12] Endemann DH, Schiffrin EL. Endothelial dysfunction. *J Am Soc Nephrol* 2004; 15: 1983-92.
- [13] Shah R. Endothelins in health and disease. *Eur J Intern Med* 2007; 18: 272-82.
- [14] Irving RJ, Noon JP, Watt GC, Webb DJ, Walker BR. Activation of the endothelin system in insulin resistance. *Qjm* 2001; 94: 321-6.
- [15] Strawbridge AB, Elmendorf JS. Phosphatidylinositol 4,5-bisphosphate reverses endothelin-1-induced insulin resistance *via* an actin-dependent mechanism. *Diabetes* 2005; 54: 1698-705.
- [16] Strawbridge AB, Elmendorf JS. Endothelin-1 Impairs Glucose Transporter Trafficking *via* a Membrane-Based Mechanism. *J Cell Biochem* 2006; 97: 849-56.
- [17] Tiret L, Poirier O, Hallet V, McDonagh TA, Morrison C, McMurray JJ, *et al.* The Lys198Asn polymorphism in the endothelin-1 gene is associated with blood pressure in overweight people. *Hypertension* 1999; 33: 1169-74.
- [18] Asai T, Ohkubo T, Katsuya T, Higaki J, Fu Y, Fukuda M, *et al.* Endothelin-1 gene variant associates with blood pressure in obese Japanese subjects: the Ohasama Study. *Hypertension* 2001; 38: 1321-4.
- [19] Jin JJ, Nakura J, Wu Z, Yamamoto M, Abe M, Tabara Y, *et al.* Association of endothelin-1 gene variant with hypertension. *Hypertension* 2003; 41: 163-7.
- [20] Castro MG, Rodriguez-Pascual F, Magan-Marchal N, Reguero JR, Alonso-Montes C, Moris C, *et al.* Screening of the endothelin1 gene (EDN1) in a cohort of patients with essential left ventricular hypertrophy. *Ann Hum Genet* 2007; 71(Pt 5): 601-10.
- [21] Palacin M, Rodriguez-Pascual F, Reguero JR, Rodriguez I, Avanzas P, Lozano I, *et al.* Lack of association between endothelin-1 gene variants and myocardial infarction. *J Atheroscler Thromb* 2009; 16: 388-95.
- [22] Panoulas VF, Douglas KM, Smith JP, Taffe P, Stavropoulos-Kaliloglou A, Toms TE, *et al.* Polymorphisms of the endothelin-1 gene associate with hypertension in patients with rheumatoid arthritis. *Endothelium* 2008; 15: 203-12.
- [23] Tobe SW, Baker B, Hunter K, Kiss A, Perkins N, Gomez L, *et al.* The impact of endothelin-1 genetic analysis and job strain on ambulatory blood pressure. *J Psychosom Res* 2011; 71: 97-101.
- [24] Zhu G, Carlsen K, Carlsen KH, Lenney W, Silverman M, Whyte MK, *et al.* Polymorphisms in the endothelin-1 (EDN1) are associated with asthma in two populations. *Genes Immun* 2008; 9: 23-9.
- [25] Yu JC, Pickard JD, Davenport AP. Endothelin ETA receptor expression in human cerebrovascular smooth muscle cells. *Br J Pharmacol* 1995; 116: 2441-6.
- [26] Li C, Chen W, Jiang F, Simino J, Srinivasan SR, Berenson GS, *et al.* Genetic association and gene-smoking interaction study of carotid intima-media thickness at five GWAS-indicated genes: The Bogalusa Heart Study. *Gene* 2015; 562: 226-31.
- [27] Lopez-Mejias R, Genre F, Garcia-Bermudez M, Ubilla B, Castaneda S, Llorca J, *et al.* Lack of association between ABO, PPA2B, ADAMST7, PIK3CG, and EDNRA and carotid intima-media thickness, carotid plaques, and cardiovascular disease in patients with rheumatoid arthritis. *Mediators Inflamm* 2014; 2014:756279.
- [28] Purcell S, Neale B, Todd-Brown K, Thomas L, Ferreira MA, Bender D, *et al.* PLINK: a tool set for whole-genome association and population-based linkage analyses. *Am J Hum Genet* 2007; 81: 559-75.
- [29] Barrett JC, Fry B, Maller J, Daly MJ. Haploview: analysis and visualization of LD and haplotype maps. *Bioinformatics* 2005; 21: 263-5.
- [30] Wiltshire S, Powell BL, Jennens M, McCaskie PA, Carter KW, Palmer LJ, *et al.* Investigating the association between K198N coding polymorphism in EDN1 and hypertension, lipoprotein levels, the metabolic syndrome and cardiovascular disease. *Hum Genet* 2008; 123: 307-13.
- [31] Liu F, He J, Gu D, Rao DC, Huang J, Hixson JE, *et al.* Associations of Endothelial System Genes With Blood Pressure Changes and Hypertension Incidence: The GenSalt Study. *Am J Hypertens* 2014.
- [32] Yasuda H, Kamide K, Takiuchi S, Matayoshi T, Hanada H, Kada A, *et al.* Association of single nucleotide polymorphisms in endothelin family genes with the progression of atherosclerosis in patients with essential hypertension. *J Hum Hypertens* 2007; 21: 883-92.
- [33] Dai DZ, Dai Y. Role of endothelin receptor A and NADPH oxidase in vascular abnormalities. *Vasc Health Risk Manag* 2010; 6: 787-94.
- [34] Vadapalli S, Rani HS, Sastry B, Nallari P. Endothelin-1 and endothelial nitric oxide polymorphisms in idiopathic pulmonary arterial hypertension. *Int J Mol Epidemiol Genet* 2010; 1: 208-13.

Original article

The medical diagnostic approaches with phylogenetic analysis for rare *Brucella* spp. diagnosis in Taiwan

Ni Tien^{ab}, Yun-Ju Sung^a, Yi-Chih, Chang^b, Bang-Jau You^c, Michelle Liang^d, Yun-Ping Lim^e, Wen-Yu Ho^f, Hsiu-Shen Lin^a, Mao-Wang Ho^g, Chen-Mao Ho^{ag}, Chao-Chin Chang^h, Yu-Ching Lan^{i,*}

^aDepartment of Laboratory Medicine, China Medical University Hospital, Taichung 404, Taiwan

^bDepartment of Medical Laboratory Science and Biotechnology, China Medical University, Taichung 404, Taiwan

^cDepartment of Chinese Pharmaceutical Sciences and Chinese Medicine Resources, China Medical University, Taichung 404, Taiwan

^dDepartment of Microbiology, UCLA, CA 90095, USA

^eDepartment of Pharmacy, College of Pharmacy, China Medical University, Taichung 404, Taiwan

^fDepartment of Laboratory Medicine, China Medical University Beigang Hospital, Taichung 651, Taiwan

^gDepartment of Internal Medicine, School of Medicine, China Medical University, Taichung 404, Taiwan

^hGraduate Institute of Microbiology and Public Health, National Chung Hsing University, Taichung 402, Taiwan

ⁱDepartment of Health Risk Management, China Medical University, Taichung 404, Taiwan

Received 1st of April 2015 Accepted 22nd of April 2015

© Author(s) 2015. This article is published with open access by China Medical University

Keywords:

Brucella;
Traditional biochemical methods;
6s *rRNA*;
Phylogenetic analysis;
Anti-microbial susceptibility test

ABSTRACT

Brucellosis is a bacterial zoonotic disease which can be easy to misdiagnose in clinical microbiology laboratories. In the present study, we have tried to improve the current clinical method for detecting *Brucella* spp. and its antibiotic characteristics. Our method begins with detecting the clinical isolate through traditional biochemical methods and automatic identification systems. Then, we move on to editing the sequence for BLAST allows us to compare 16s *rRNA* sequences with sequences from other species, allowing the gene level to be determined. Next, the phylogenetic analysis of multiple genetic loci is able to determine the evolutionary relationships between our bacteria strain and those from other locations. Finally, an anti-microbial susceptibility test hones in on the level of antibacterial activity that the bacteria displays. Employing these four steps in concert is extremely effective in identifying rare bacteria. Thus, when attempting to determine the identity of rare bacteria such as *Brucella*, utilizing these four steps from our research should be highly effective and ultimately prevent further identification errors and misdiagnoses. The standards we have suggested to identify rare bacteria strains is applicable not only to *Brucella*, but also to other rarely encountered bacteria.

1. Introduction

Brucellosis is one of the most common zoonotic diseases, with more than 500,000 new cases yearly. Its prevalence is more than 10/100,000 population in some endemic areas such as France, Israel, and most of Latin America, the Middle East, northern Africa, and central Asia [1, 2]. The disease is transmitted by consumption of unpasteurized dairy products or by occupational contact with infected animals. In the past 15 years, the epidemiology of human brucellosis has increasingly evolved through tourism and cases of animal brucellosis [2]. Furthermore, infected objects are the most common cause of laboratory-transmitted infections in laboratory workers [3, 4]. *Brucella* spp. has been classified in the high risk group of pathogens [5].

Since *Brucella* spp are intracellular bacteria, relapse is often seen [6-9]. The features of *Brucella* spp include being a faculta-

tive intracellular pathogen, lacking capsules, flagellates, endospores or native plasmids, and being slow growing and small (0.5-0.7 × 0.6-1.5 μm) gram-negative coccobacilli (GNCB). Brucellosis usually causes systemic diseases in the osteoarticular, hematological, hepatobiliary, gastrointestinal, cardiovascular, and central nervous systems [10]. Common clinical symptoms of brucellosis are characterized by high fever, myalgia, and arthralgia of the large joints. Apart from these main symptoms, brucellosis can also mimic various multisystem diseases by exhibiting wide clinical polymorphism and nonspecific symptoms, which frequently lead to misdiagnosis and treatment delay [11, 12]. Brucellosis may be difficult to diagnose because of its wide clinical polymorphism. Previous identification experiences have had problems with errors. Laboratories had been report some cases of *Brucella* initially misdiagnosed by automatic identification systems before. These errors can lead to misdiagnosis, delayed treatment, and ul-

*Corresponding author. Department of Health Risk Management, China Medical University, No. 91, Hsueh-Shih Road, Taichung 404, Taiwan.

E-mail address: yclan@mail.cmu.edu.tw (Y.-C. Lan)

timately, the infection of even more individuals [11-14].

Since 1980, Taiwan has been free of this disease after an eradication program was implemented [15-17]. However, in 2011 a few cases were reported. These cases were traced back to North Africa and Malaysia [16-18]. They indicate that the pathogen can still pose a threat to public health in Taiwan despite previously being eradicated. There are worries that the overall capacity of Taiwanese physicians may be lacking due to inexperience in identification of the bacteria and subsequent misdiagnoses in clinical microbiology laboratories.

Therefore, the aim of this report is to share our experiences, to culture and identify the findings of this rare pathogen in Taiwan, and to compare the phylogenetic relevance of our genetic sequence with other epidemic strains in the geographical areas mentioned above. This research will aid in refining our understanding about the source of pathogens, thus allowing clinical microbiology laboratory workers to pay more attention to the identification and diagnosis of the rare *Brucella* spp. [19].

2. Materials and methods

In this study, we detected the clinical isolate by utilizing traditional biochemical methods and automatic identification systems which include the BD Phoenix system and API 20E and 32 GN identification kits. Furthermore, we used the 16s *rRNA* sequences method for determining gene level. We performed an antibiotic sensitivity test. In addition, we also carried out phylogenetic analysis. By analyzing our strain of bacteria and comparing it with those from other geographical areas, we were able to determine the evolutionary relationship between the strain from Taiwan and other areas' strains.

2.1. Collection and identification of bacteria isolate

The conventional biochemical tests used included Oxidase-positive, urease-positive, H₂S production, dye tolerance such as basic fuchsin and thionin and sero-agglutination tests. We routinely employed the BD Phoenix NMIC/ID-2 commercial kit (Becton Dickinson diagnostic System, Sparkes, MD, USA). Inoculation was performed according to the manufacturer's instructions. The API 20E and 32 GN systems (Biomérieux SA, Marcy l'Etoile, France) were also used to identify the strain. Inoculation, reading, and interpretation of panels were performed according to the manufacturer's instructions [20].

2.2. 16S ribosomal RNA gene sequencing

Sampling and sample preparation: The bacteria from positive blood culture specimens of the patient were plated on Trypticase soy agar with 5% defibrinated sheep blood (BBL Microbiology Systems, Cockeysville, Md.) and incubated aerobically for 2 days at 37°C. Several visible colonies were selected and suspended in 600 µl TE buffer and adjusted to MacFaland 3.0 cell density for nucleic acid extraction.

Nucleic acid extraction: DNA was extracted from fluid samples (600 µl) using the Genomic DNA Mini Kit (Geneaid, Taiwan). The appropriate protocols were followed according to the manufacturer's instructions; with a final elution volume of 50 µL. Extracted DNA was stored at 4°C until required for PCR.

Amplification of 16s *rRNA* genes: The 16s *rRNA* gene from the microorganisms was amplified by PCR. A primer pair con-

sisting of 8f (5'-GAGAGTTTGATCTGGCTCAG-3') and 1492r (5'-TACGGCTACCTTGTTACGACT-3') [21, 22] was used to amplify nearly 1500-bp fragments of the 16s *rRNA* genes. The samples were amplified in the following PCR mixture: 10 µmol of each primer in a 2X buffer containing 4 mM MgCl₂, 0.4 mM of each deoxynucleoside triphosphate, 0.05 U *Taq* DNA polymerase, and 40 mM (NH₄)₂SO₄ (Ampliqon, Skovlunde, Denmark) in a final volume of 50 µL. The following temperature cycles were used: 94°C for 5 min, 30 cycles of 94°C for 1 min, 55°C for 1 min, and 72°C for 1 min and 30 s, and a final extension at 72°C for 7 min. All reactions were conducted in a GeneAmp 9700 thermocycler (Applied Biosystems, Foster City, Calif.).

16s *rRNA* gene sequencing and alignment: Sequencing primers were chosen from a pair of previously described oligonucleotides, 8f and 1492r. Sequencing was performed with a 3730xl DNA Analyzer (Applied Biosystems, Foster City, Calif.). Sequences were aligned using the BioEdit suite of programs (www.mbio.ncsu.edu/BioEdit/bioedit.html), and the identity was evaluated by checking against existing sequences using BLAST (<http://www.ncbi.nlm.nih.gov/BLAST>). Sequencing of the 16s *rRNA* gene fragments showed a clear division of sequences into *Brucella melitensis* [22-24].

2.3. The multiple genetic loci for phylogenetic relationship identification

A previous study already successfully determined the sequences of multiple genetic loci in order to examine the relationships between *Brucella* isolates [25]. In order to further identify the genetic relationship among *Brucella* strains in this study and others strains in the GenBank, we extracted the *Brucella* DNA and amplified multiple genetic loci of the isolate, including *aroA*, *gIK*, *dank*, and *gyrB* partial gene fragments (Table 1) for phylogenetic analysis [25].

2.4. Polymerase chain reactions (PCRs) and sequencing

Four distinct genome fragments were amplified by PCR using the primers shown in Table 1. PCR reaction mixes were prepared for each sample by mixing 10 µmol of each primer in a 2X buffer containing 4 mM MgCl₂, 0.4 mM of each deoxynucleoside triphosphate, 0.05 U *Taq* DNA polymerase, and 40 mM (NH₄)₂SO₄ (Ampliqon, Skovlunde, Denmark) in a final volume of 30 µL. Cycling parameters were as follows: 94°C for 5 min. followed by 30 cycles of 94°C for 1 min., 53°C for 1 min. and 72°C for 1 min., and a final polishing step of 72°C for 10 min. Products were separated by agarose gel electrophoresis to check for efficiency of amplification and to ensure that only a single product of the expected size was present. The DNA products were sequenced by using a GeneAmp 9700 thermocycler (Applied Biosystems, Foster City, Calif.).

2.5. Phylogenetic analysis

The *aroA*, *gIK*, *dank* and *gyrB* gene partial segments sequence data were edited using Bioedit for alignment, and then these data were combined with each other and before undergoing phylogenetic analysis. Sequences of the four loci were concatenated to produce a 1675 bp sequence for each genotype sequence. Phylogenetic analysis was performed with the MEGA software, Version 3.1. The neighbor joining tree was constructed with the concatenated sequence data of the four loci (1,675 bp) using the neighbor

Table 1 – Oligonucleotide sequences used for the amplification and sequencing of four genetic loci.

Locus	Function	Primer sequences	Length (bp)
<i>aroA</i>	3-phosphoshikimate 1-carboxyvinyltransferase	5' GACCATCGACGTGCCGGG 3' 5' YCATCAKGCCCATGAATTC 3'	565
<i>glK</i>	glucokinase	5' TATGGAAMAGATCGGCGG 3' 5' GGGCCTTGTCTCGAAGG 3'	475
<i>danK</i> ,	chaperone protein	5' CGTCTGGTCTCGAATATCTGG 3' 5' GCGTTTCAATGCCGAGCGA 3'	470
<i>gyrB</i>	DNA gyrase B subunit	5' ATGATTTTCATCCGATCAGGT 3' 5' CTGTGCCGTTGCATTGTC 3'	469

joining approach. The Jukes-Cantor model, which is based on the assumption that all nucleotide substitutions are equally likely, was used to determine genetic distances. The percentage bootstrap confidence levels of internal branches were calculated from 1,000 resamplings of the original data.

2.6. Antimicrobial susceptibility test of *Brucella* isolate from clinical specimens

The antibiotic susceptibility test applied the paper disc diffusion method and the minimal inhibition concentration test; MIC. Tigecycline (TGC) MICs were determined by the E test (Biomerieux, Sweden). Mueller-Hinton agar supplemented with 5% sheep's blood agar plate (Oxoid, UK) was inoculated with bacterial suspensions with a equivalent to a 0.5 McFarland turbidity and was interpreted 2 days after incubation in ambient air. The susceptibility testing of tetracycline (Te) (30 µg/ml), streptomycin (STR) (300, 10 µg/ml), rifampin (RIF) (5 µg/ml), and trimethoprim-sulfamethoxazole (TMP-SMZ) (1.25/23.75 µg/ml) was determined by disk diffusion method. Mueller-Hinton agar supplemented with 5% sheep's blood was inoculated with suspensions of bacteria with equivalent 0.5 McFarland turbidity and was interpreted 48 h after incubation in ambient air.

3. Results

3.1. Conventional identification

The gram-negative coccobacilli on the BAP plate are better growth and appeared small and white. The glossy quality of the better growth suggests that the gram-negative coccobacilli were of the smooth-quality type. The size of the bacteria was about 0.5-0.8 µm × 0.6-1.5 µm. There were no colonies growing on the EMB plate. The conventional biochemical tests showed a positive reaction that included the catalase, oxidase, and urease. Automated instruments and the API system (32 GN and 20 E) were employed to identify the bacteria. The results presented two species, *Ochrobactrum antropi* and *Myroides* spp., respectively. The Phoenix instrument gave an *Ochrobactrum antropi* result, and the species was identified with 90% confidence. The API 20E identification was analyzed, and then code number 0210004 presented *Myroides* / *Chryseobacterium indologenes* (% id: 47.4, T = 0.92), *Bordetella* / *Alcaligenes* / *Moraxella* spp. (% id: 25.7, T = 0.87) and *Ochrobactrum antropi* (% id: 21.7, T = 0.82). The API 32 GN identification code number 0000000002 was *Myroides* spp. (% id: 90.0, T = 1.00).

3.2. 16S ribosomal RNA gene sequencing

The 16s *rRNA* gene sequences were aligned by the BioEdit program and BLAST. A 99% similarity between *Brucella melitensis* and *Brucella ovis* was discovered. The 16s *rRNA* gene sequence illustrated a homology between these two species. We further conducted phylogenetic analysis from multiple genetic loci in order to examine the relationships between *Brucella* isolates.

3.3. The phylogenetic relationships with other *Brucella*

To recognize the phylogenetic relationships of this *Brucella* strain, sequences of the four loci were concatenated to produce a 1675 bp sequence. The multiple genetic loci that were analyzed included *aroA*, *glK*, *dank* and *gyrB* partial gene fragments. The reference sequences with whole genomes came from the GenBank. The topology of the phylogenetic reference tree from the four loci was similar to the tree from the whole genome. The percentage bootstrap confidence levels of internal branches were calculated from 1,000 re-samplings of the original data. After comparison with the brucellosis in the Genbank as reference sequences, the bacterial strain in this study was clustered with the *Brucella melitensis* strains in a significantly monophyletic branch of the neighboring joining tree. The branch lengths represent the genetic variation between Taiwan *Brucella melitensis* and strains from other geographic areas.

3.4. Antimicrobial susceptibility test

In the tigecycline MICs, results were determined by the E test with turbidity between 0.5, 0.75, and 1.0 McFarland, but the results appeared all the same as 0.094 µg/ml (Figure 1). The inhibitory zone size of tetracycline (Te), streptomycin (STR), rifampin (RIF) and trimethoprim-sulfamethoxazole (TMP-SMZ) are shown in Table 2.

4. Discussion

Brucellosis has become a rare disease in developed and developing countries. As the infectious dose is very low, infections are an occupational risk for farmers, veterinarians, abattoir workers, laboratory personnel, and others who work with animals and consume their products [18, 26]. The increase in business and leisure travel to brucellosis-endemic countries has led to the importation of the disease into non-endemic areas [26]. Two problems arise from this importation. First, clinicians in non-endemic areas often

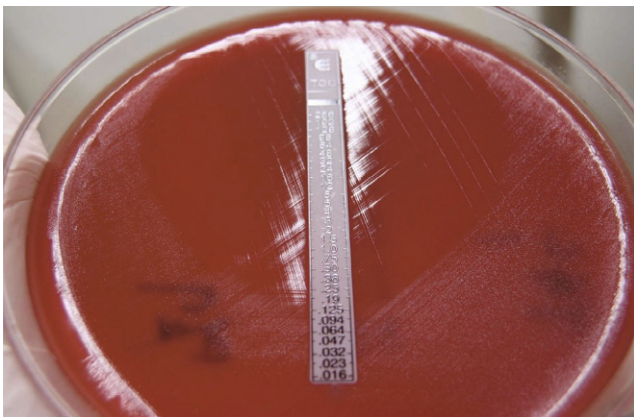


Fig. 1 - Tigecycline MICs results were determined by the E test.

have insufficient experience with brucellosis and have difficulty making the correct diagnosis. Second, there could be failures in notifying laboratories, and brucellosis bacteria could be misidentified by using commercial automatic diagnosis systems. These two problems are serious enough to deserve special attention in Taiwanese clinical microbiology laboratories [27].

The “gold standard” in the diagnosis of brucellosis is bacterial isolation, which requires long cultivation periods and is often unsuccessful. Because of this, we back-tracked the identification process and found that *Brucella* spp. is not included regularly in the database of automatic identification systems. The results of our tests presented *Ochrobactrum antropi* and *Myroides / Chryseobacterium indologenes*, respectively, and were given by two identification systems, the Phoenix and the API 20E systems. The confirmed rates were untrustworthy [9, 12, 13]. Whereas *Brucella* spp. are classified as highly pathogenic biosafety level 3 agents, only two species of the genus *Ochrobactrum* (*O. anthropi* and *O. intermedium*) have been associated with opportunistic immunocompromised human disease [28]. It can be seen that errors in identification of *Brucella* spp. may not only affect physicians’ treatments, they may also affect the safety of laboratory personnel.

Ochrobactrum represent a distinct genus distantly related to *Achromobacter* but phylogenetically closely related to the *rRNA* superfamily IV of the *Alphaproteobacteria*—in particular, to *Brucella* and *Phyllobacterium* [9]. The close relationship to *Brucella* was emphasized in 1998 by Velasco *et al.* [29]. This close relationship has led to misidentification of *Brucella melitensis* as *Ochrobactrum anthropi* in the past. In previous research, the 16s *rRNA* sequences of *Brucella* spp. and *O. intermedium* were found to be 98.6% identical [29]. Like the previous research group report [14], our study also had a similar misclassification experience with *Brucella* spp. in our automatic identification and 16s nucleotides blast. The result of our 16s *rRNA* BLAST illustrated a homology between *Brucella melitensis* and *Brucella ovis*.

Results that are not accurate have the very real potential of misleading the examiner(s) of these bacteria. One could potentially send the wrong bacteria culture report and cause clinicians to misdiagnose [12, 13]. There is currently a growing trend in errors due to the increasing utilization of automated equipment for microbial identification. Limitations in the instruments’ databases and inability to distinguish similar phenotype strains mean laboratory staff must sometimes use traditional options such as

Table 2 – Susceptibility testing results were determined via disk diffusion method.

Antibiotics	Concentration (µg/ml)	Inhibitory zone (mm)
Tetracycline	30	28
Streptomycin	10	30
	300	40
Rifampin	5	21
Trimethoprim-sulfamethoxazole	1.25/23.75	22

characterizing bacterial colonies and examining staining patterns as well as biochemical reactions to determine what bacteria are in a given sample. However, a clinical microbiology laboratory can also think ahead and identify bacteria and bacterial genotypes using molecular biological techniques. 16s *rRNA* analysis methods and phylogenetic analysis can provide more accurate reports in order to make up for the inability of automated systems to distinguish between closely related bacterial strains.

Ever since the early microbiological work performed by Wilson (30), researchers have been developing increasingly sophisticated methods of classifying *Brucella* species. However, despite technical advances in genotyping, the methods we have chosen have been able to roughly generate the same evolutionary relationships as those seen in whole genome phylogenies, especially in clinical approaches with a short time-span. Multilocus sequence typing trees in our study of *Brucella* roughly approximate the whole-genome phylogeny but use only four housekeeping genes. Although each approach to genotyping has its value, particularly when low-cost genotyping is the goal, only whole-genome sequencing can capture the full extent of genetic variation. Furthermore, only whole-genome phylogenies allow us to gauge the accuracy of previous genetic methods. Understanding the evolutionary framework of the genus *Brucella* is essential for designing assays that differentiate the various strains or biovars, and only by rooting our phylogeny can we understand the directionality of the evolutionary process. A future study might pursue a strategy for tracing the relationship between strains of *Brucella* in Taiwan, China or other neighboring countries.

The CLSI-M100-S20 specification standards of susceptibility of *Brucella* spp. illustrated streptomycin ≤ 8 µg/ml, tetracycline ≤ 1 µg/ml, doxycycline ≤ 1 µg/ml, gentamicin ≤ 4 µg/ml, trimethoprim-sulfamethoxazole (SXT) $\leq 2/38$ µg/ml. When we manipulated the antibiotic sensitivity test, we found that when bacterial growth is slow and the colonies are small, they cannot take advantage of automated identification systems to perform the MIC test. The interpretation of inhibition zone size does not follow the CLSI standards. The same scenario is found in a previous report [11, 12]. Resistance to *Brucella* is not common, but research has pointed out that minimum inhibitory concentration of ceftriaxone and streptomycin (MIC) has been on the rise [7]. Intermediate rifampin susceptibility strains also have become widespread [8]. Kuwait and Mexico have found a good bacteriostatic effect that includes tetracycline, amikacin, gentamicin [11, 12], streptomycin and ciprofloxacin for *Brucella* spp. However, rifampin and trimethoprim-sulfamethoxazole’s (SXT) antibacterial effects have been decreasing. The anti-microbial susceptibility test used in previous studies [15, 17] was the disk diffusion method. But the disk diffusion method is an atypical anti-microbial susceptibility

test, meaning it is nearly impossible to interpret the results. In our interpretation, we have followed the standard that ≤ 16 mm indicates low anti-*Brucella* activity and >16 mm is evidence of good anti-*Brucella* activity.

Contrary to cases of brucellosis previously discovered in Taiwan, our report may be the first to suspect cases of local infection. A review of brucellosis infection cases in Taiwan found that the first cases of infection of *B. abortus* occurred in 1978 when university veterinary students came into contact with infected cattle. Later in 1994, a report from 1980-1981 tracked and collected all contacts with infected cattle or other animals by veterinarians, laboratory workers, and farmers, and analyzed if they had been infected with *B. abortus*. Results showed about a 42.1% sero-positive reaction. But these results were never confirmed as being from outside or local cases [22]. However, in 2011 Taiwan also had four cases confirmed from outside the country [23]. In Taiwan it is still possible to become infected by touching infected animals such as deer. The main clinical signs of human Brucellosis are often nonspecific clinical manifestations. Clinicians in Taiwan may easily overlook the possibility of a Brucellosis infection. From this study, our aim is to increase the awareness of laboratory staff as well as aid physicians in their clinical and diagnostic abilities. In addition, we hope to raise awareness about the process of identifying bacteria in clinical microbiology laboratories.

5. Conclusion

This is the first study to provide both an improved genotype and phenotype analysis of Taiwan *Brucella* infection in clinical works. Through our research, we built a standard method of four steps for detecting the *Brucella* spp. and its antibiotic characteristics. We have worked to improve the standards by which we identify rare bacteria strains, and to make them applicable not only to *Brucella*, but also to other rarely-encountered bacteria. Our standard method begins with detecting the clinical isolate through traditional biochemical methods and automatic identification systems. The second step is the editing sequence for BLAST that allows one to compare 16s *rRNA* sequences with sequences from other species, allowing the gene level to be determined. In the third step, a phylogenetic analysis of multiple genetic loci is able to determine evolutionary relationships between our bacteria strain and those from other locations. Finally, an anti-microbial sensitivity test hones in on the level of antibacterial activity that the bacteria displays. Employing these four steps in concert is extremely effective in identifying rare bacteria. Thus, when attempting to determine the identity of rare bacteria such as *Brucella*, utilizing these four steps from our research will be highly effective and will hopefully ultimately prevent further identification errors and misdiagnoses.

Acknowledgments

The authors appreciate the collaborating work with the staff at the Department of Laboratory Medicine, China Medical University Hospital, Taichung, Taiwan. This work was supported by the grants CMU97-244, CMU98-S-16, CMU99-S-03; DMR-102-081 and DMR-102-078 from China Medical University and China Medical University Hospital, Taichung, Taiwan; and the grant NSC99-2314-B-039-022-MY3 from the National Science Council.

Open Access This article is distributed under terms of the Creative Commons Attribution License which permits any use, distribution, and reproduction in any medium, provided original author(s) and source are credited.

REFERENCES

- [1] Organization WH. 1997. Fact Sheet N173. Geneva: World Health Organization.
- [2] Pappas G, Papadimitriou P, Akritidis N, Christou L, Tsianos EV. The new global map of human brucellosis. *The Lancet infectious diseases* 2006; 6: 91-9.
- [3] Fiori PL, Mastrandrea S, Rappelli P, Cappuccinelli P. *Brucella abortus* infection acquired in microbiology laboratories. *Journal of clinical microbiology* 2000; 38: 2005-6.
- [4] Robichaud S, Libman M, Behr M, Rubin E. Prevention of laboratory-acquired brucellosis. *Clinical infectious diseases: an official publication of the Infectious Diseases Society of America* 2004; 38: e119-22.
- [5] Gilligan PH YM. Basic protocols for level A laboratories for the presumptive identification of *Brucella* species. Washington: American Society for Microbiology. 2002.
- [6] E.J. Young GLM, J.E. Bennett, R. Dolin (Eds.). 2005. *Brucella* species in Principles and practice of infectious diseases (6th ed.), p. 2669-2672. Churchill Livingstone, Philadelphia, PA, USA, 2005.
- [7] Gotuzzo E, Celillo E. *Brucella* in: Gorbach SI, Bartlett JG, Blacklow NR, editors. *Infectious Diseases*. Philadelphia: Harcourt Brace Jovanovich Inc 1992; 1513-8.
- [8] Hall WH (1991): Brucellosis. In: Evans AS & Brachman PS (Eds.). *Bacterial infections in humans*. Plenum, New York. pp. 133-49.
- [9] Elsaghir AAF, James EA. Misidentification of *Brucella melitensis* as *Ochrobactrum anthropi* by API 20NE. *Journal of Medical Microbiology* 2003; 52: 441-2.
- [10] Buzgan T, Karahocagil MK, Irmak H, Baran AI, Karsen H, Evirgen O, *et al.* Clinical manifestations and complications in 1028 cases of brucellosis: a retrospective evaluation and review of the literature. *International journal of infectious diseases: IJID: official publication of the International Society for Infectious Diseases* 2010; 14: e469-78.
- [11] Peiris V, Fraser S, Fairhurst M, Weston D, Kaczmarek E. Laboratory diagnosis of *brucella* infection: some pitfalls. *The Lancet* 1992; 339: 1415-6.
- [12] Batchelor BI, Brindle RJ, Gilks GF, Selkon JB. Biochemical misidentification of *Brucella melitensis* and subsequent laboratory-acquired infections. *The Journal of hospital infection* 1992; 22: 159-62.
- [13] Barham WB, Church P, Brown JE, Paparello S. Misidentification of bruceila species with use of rapid bacterial identification systems. *Clinical Infectious Diseases* 1993; 17: 1068-9.
- [14] Yang J, Ren XQ, Chu MI, Meng DY, Xue WC. Mistaken identity of brucella infection. *Journal of clinical microbiology* 2013; 51: 2011.
- [15] Lu YS LY, Lin DF, Tsai HJ. Case study on human brucellosis of bovine-origin in Taiwan. *Taiwan Prov Res Inst Anim Hlth Exp Rep* 1994; 30: 127-34.
- [16] Chuang YC, Chen SC, Mu JJ, Lin HY, Chang CH, Yang WS, *et al.* Brucellosis, Taiwan, 2011. *Emerg Infect Dis* 2011; 17: 2374-5.

- [17] Huang XT WY, Tung HP, Chen WC, Su CP, Chang SJ, Lai CL. Case report of two imported Brucellosis cases, May 2011. *Taiwan Epidemiology Bulletin*. 2011.
- [18] Smits HL SC. Contributions of biotechnology to the control and prevention of brucellosis in Africa. *Afr J Biotechnol* 2004; 3: 631-6.
- [19] Araj GF. Update on laboratory diagnosis of human brucellosis. *Int J Antimicrob Agents* 2010; 36 Suppl 1: S12-7.
- [20] Brigante G, Luzzaro F, Bettaccini A, Lombardi G, Meacci F, Pini B, *et al*. Use of the phoenix automated system for identification of streptococcus and enterococcus spp. *Journal of clinical microbiology* 2006; 44: 3263-7.
- [21] James G. Universal Bacterial Identification by PCR and DNA Sequencing of 16S rRNA Gene, p. 209-214. *In* Schuller M, Sloots TP, James GS, Halliday CL, Carter IWJ (ed.), *PCR for Clinical Microbiology*. Springer Netherlands. 2010.
- [22] Clarridge JE, 3rd. Impact of 16S *rRNA* gene sequence analysis for identification of bacteria on clinical microbiology and infectious diseases. *Clin Microbiol Rev* 2004; 17: 840-62.
- [23] Janda JM, Abbott SL. 16S *rRNA* gene sequencing for bacterial identification in the diagnostic laboratory: pluses, perils, and pitfalls. *Journal of clinical microbiology* 2007; 45: 2761-4.
- [24] Weisburg WG, Barns SM, Pelletier DA, Lane DJ. 16S ribosomal DNA amplification for phylogenetic study. *Journal of bacteriology* 1991; 173: 697-703.
- [25] Whatmore A, Perrett L, MacMillan A. Characterisation of the genetic diversity of *Brucella* by multilocus sequencing. *BMC Microbiology* 2007; 7: 34. doi: 10.1186/1471-2180-7-34.
- [26] Corbel M. *Brucellosis in humans and animals*. Geneva (Switzerland): World Health Organisation. 2006.
- [27] Gwida M, Al Dahouk S, Melzer F, Rosler U, Neubauer H, Tomaso H. Brucellosis - regionally emerging zoonotic disease? *Croat Med J* 2010; 51: 289-95.
- [28] Vaidya SA, Citron DM, Fine MB, Murakami G, Goldstein EJC. Pelvic Abscess Due to *Ochrobactrum anthropi* in an Immunocompetent Host: Case Report and Review of the Literature. *Journal of clinical microbiology* 2006; 44: 1184-6.
- [29] Velasco J, Romero C, Lopez-Goni I, Leiva J, Diaz R, Moriyon I. Evaluation of the relatedness of *Brucella* spp. and *Ochrobactrum anthropi* and description of *Ochrobactrum intermedium* sp. nov., a new species with a closer relationship to *Brucella* spp. *Int J Syst Bacteriol* 48 Pt 1998; 3: 759-68.
- [30] Wilson GS. The classification of the *Brucella* group: a systematic study. *J Hyg (Lond)* 1933; 33: 516-41.

Original article

P-coumaric acid regulates exon 12 splicing of the *ATP7B* gene by modulating hnRNP A1 protein expressions

Ying-Ju Lin^{a,b,†}, Tsung-Jung Ho^{b,c,d,†}, Ting-Hsu Lin^a, Wei-Yi Hsu^a, Shao-Mei Huang^a, Chiu-Chu Liao^a, Chih-Ho Lai^f, Xiang Liu^f, Hsinyi Tsang^f, Chien-Chen Lai^{g,*}, Fuu-Jen Tsai^{a,b,h,*}

^aGenetic Center, Department of Medical Research, China Medical University Hospital, Taichung 404, Taiwan

^bSchool of Chinese Medicine, China Medical University, Taichung 404, Taiwan

^cDivision of Chinese Medicine, China Medical University Beigang Hospital, Yunlin County 651, Taiwan

^dDivision of Chinese Medicine, Tainan Municipal An-Nan Hospital -China Medical University, Tainan 709, Taiwan

^eDepartment of Microbiology, School of Medicine, China Medical University, Taichung 404, Taiwan

^fNational Institute of Allergy and Infectious Diseases, National Institutes of Health, Bethesda, Maryland 20892, USA

^gInstitute of Molecular Biology, National Chung Hsing University, Taichung 402, Taiwan

^hDepartment of Biotechnology, Asia University, Taichung 413, Taiwan

Received 11th of February 2015 Accepted 20th of March 2015

© Author(s) 2015. This article is published with open access by China Medical University

Keywords:

Wilson's disease;
Schizonepeta;
p-coumaric acid;
hnRNP A1;
Alternative splicing

ABSTRACT

Background: Wilson's disease (WD) is a genetic disorder involving the metabolism of copper. WD patients exhibit a wide range of disease phenotypes, including Kayser-Fleischer rings in the cornea, predominant progressive hepatic disease, neurological diseases, and/or psychiatric illnesses, among others. Patients with exon12 mutations of the *ATP7B* gene have progressive hepatic disease. An *ATP7B* gene that lacks exon12 retains 80% of its copper transport activities, suggesting that alternative splicing of *ATP7B* gene may provide alternative therapeutic ways for patients with inherited sequence variants and mutations of this gene.

Purpose: We aimed to search for possible Chinese herbs and related compounds for modulating *ATP7B* pre-mRNA splicing.

Methods: We used an *ATP7B* exon11-12-13 mini-gene vector as a model and screened 18 Chinese herbal extracts and four compounds from *Schizonepeta* to determine their effects on *ATP7B* pre-mRNA splicing *in vitro*.

Results: We found that *Schizonepeta* demonstrated the greatest potential for alternative splicing activity. Specifically, we found that *p-coumaric acid* from this herb enhanced *ATP7B* exon12 exclusion through the down-regulation of heterogeneous ribonucleoprotein (hnRNP) A1 protein expressions.

Conclusion: These results suggest that there are herbs or herb-related compounds that could modify the alternative splicing of the *ATP7B* gene *via* a mechanism that regulates pre-mRNA splicing.

1. Introduction

Wilson's disease (WD; MIM number: 277900) is a genetic disorder involving the metabolism of copper [1, 2]. The incidence of the disease is approximately 1 in 30,000 worldwide. It is characterized by copper accumulations, particularly in the liver, kidney, brain, and cornea, resulting from the impairment of the incorporation of copper into ceruloplasmin, with the subsequent excretion of copper through the bile. Patients with WD exhibit a wide range of disease phenotypes, including Kayser-Fleischer rings in the cornea, predominant progressive hepatic disease, neurological diseases, and/or psychiatric illnesses, among others [3]. In addition,

these phenotypes can present as early as 3 years of age up to as late as the seventh decade of a person's life. The clinical treatment for WD is copper-chelating agents for the removal of excess copper [4, 5].

The gene responsible for WD is the *ATPase Cu⁺⁺ transporting beta polypeptide* (*ATP7B*, MIM number: 606882). *ATP7B* encodes a copper transporting P-type ATPase, a protein of approximately 160 kDa that contains eight membrane-spanning domains, an ATPase consensus sequence, a hinge domain, a phosphorylation domain, and six copper-binding domains [6]. Over 300 sequence variants and mutations have been identified and collected in the WD Mutation Database to date [1]. We previously

* Corresponding author. Department of Medical Research, China Medical University Hospital, No. 2, Yuh-Der Road, Taichung 404, Taiwan.

† Ying-Ju Lin and Tsung-Jung Ho contributed equally to this work.

E-mail address: d0704@mail.cmuh.org.tw (F.-J. Tsai); lailai@dragon.nchu.edu.tw (C.-C. Lai).

observed that predominant mutation hotspots are located in exons 8 and 12 in Taiwanese WD patients [7]. Mutations (Arg919Gly, Thr935Met, Gly943Asp, and 2810delT) in the Transmembrane 6 region (exon12) accounted for 9.62% of all mutations observed in Taiwanese WD patients. These patients with exon12 mutations have progressive hepatic disease [3]. Functional characterization of *ATP7B* showed that variants lacking exon12 retained 80% of their copper transport activities [7], suggesting that the alternative splicing of *ATP7B* gene may provide alternative therapeutic ways for patients with inherited sequence variants and mutations of this gene.

Alternative splicing of mRNA precursors requires specific sequences and splicing factors. Exons frequently contain positive elements known as exonic splicing enhancers (ESEs), which are most often recognized by the serine/arginine-rich family of splicing factors (SR proteins) [8]. Furthermore, exons may also contain splicing silencer elements (ESSs), which are recognized by heterogeneous ribonucleoproteins (hnRNPs) [9]. The presence of ESEs and/or ESSs along with splicing factors regulates alternative splicing. One example of a disease model for alternative splicing that is modulated by SR and hnRNP proteins is spinal muscular atrophy (SMA) disease [10, 11]. This screening model, which prevents exon7 exclusion in the *SMN2* gene, has been widely used, and several pharmacological compounds have been investigated for their splicing correction abilities in order to maintain the full length of SMN2 proteins for therapeutic strategies of SMA disease [12-14].

In the present study, we screened 18 Chinese herbal extracts and four compounds from *Schizonepeta* to determine their effects on *ATP7B* pre-mRNA splicing *in vitro*. We used an *ATP7B* exon11-12-13 mini-gene vector as a model to search for the Chinese herb candidates that modulated alternative *ATP7B* pre-mRNA splicing. This model was based on an *ATP7B* exon11-12-13 mini-gene and its alternative splicing products [7]. The mini-gene contains three exons and two introns and produces two major alternatively spliced isoforms when expressed in cells. The inclusion form (+ex12) of exon12 produces *ATP7B* mRNA for activating copper-transporting P-type adenosine triphosphatase (ATPase) activities. The exclusion form (-ex12) lacks exon12 of the mini-gene and results in reduced copper transporting ATPase activity, but retains 80% of its biological activities [7]. Exon12 exclusion represents an interesting target due to the mutation hotspots in these regions in Taiwanese WD patients [7, 15]. These patients with exon12 mutations have progressive hepatic disease [3]. In addition, an alternative splice variant of *ATP7B* lacking exon12 was observed in one patient who had a homozygous 2810delT mutation (located in exon12), and showed very mild clinical symptoms [7]. Therefore, it would be useful to identify possible candidate herbs or herb-related compounds that could modify alternative splicing patterns of the *ATP7B* gene. This strategy would be of benefit for alternative splicing therapy for the hundreds of different mutations associated with WD.

2. Materials and methods

2.1. Plasmids

The *ATP7B* exon11-12-13 mini-gene plasmid has been described previously [7] (Fig. 1A). Briefly, the *ATP7B* (from exon11 to exon13, total 4.5 kb) mini-gene construct was polymerase chain reaction (PCR)-amplified from control genomic DNA by using

the forward primer (5' - GTGAGATGGCTTGTTCATGT-3) and the reverse primer (5' - AACCCAGTGCAGGGCTCACAC-3). The PCR-amplified fragment was cloned into a pcDNATM 3.1 (Invitrogen) vector, and this fragment was verified by DNA sequencing.

2.2. Mammalian cell transfection

CHO-K1 cells were grown in a 6-well plate, and 2.5 µg of the *ATP7B* exon11-12-13 mini-gene plasmid was transiently transfected using Lipofectamine 2000 (Invitrogen). The transfected cells were harvested using trypsin 24 h after transfection, and RNAs were isolated using the RNeasy Mini Kit (QIAGEN).

2.3. cDNA synthesis and PCR

Total RNAs from the transfected cells were used for reverse-transcription (RT)-PCR using M-MLV reverse transcriptase (Invitrogen), according to manufacturer guidelines. One µL of cDNA was amplified using the forward primer in exon11 (5' - GAGAAGCCATGCCAGTCACTA-3) and the reverse primer in exon13 (5' - CTTGTGCGCCATCTCCAGG -3). Band intensities were quantified using ImageJ software.

2.4. Preparation of herbal extracts

Crude extract powders from 18 herbs (Fig. 1) used in traditional Chinese medical practices were obtained from Timing Pharmaceutical, a good manufacturing process (GMP)-certified traditional Chinese medicine manufacturer based in Taiwan. Briefly, each fine herb powder was prepared by milling dry herbal plants with a mechanical grinder and filtering it through a 20-mesh metal sieve, followed by mixing 1.0 g of the powder with 40 mL of distilled water. After boiling for 40 min, the mixture was filtered through a 100-mesh metal sieve. The filtrate (crude water extract) was sterilized using a 0.44 µm syringe filter.

2.5. Chemicals

Apigenin, luteolin, caffeic acid, and p-coumaric acid were purchased from Sigma Chemical (St. Louis, MO, USA) (Fig. 2). The chemical structures of these compounds are shown in Fig. 2A.

2.6. High-performance liquid chromatography with tandem mass spectrometry (HPLC/MS/MS) analyses

HPLC was used to determine the relative abundances of apigenin, luteolin, caffeic acid, and p-coumaric acid in *Schizonepeta* extract. Chromatography was performed using a Finnigan SurveyorTM HPLC system. HPLC analysis was performed on a 3 µm C18 column (Waters, Atlantis 2.1 mm i.d. × 100 mm). A guard column (Waters, Atlantis, 2.1 mm i.d. × 10 mm) was used to prolong the HPLC column life. The two mobile phases were buffer A, H₂O (0.1% FA) and buffer B, ACN (0.1% FA). The flow rate was 0.20 mL/min. The gradient conditions were as follows: isocratic elution (75% A) for 5 min, followed by an 8 min gradient to 70% B and then a 12 min gradient to 95% B. Analyses generally lasted for 25 min; an additional 10 min were required for column re-equilibration. We used a Finnigan SurveyorTM autosampler fitted with a 2 µL sample loop. HPLC and autosampler systems were synchronized using Xcalibur software.

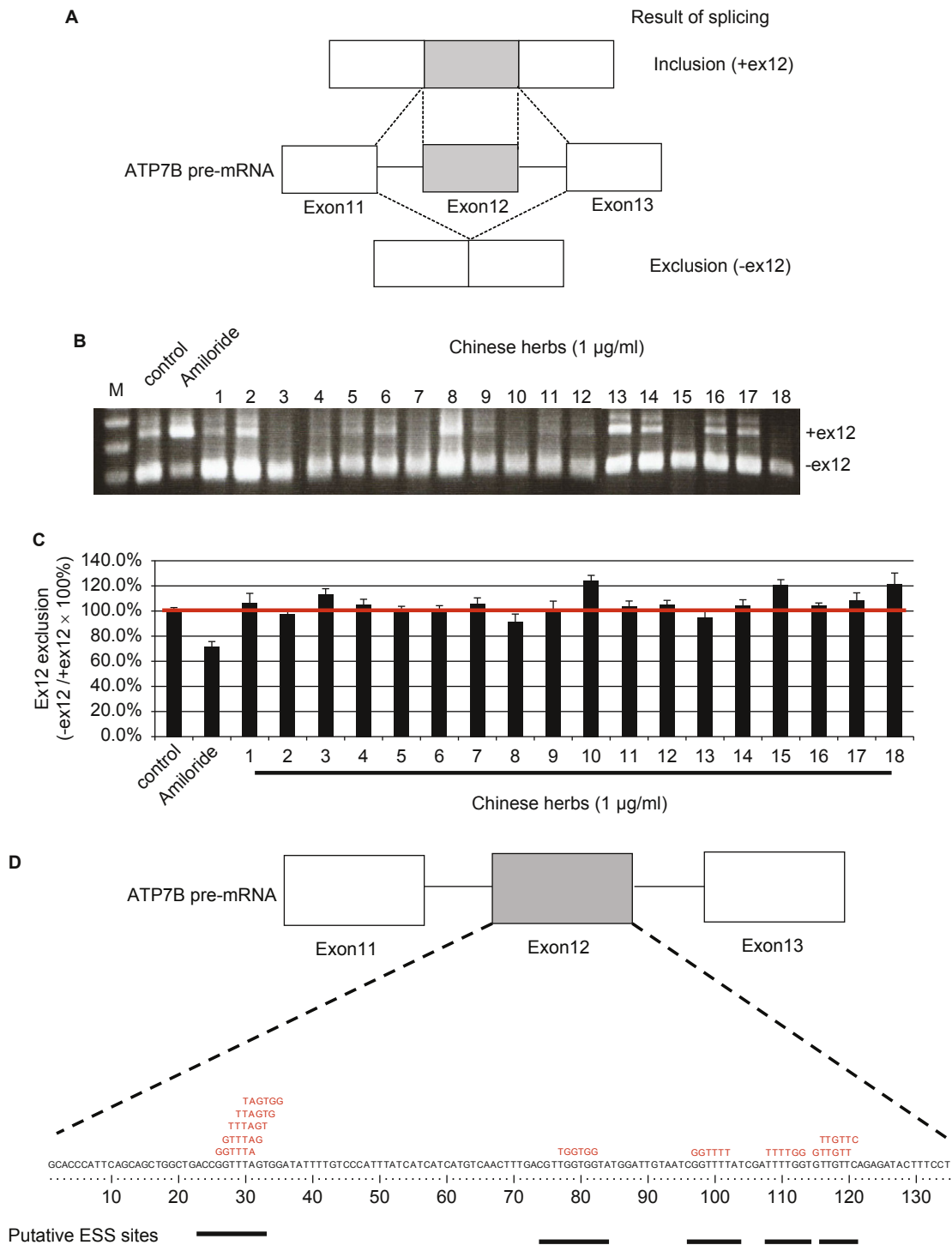


Fig. 1 - *ATP7B* exon12 exclusion pattern of Chinese herbal extracts: *ATP7B* exon11-12-13 mini-gene vector. (A) Schematic representations of *ATP7B* exon11-12-13 mini-gene vector and its two alternative splicing products. The *ATP7B* mini-gene vector has three exons and two introns and produces two major alternatively spliced isoforms when expressed in cells. (B) RT-PCR analysis of various types of Chinese herbal extracts or Amiloride on *ATP7B* exon11-12-13 mini-gene splicing. CHO-K1 cells were transfected with the *ATP7B* exon11-12-13 mini-gene, held for 24 h, and then treated with various kinds of herbal extracts (1 µg/mL) for another 24 h. Cells were harvested, total RNAs were extracted, and *ATP7B* splicing products were analyzed by RT-PCR. Controls are cells transfected with the *ATP7B* exon 11-12-13 mini-gene vector without any herbs or drugs treatments. Amiloride-treated cells were used for the inhibition of ex12 exclusion controls. (C) Ex12 exclusion ratio analysis of various kinds of Chinese herbal extracts or Amiloride on *ATP7B* exon11-12-13 mini-gene splicing. Quantification was carried out using SynGene Gene Tools. The ex12 exclusion ratio was expressed as: (PCR product (-ex12))/(PCR product (-ex12) + PCR product (+ex12)). Data are expressed as ex12 exclusion ratios (Cell with medium only = 100%) from three independent experiments, each performed in triplicate. (D) Putative ESS sites for hnRNP A1 protein binding.

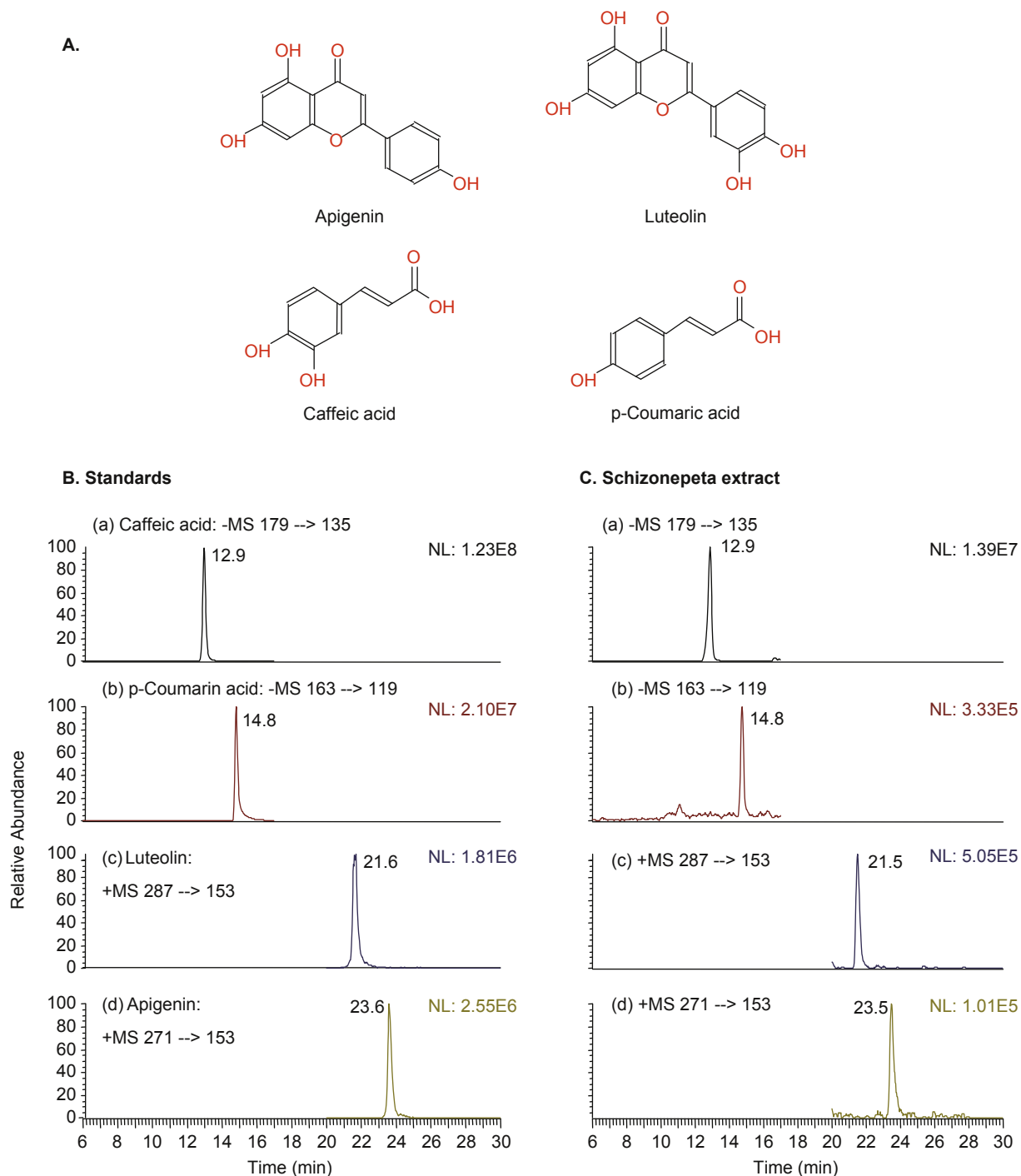


Fig. 2 - A. Chemical structures of four *Schizonepeta* constituents. Typical multiple reaction monitoring (SRM) chromatograms of of B. Standards: (a) Caffeic acid; (b) p-Coumaric acid; (c) Luteolin; (d) Apigenin; and C. *Schizonepeta* extract.

2.7. Antibodies and reagents

Anti-SRp20 (Abcam ab125124), anti-SRSF1 (Abcam ab38017, Taipei, Taiwan), and anti-hnRNP A1 (Abcam ab137780, Taipei, Taiwan) antibodies were purchased from Abcam Taipei, Taiwan. The anti-beta tubulin antibody was obtained from GeneTex (GeneTex GTX101279, Taipei, Taiwan).

2.8. Western blot analysis

CHO-K1 cells were added to media containing various chemicals (50 μM) and incubated for 24 h at 37°C. Cells were harvested, washed, and lysed in a lysis buffer (50 mM Tris-HCl [pH 7.5], 150 mM NaCl, 5 mM EDTA, 1% Triton X-100, 0.1% sodium dodecyl sulfate (SDS)) that was supplemented with a protease inhibitor cocktail (Roche). The lysates were resolved by 12% SDS-polyacrylamide gel electrophoresis (PAGE) and transferred to polyvinylidene fluoride membranes (Millipore). The membrane was incubated with primary antibodies overnight at 4°C, and then

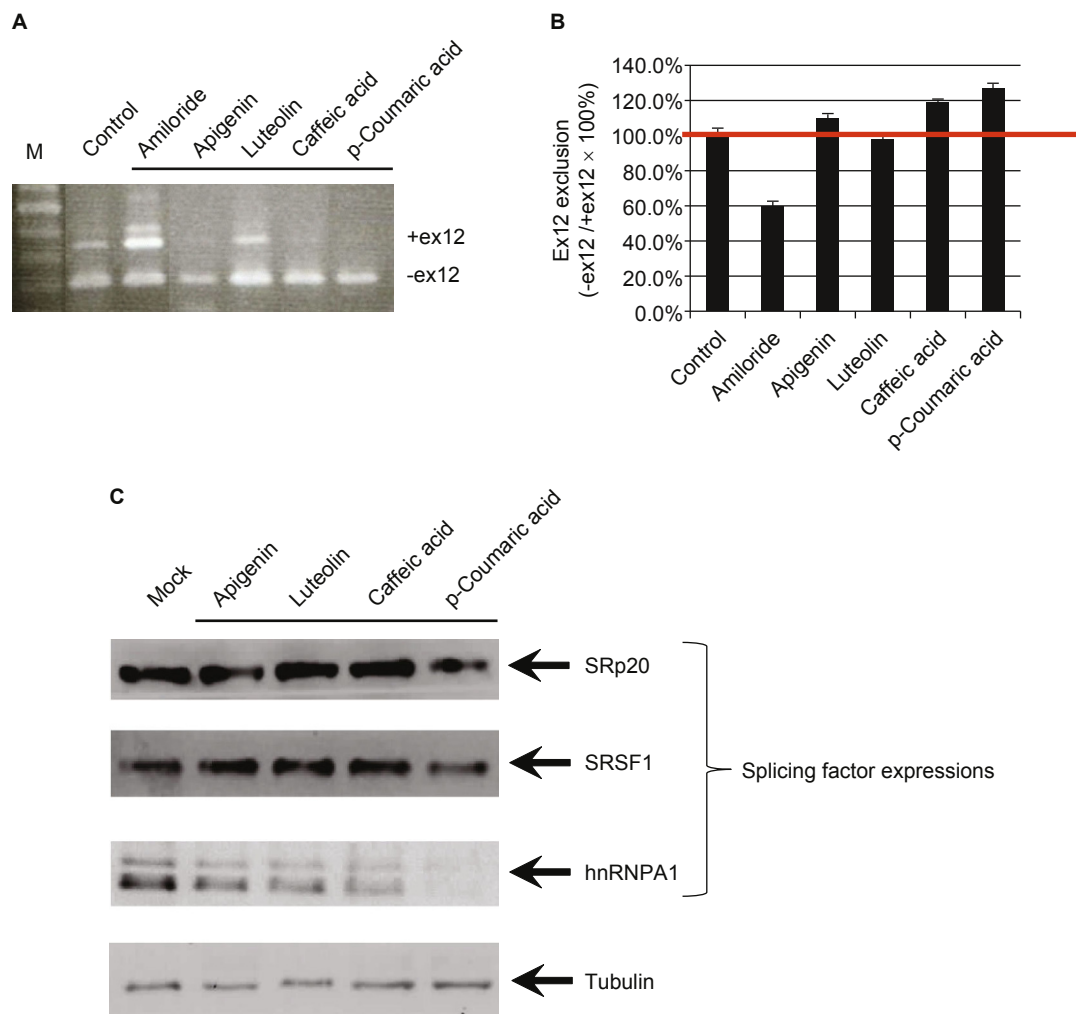


Fig. 3 - *ATP7B* exon12 exclusion pattern of compounds from *Schizonepeta*: *ATP7B* exon11-12-13 mini-gene vector. (A) RT-PCR analysis of various kinds of compounds on *ATP7B* exon11-12-13 mini-gene splicing. CHO-K1 cells were transfected with the *ATP7B* exon11-12-13 mini-gene vector, held for 24 h, and then treated with various kinds of compounds for another 24 h. Cells were harvested, total RNAs were extracted, and *ATP7B* splicing products were analyzed by RT-PCR. Controls are cells transfected with the *ATP7B* exon11-12-13 mini-gene vector without any compound treatment. Amiloride-treated cells were used for the inhibition of ex12 exclusion controls. (B) Ex12 exclusion ratio analysis of various kinds of compounds or Amiloride on *ATP7B* exon11-12-13 mini-gene splicing. Quantification was carried out using SynGene Gene Tools. The ex12 exclusion ratio was expressed as: (PCR product (-ex12))/(PCR product (-ex12) + PCR product (+ex12)). Data are expressed as previously described. (C) Western blot analysis of SRp20, SRSF1, and hnRNP A1 protein expression levels modulated by compounds derived from *Schizonepeta*. CHO-K1 cells were respectively treated with apigenin, luteolin, caffeic acid, and p-coumaric acid for 24 h at 37°C. Cells were harvested, washed, and lysed. The lysates were resolved by 12% SDS-PAGE and western blotting. Briefly, the membrane was incubated with primary antibodies, and then incubated with alkaline phosphatase-conjugated secondary antibodies (Sigma-Aldrich). Signals were visualized using chemiluminescence following the manufacturer's protocol (Chemicon).

incubated with alkaline phosphatase-conjugated secondary antibodies (Sigma-Aldrich). Signals were visualized using chemiluminescence following the manufacturer's protocol (Chemicon).

2.9. Short interfering RNAs (siRNAs)

siRNAs targeting transcripts for *SRp20* (siSRp20: CCGAAGUGUGUGGUUGCUAGAAAC; GUUUCUAGCAACCCACACACUUCGG), *SRSF1* (siSRSF1: UGGUGUCGUGGAGUUU-GUACGGAAA; UUUCGUACAAACUCCACGACACCA),

and *HNRNP A1* (sihnRNP A1: GGTAGGCTGGCAGATACGT-TCGCA; TGACGAACGTATCTGCCAGCCTACC) were purchased from Invitrogen, Taipei, Taiwan, as was the non-targeting siRNA control (siNC).

2.10. siRNA transfection

CHO-K1 cells (2×10^5) were seeded in 24-well plates and cultured for 24 h. siRNAs targeting *SRp20* (NM_003017), *SRSF1* (NM_006924.4), and *hnRNP A1* (NM_031157.2) (Fig. 6A, B, and

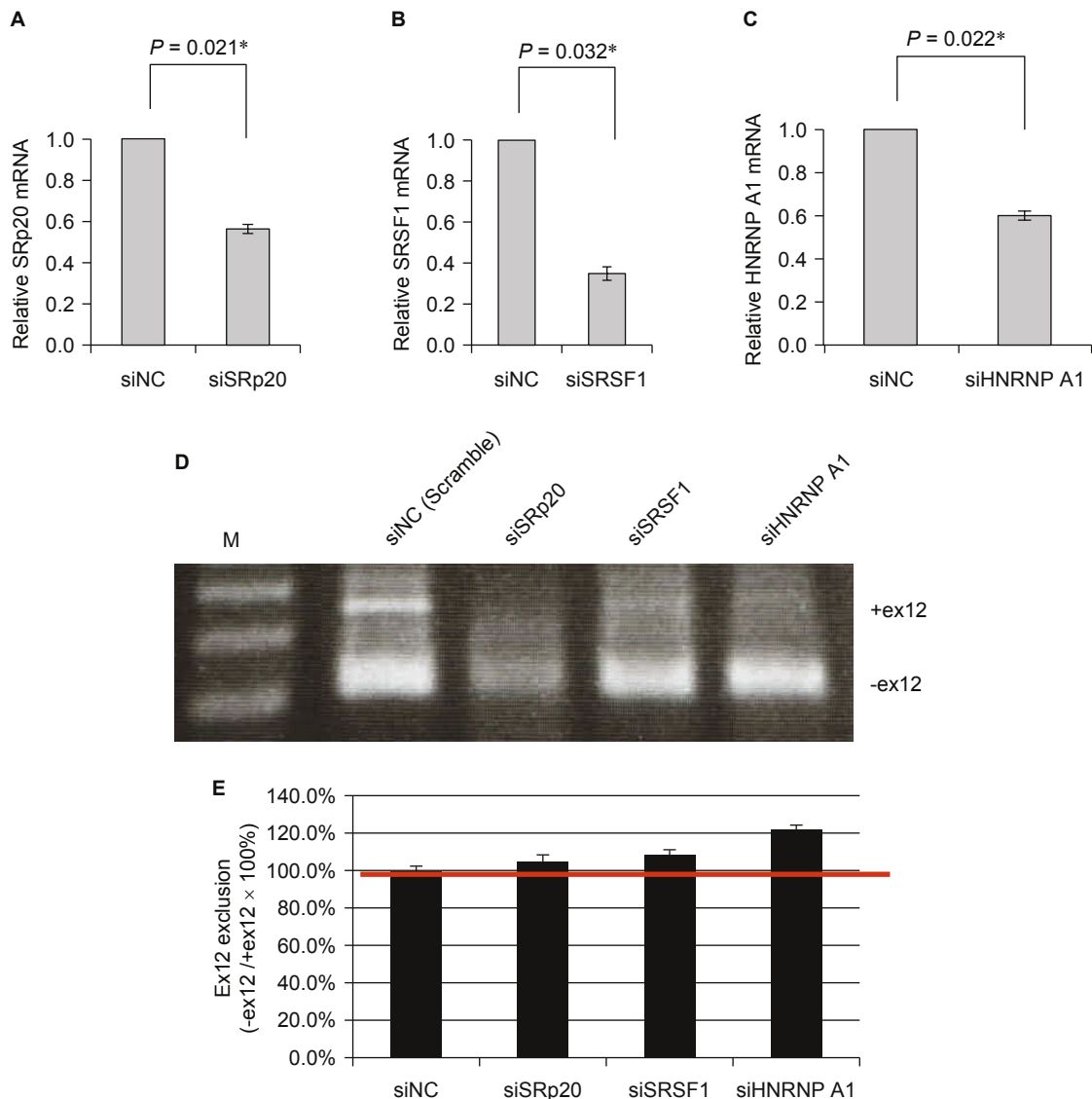


Fig. 4 - RT-PCR analysis of *ATP7B* exon12 exclusion by siRNAs targeting *SRp20* (siSRp20), *SRSF1* (siSRSF1), and *hnRNP A1* in CHO-K1 cells. (A) RT-qPCR analysis of relative *SRp20* mRNA expression levels. (B) RT-qPCR analysis of relative *SRSF1* mRNA expression levels. (C) RT-qPCR analysis of relative *hnRNP A1* mRNA expression levels. (D) RT-PCR analysis of various kinds of splicing factors on *ATP7B* exon11-12-13 mini-gene splicing using RNA interference. Controls are cells co-transfected with siNC and the *ATP7B* exon11-12-13 mini-gene. (E) Ex12 exclusion ratio analysis of various kinds of splicing factors on *ATP7B* exon11-12-13 mini-gene splicing. Quantification was carried out using SynGene Gene Tools. The ex12 exclusion ratio was expressed as previously described.

C) were transfected into CHO-K1 cells using Amaxa Nucleofection technology (Lonza) following the manufacturer's recommendations. Cells were then recovered and seeded in pre-warmed 24-well plates. After 24 h incubation, cells were used for *ATP7B* exon12 exclusion analysis (Fig. 4).

2.11. cDNA plasmid transfection

For cDNA plasmid transfection assays, CHO-K1 cells (2×10^5) were seeded in 24-well plates and cultured for 24 h. Cells were transiently transfected with the wild-type expression plasmids, pSRp20, pSRSF1, and phnRNP A1, or with the pcDNA3.0 expression plasmid as a mock control using Amaxa Nucleofection technology (Lonza) following the manufacturer's recommenda-

tions. Cells were then recovered and seeded in pre-warmed 24-well plates. After 24 h incubation, cells were used for *ATP7B* exon12 exclusion analysis (Fig. 5).

3. Results and discussion

CHO-K1 cells were transfected with the *ATP7B* exon11-12-13 mini-gene. Twenty-four hours later, various kinds of herbal extracts (1 $\mu\text{g/mL}$) were added to the cells (Fig. 1). Cells were harvested, total RNAs were extracted, and *ATP7B* splicing products were analyzed by RT-PCR. The molar ratio of each isoform was analyzed using SynGene Gene Tools. Three of the Chinese herbs evaluated exhibited the most significant splicing efficiency: over

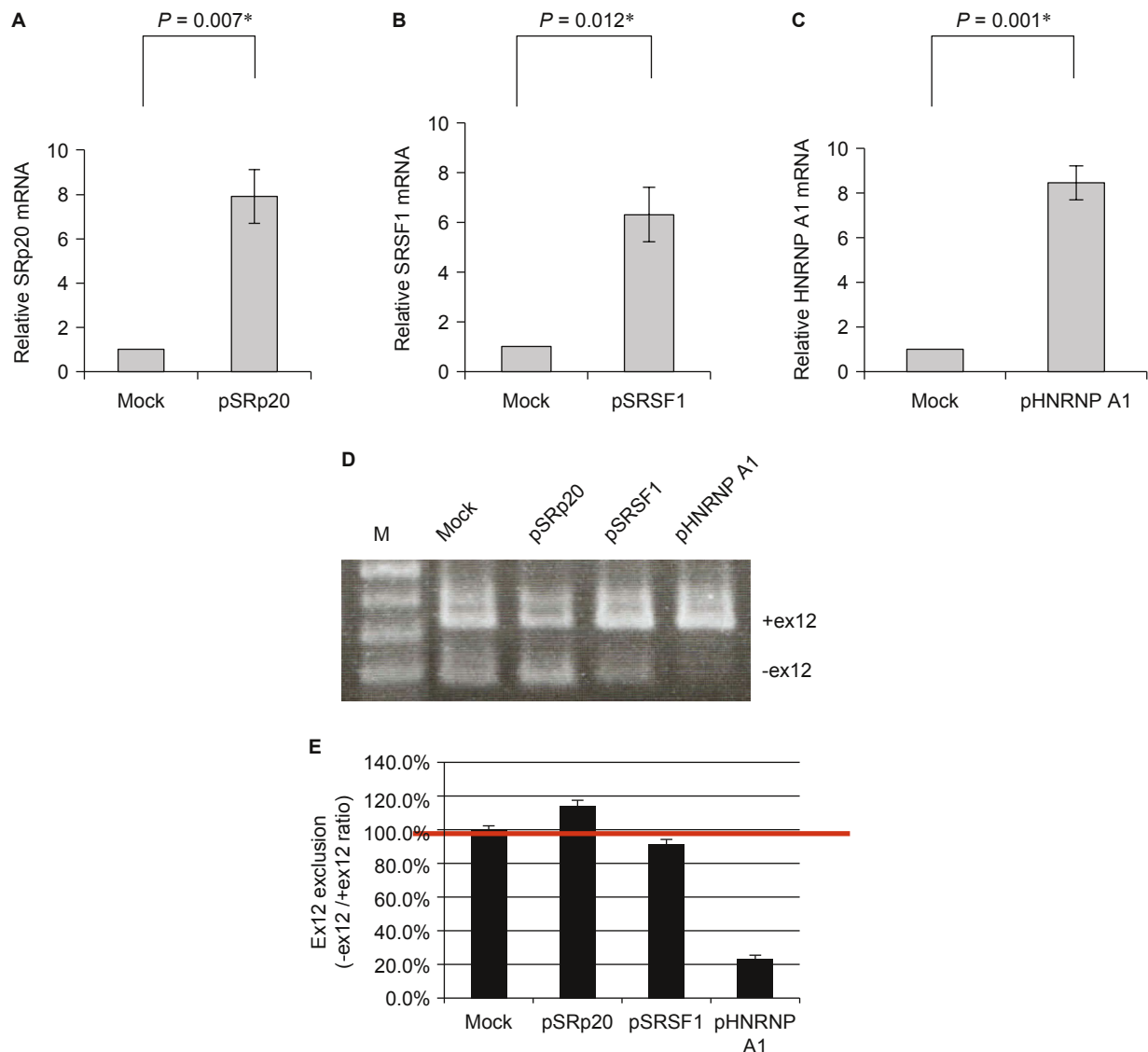


Fig. 5 - RT-PCR analysis of *ATP7B* exon12 exclusion by over-expression of mammalian expression constructs encoding SRp20, SRSF1, and hnRNP A1 in CHO-K1 cells. (A) RT-qPCR analysis of relative *SRp20* mRNA expression levels. (B) RT-qPCR analysis of relative *SRSF1* mRNA expression levels. (C) RT-qPCR analysis of relative *HNRNP A1* mRNA expression levels. (D) RT-PCR analysis of various kinds of splicing factors on *ATP7B* exon11-12-13 mini-gene splicing by using over-expression of mammalian expression constructs encoding SRp20, SRSF1, and hnRNP A1. Controls are cells co-transfected with pcDNA3.1 vector only and the *ATP7B* exon11-12-13 mini-gene. (E) Ex12 exclusion ratio analysis of various kinds of splicing factors on *ATP7B* exon11-12-13 mini-gene splicing. Quantification was carried out using SynGene Gene Tools. The ex12 exclusion ratio was expressed as previously described.

120% compared to untreated cells. Among these three herbs, cells treated with *Schizonepeta tenuifolia* Briq. exhibited the most efficient exon12 exclusion activity at 124.1%. This result suggests that the Chinese herbs *Schizonepeta tenuifolia* Briq., JYH GAN TASSO TANG, and CHI BAO MEEI RAN DAN have the ability to modulate alternative splicing through the enhancement of exon12 exclusion of the *ATP7B* gene (Fig. 1).

Among these three herbs, *Schizonepeta tenuifolia* Briq. is the only herbal extract that originates from only one type of plant resource. Derived from the dried aerial parts of *Schizonepeta tenuifolia* Briq. (a member of the Labiatae family of plants), this extract is widely used in Asian countries as an herbal constituent included in treatments for the common cold with fever, otitis

media, skin inflammations, as well as anti-pruritic, anti-microbial, and hemostatic activities [16, 17]. It is categorized as a surface-relieving agent in modern Chinese Materia Medica guides. Several studies have suggested that *Schizonepeta tenuifolia* Briq. displays immunomodulatory, anti-inflammatory, and anti-oxidant effects. This study is the first to show that the water extract of *Schizonepeta tenuifolia* Briq. also exhibits the ability to modulate alternative splicing via the enhancement of exon12 exclusion of the *ATP7B* gene.

Similar strategies have been widely used in treatments for spinal muscular atrophy (SMA) disease. SMA is caused by the deletion of or mutations in the *SMN1* gene but with the retention of the *SMN2* gene [18]. However, the *SMN2* gene is unable to

produce sufficient amounts of SMN proteins for the survival of motor neurons. This is due to the fact that the *SMN2* mRNA transcripts lack exon7, which results in a defective SMN protein [19]. SMA treatment strategies targeting *SMN2* have been proposed [12]; however, unlike the WD strategy, the SMA strategy is aimed at identifying compounds that can enhance the inclusion of exon7 in *SMN2* [12].

Results from HPLC analyses indicated the presence of apigenin, luteolin, caffeic acid, and p-coumaric acid in our *Schizonepeta* water extract (Fig. 2). The HPLC-MS/MS analysis results for four *Schizonepeta*-associated compounds are shown in Fig. 2. HPLC-MS/MS for apigenin (23.6 min retention time), luteolin (21.6 min retention time), cinnamic acid (18.7 min retention time), and p-coumaric acid (14.8 min retention time) from *Schizonepeta* water extract are shown in Fig. 2C. Combined, these results indicated the presence of apigenin, luteolin, caffeic acid and p-coumaric acid in our *Schizonepeta* water extract.

In order to search for chemical compounds from *Schizonepeta* that could modulate alternative *ATP7B* pre-mRNA splicing, CHO-K1 cells transfected with the *ATP7B* exon11-12-13 mini-gene were treated with apigenin, luteolin, caffeic acid, and p-coumaric acid, respectively (Fig. 3A and B). Cells were harvested, total RNAs were extracted, and *ATP7B* splicing products were analyzed by RT-PCR. As shown, two compounds, caffeic acid and p-coumaric acid, exhibited the most significant splicing efficiency. Several pharmacological compounds have been investigated and found to modulate the inclusion of exon7 in *SMN2* mRNA. These compounds include aclarubicin (anthracycline antibiotics) [13], benzamide M344 (a histone deacetylase (HDAC) inhibitor) [20], indoprofen (a nonsteroidal anti-inflammatory drug and cyclooxygenase inhibitor) [21], sodium vanadate (a phosphatase inhibitor) [12], 5-(N-ethyl-N-isopropyl)-amiloride (an Na^+/H^+ exchanger inhibitor) [14], sodium butyrate (an HDAC inhibitor) [22], and valproic acid (an HDAC inhibitor) [23]. We found that caffeic acid and p-coumaric acid could both enhance exon12 exclusion from the *ATP7B* gene. Caffeic acid and p-coumaric acid are HDAC inhibitors [24]. The HDAC inhibitors, such as benzamide M344, and VPA, also present the ability to correct the splicing abnormality in SMA via regulating splicing factor expression patterns [20, 23]. The present study is the first to demonstrate that caffeic acid and p-coumaric acid can enhance exon12 exclusion from the *ATP7B* gene.

Several studies have suggested that the alternative splicing is modulated by SR and hnRNP proteins in some disease models, including SMA [10, 11]. Furthermore, some HDAC inhibitors, including benzamide M344, and VPA, could also correct the splicing abnormality in SMA, mainly through the regulation of splicing factors [20, 23]. An alternative splicing pattern related to RNA processing machinery was also observed in a mouse model of WD, suggesting that copper elevation selectively alters the protein machinery involved in RNA biogenesis, which is associated with a distinct modification of the splicing pattern [25]. To further explore the mechanism underlying the effect of compounds derived from *Schizonepeta* on *ATP7B* pre-mRNA splicing, CHO-K1 cells were respectively treated with apigenin, luteolin, caffeic acid, and p-coumaric acid (Fig. 3). The change in the levels of several SR and hnRNP proteins was examined by western blotting. The results showed that p-coumaric acid markedly decreased the levels of hnRNP A1. These results suggest that p-coumaric acid may modulate *ATP7B* exon12 exclusion through down-regulation of hnRNP A1 protein expressions.

The hnRNP A1 protein belongs to the A/B subfamily of ubiquitously expressed hnRNPs [26]. These proteins are RNA-binding proteins; they form a complex with heterogeneous nuclear RNA (hnRNA); and they modulate pre-mRNA splicing. ESSs are cis-regulatory elements that inhibit the use of adjacent splice sites and prevent exon exclusions [27]. hnRNPs typically function at ESSs and regulate the alternative splicing process. Interestingly, the progression of several diseases is also affected by hnRNP A1-dependent ESS interactions, including Alzheimer's disease, breast cancer, and SMA [28-30]. Using the ESS prediction website (<http://genes.mit.edu/fas-ess/>), we observed several putative ESS sites in exon12 of *ATP7B* (Fig. 1D) [27]. These putative ESSs are potential targets for hnRNP A1 protein binding to prevent *ATP7B* exon12 exclusion.

To address whether or not *ATP7B* exon12 exclusion can be modulated by these splicing factors, *in vivo* splicing assays were performed in CHO-K1 cells using RNA interference experiments (Fig. 4). CHO-K1 cells were transiently co-transfected with siRNAs targeting SRp20 (siSRp20), SRSF1 (siSRSF1), and hnRNP A1 (sihnRNP A1), respectively, along with the *ATP7B* exon11-12-13 mini-gene, and the effect was assessed by real-time quantitative PCR (qPCR) (Fig. 4 A, B, and C). Cells were harvested, total RNAs were extracted, and *ATP7B* splicing products were analyzed by RT-PCR. As shown in Fig. 4D, compared to the negative control siRNA (siNC), transfection with sihnRNP A1 exhibited the most significant splicing efficiency. This result suggests that down-regulation of the hnRNP A1 protein is able to modulate alternative splicing by the enhancement of exon12 exclusion of the *ATP7B* gene (Fig. 4 D and E).

To further address whether or not *ATP7B* exon12 exclusion can be modulated by these splicing factors, *in vivo* splicing assays were also performed in CHO-K1 cells by overexpression experiments using mammalian expression constructs encoding SRp20, SRSF1, and hnRNP A1 (Fig. 5). The effect was assessed by real-time qPCR (Fig. 5 A, B and C). The CHO-K1 cells were co-transfected with these expression constructs and the *ATP7B* exon11-12-13 mini-gene. Cells were harvested, total RNAs were extracted, and *ATP7B* splicing products were analyzed by RT-PCR. As shown in Fig. 5D, compared to the control pcDNA3.1 vector only, transfection with phnRNP A1 exhibited the most significant splicing efficiency. This result suggests that overexpression of the hnRNP A1 protein can modulate alternative splicing by the inhibition of exon12 exclusion of the *ATP7B* gene (Fig. 5 D and E).

In this study, we first found that the HDAC inhibitor, p-coumaric acid, from *Schizonepeta* water extract could inhibit the expression of the splicing factor, hnRNP A1. There are several putative ESS sites found in exon12 for hnRNP A1 protein binding. RNA interference of hnRNP A1 promoted *ATP7B* exon12 exclusion. In addition, over-expression of the hnRNP A1 protein promoted *ATP7B* exon12 inclusion. The protein patterns of host splicing proteins may be altered when cells are treated with p-coumaric acid, and induced or inhibited cellular proteins associated with ESS may influence pre-mRNA splicing. Additional studies are required to determine whether these HDAC inhibitors and induced or inhibited ESS binding proteins are essential for alternative splicing or not, and to identify new targets for agent development.

The authors declare that they have no competing interests.

Competing interests

The authors declare that they have no competing interests.

Acknowledgments

This research was supported by grants from the China Medical University (CMU102-PH-01), the China Medical University Hospital (DMR-104-029), and the Republic of China National Science Council (NSC101-2314-B-039-008-MY3). We thank Dr. Willy W. L. Hong for technical help and suggestions. We also thank the supports from the China Medical University under the Aim for Top University Plan of the Ministry of Education, Taiwan.

Open Access This article is distributed under terms of the Creative Commons Attribution License which permits any use, distribution, and reproduction in any medium, provided original author(s) and source are credited.

REFERENCES

- [1] Kenney SM, Cox DW. Sequence variation database for the Wilson disease copper transporter, ATP7B. *Hum Mutat* 2007; 28: 1171-7.
- [2] Rosencrantz RA, Schilsky ML. Mining for a diagnosis of Wilson's disease in children: genetics, score, and ore. *Hepatology* 2010; 52: 1872-4.
- [3] Ferenci P. Phenotype-genotype correlations in patients with Wilson's disease. *Ann N Y Acad Sci* 2014.
- [4] Taylor RM, Chen Y, Dhawan A. Triethylene tetramine dihydrochloride (trientine) in children with Wilson disease: experience at King's College Hospital and review of the literature. *Eur J Pediatr* 2009; 168: 1061-8.
- [5] Evans J, Zerpa H, Nuttall L, Boss M, Sherlock S. Copper chelation therapy in intrahepatic cholestasis of childhood. *Gut* 1983; 24: 42-8.
- [6] Bull PC, Thomas GR, Rommens JM, Forbes JR, Cox DW. The Wilson disease gene is a putative copper transporting P-type ATPase similar to the Menkes gene. *Nat Genet* 1993; 5: 327-37.
- [7] Wan L, Tsai CH, Hsu CM, Huang CC, Yang CC, Liao CC, *et al.* Mutation analysis and characterization of alternative splice variants of the Wilson disease gene ATP7B. *Hepatology* 2010; 52: 1662-70.
- [8] Graveley BR. Sorting out the complexity of SR protein functions. *RNA* 2000; 6: 1197-211.
- [9] Black DL. Mechanisms of alternative pre-messenger RNA splicing. *Annu Rev Biochem* 2003; 72: 291-336.
- [10] Hofmann Y, Wirth B. hnRNP-G promotes exon 7 inclusion of survival motor neuron (SMN) via direct interaction with Htra2-beta1. *Hum Mol Genet* 2002; 11: 2037-49.
- [11] Young PJ, DiDonato CJ, Hu D, Kothary R, Androphy EJ, Lorson CL. SRp30c-dependent stimulation of survival motor neuron (SMN) exon 7 inclusion is facilitated by a direct interaction with hTra2 beta 1. *Hum Mol Genet* 2002; 11: 577-87.
- [12] Zhang ML, Lorson CL, Androphy EJ, Zhou J. An *in vivo* reporter system for measuring increased inclusion of exon 7 in SMN2 mRNA: potential therapy of SMA. *Gene Ther* 2001; 8: 1532-8.
- [13] Andreassi C, Jarecki J, Zhou J, Coovert DD, Monani UR, Chen X, *et al.* Aclarubicin treatment restores SMN levels to cells derived from type I spinal muscular atrophy patients. *Hum Mol Genet* 2001; 10: 2841-9.
- [14] Yuo CY, Lin HH, Chang YS, Yang WK, Chang JG. 5-(N-ethyl-N-isopropyl)-amiloride enhances SMN2 exon 7 inclusion and protein expression in spinal muscular atrophy cells. *Ann Neurol* 2008; 63: 26-34.
- [15] Wan L, Tsai CH, Tsai Y, Hsu CM, Lee CC, Tsai FJ. Mutation analysis of Taiwanese Wilson disease patients. *Biochem Biophys Res Commun* 2006; 345: 734-8.
- [16] Tohda C, Kakihara Y, Komatsu K, Kuraishi Y. Inhibitory effects of methanol extracts of herbal medicines on substance P-induced itch-scratch response. *Biol Pharm Bull* 2000; 23: 599-601.
- [17] Fung D, Lau CB. Schizonepeta tenuifolia: chemistry, pharmacology, and clinical applications. *J Clin Pharmacol* 2002; 42: 30-6.
- [18] Lefebvre S, Burglen L, Reboullet S, Clermont O, Burlet P, Viollet L, *et al.* Identification and characterization of a spinal muscular atrophy-determining gene. *Cell* 1995; 80: 155-65.
- [19] Lorson CL, Strasswimmer J, Yao JM, Baleja JD, Hahnen E, Wirth B, *et al.* SMN oligomerization defect correlates with spinal muscular atrophy severity. *Nat Genet* 1998; 19: 63-6.
- [20] Riessland M, Brichta L, Hahnen E, Wirth B. The benzamide M344, a novel histone deacetylase inhibitor, significantly increases SMN2 RNA/protein levels in spinal muscular atrophy cells. *Hum Genet* 2006; 120: 101-10.
- [21] Lunn MR, Root DE, Martino AM, Flaherty SP, Kelley BP, Coovert DD, *et al.* Indoprofen upregulates the survival motor neuron protein through a cyclooxygenase-independent mechanism. *Chem Biol* 2004; 11: 1489-93.
- [22] Chang JG, Hsieh-Li HM, Jong YJ, Wang NM, Tsai CH, Li H. Treatment of spinal muscular atrophy by sodium butyrate. *Proc Natl Acad Sci USA* 2001; 98: 9808-13.
- [23] Brichta L, Hofmann Y, Hahnen E, Siebzehrubel FA, Raschke H, Blumcke I, *et al.* Valproic acid increases the SMN2 protein level: a well-known drug as a potential therapy for spinal muscular atrophy. *Hum Mol Genet* 2003; 12: 2481-9.
- [24] Waldecker M, Kautenburger T, Daumann H, Busch C, Schrenk D. Inhibition of histone-deacetylase activity by short-chain fatty acids and some polyphenol metabolites formed in the colon. *J Nutr Biochem* 2008; 19: 587-93.
- [25] Burkhead JL, Ralle M, Wilmarth P, David L, Lutsenko S. Elevated copper remodels hepatic RNA processing machinery in the mouse model of Wilson's disease. *J Mol Biol* 2011; 406: 44-58.
- [26] Saccone S, Biamonti G, Maugeri S, Bassi MT, Bunone G, Riva S, *et al.* Assignment of the human heterogeneous nuclear ribonucleoprotein A1 gene (HNRPA1) to chromosome 12q13.1 by cDNA competitive *in situ* hybridization. *Genomics* 1992; 12: 171-4.
- [27] Wang Z, Rolish ME, Yeo G, Tung V, Mawson M, Burge CB. Systematic identification and analysis of exonic splicing silencers. *Cell* 2004; 119: 831-45.
- [28] Donev R, Newall A, Thome J, Sheer D. A role for SC35 and hnRNP-A1 in the determination of amyloid precursor protein isoforms. *Mol Psychiatry* 2007; 12: 681-90.
- [29] Goina E, Skoko N, Pagani F. Binding of DAZAP1 and hnRNP1/A2 to an exonic splicing silencer in a natural BRCA1 exon 18 mutant. *Mol Cell Biol* 2008; 28: 3850-60.
- [30] Kashima T, Rao N, David CJ, Manley JL. hnRNP A1 functions with specificity in repression of SMN2 exon 7 splicing. *Hum Mol Genet* 2007; 16: 3149-59.

Original article

The relationships of the pulmonary arteries to lung lesions aid in differential diagnosis using computed tomographyChien-Heng Lin^{a,b}, Tsai-Chung Li^c, Po-Pang Tsai^d, Wei-Ching Lin^{d,e,*}^aDepartment of Pediatrics, Children's Hospital, China Medical University Hospital, Taichung 404, Taiwan^bDepartment of Biomedical Imaging and Radiological Science, China Medical University, Taichung 404, Taiwan^cGraduate Institute of Biostatistics, China Medical University, Taichung 404, Taiwan^dDepartment of Radiology, China Medical University Hospital, Taichung 404, Taiwan^eSchool of Medicine, China Medical University, Taichung 404, TaiwanReceived 7th of April 2015 Accepted 29th of April 2015

© Author(s) 2015. This article is published with open access by China Medical University

*Keywords:*Lung lesion;
Pulmonary artery;
Multidetector
computed tomography**ABSTRACT**

The improvement of the resolution of rapid scanning in multidetector computed tomography (CT) has an increased accuracy that allows for the demonstration of the relationship of the pulmonary arteries and lung lesions, even in the peripheral lung. The purpose of this study is to evaluate the relationship between the pulmonary arteries and lung lesions by CT, and to use this relationship to distinguish between benign and malignant lung lesions. The relationships of the lung lesions and the adjacent pulmonary artery were recorded as encasement, displacement, penetration, in the margin, and disconnection. Statistical analyses were then performed to evaluate the relationship of the pulmonary arteries to each lesion with a focus toward the possibility of malignancy and the degree of pulmonary arterial encasement in the lesion. The relationship between the pulmonary arteries and lung lesions had a statistically significant difference between benignity and malignancy ($P < 0.001$). Inter-observer agreement was substantial ($\kappa = 0.639$; 95% CI: 0.518-0.719). The average degrees of pulmonary arterial encasement in benign and malignant lesions were $52.1\% \pm 27.3\%$ and $71.8\% \pm 18.8\%$, respectively ($P = 0.011$). The ROC curve showed that the degree of pulmonary arterial encasement had a moderate discriminating ability in diagnosing lung carcinoma, and the area under the curve was 0.738. The best cutoff value was 44.4%. The relationships of the pulmonary arteries to lung lesions and the degree of pulmonary arterial encasement could be used in differentiating benignity from malignancy not only for central lung lesions but also peripheral lung lesions.

1. Introduction

A solitary pulmonary tumor is a common radiological finding. And while computed tomography (CT) is considered to be one of the most important non-invasive diagnostic tools in clinical practice, differentiating between a malignant and a benign lesion on CT is not an easy task for a radiologist [1, 2].

The lung has a dual blood supply: one source is the bronchial arteries, and the other is the pulmonary arteries. Generally, the bronchial artery provides the blood supply to bronchogenic carcinoma. Using the relationship of the bronchial artery to lung lesions in distinguishing said lesions' benignity from malignancy in CT usually has limitations because tracing the whole course of the bronchial artery to the lung carcinoma is still a challenge [3].

The pulmonary vessels are usually encased or invaded by lung carcinoma. Therefore, the relationship of nodules to both the pulmonary arteries and veins has been reported as the parameter in the neural network to distinguish benignity from malignancy [4, 5].

nancy [4, 5].

In our preliminary study, we found that the pulmonary vein was easily encased, compressed, or invaded by benign and malignant lesions due to low blood pressure, but we were unable to differentiate whether each vein was encased, compressed, or invaded by each lesion.

The pulmonary artery has a relatively higher blood pressure than the pulmonary vein, and so may not be as easily affected as the pulmonary vein. Therefore, it may be better used as a parameter to differentiate benignity from malignancy.

Improvement of the temporal and spatial resolution in the multidetector CT (MDCT), along with rapid coverage of the whole thorax and power auto-injector and CT software techniques, has made it possible to time the initiation of a scan to take into consideration peak enhancement so that the pulmonary arteries can be shown clearly, even in the peripheral lung. In addition, multiple windows and levels are visible simultaneously with multiplanar reformations (MPR), and maximum or minimum inten-

* Corresponding author. Department of Radiology, China Medical University Hospital, No. 2, Yuh-Der Road, Taichung 404, Taiwan.
E-mail address: a0975681278@gmail.com (W.-C. Lin).

Table 1 – Methods to prove the final diagnosis in malignancy and benignancy.

Methods to prove final diagnosis	Case numbers
Malignancy	77
Ultrasonography guided biopsy	10
CT guided biopsy	3
Transbronchial biopsy	41
Transbronchial brush	33
Transbronchial wash	33
Thoracotomy	14
Benignancy	23
CT guided biopsy	2
Transbronchial wash	4
Thoracotomy	4
Sputum culture and F/U	13

CT = computed tomography, F/U = follow up until the lesion resolves (about 6-18 months).

sity projections (MIP and minIP) tools can be used interactively at the workstation so that radiologists can trace the whole course of each pulmonary artery and differentiate the relationships between the lung lesion more accurately than with conventional CT, even in the peripheral small lung nodules [1].

The aim of this study was to evaluate the ability of the relationships between the pulmonary arteries and lung lesions to distinguish benignancy from malignancy in said lesions. In addition, the degree of pulmonary arterial encasement in predicting malignancy was evaluated with the receiver operating characteristic (ROC) curve.

2. Patients and methods

2.1. Patients

We reviewed all of the chest CT images from August 2005 to December 2005. There were 100 patients with solitary pulmonary nodules or mass who underwent a 16-slice MDCT study. The final diagnosis was made by the pathological biopsy or the sputum culture (Table 1). Age and sex were assessed in patients with either benign or malignant lesions. This study was approved by the Institutional Review Board with patients signing a waiver of informed consent.

2.2. CT protocol and image analysis

All of the CT imaging was performed with a 16-slice MDCT (LightSpeed and BrightSpeed, General Electric Medical Systems). Before dynamic CT was performed, high resolution CT (HRCT) images were obtained. One-mm-thick images were taken at 10-mm spacings from lung apexes to lung bases, with the patient breathing out fully for each image. Then, 100 ml of iodinated contrast medium (Omnipaque 350 mg I/ml) was intravenously injected with a power injector at a rate of 3 ml/sec. The scanning was then performed from the lung apexes to the middle pole of both kidneys. Smart preparation technique-scanning delay was automatically determined with bolus tracking in the aorta, and

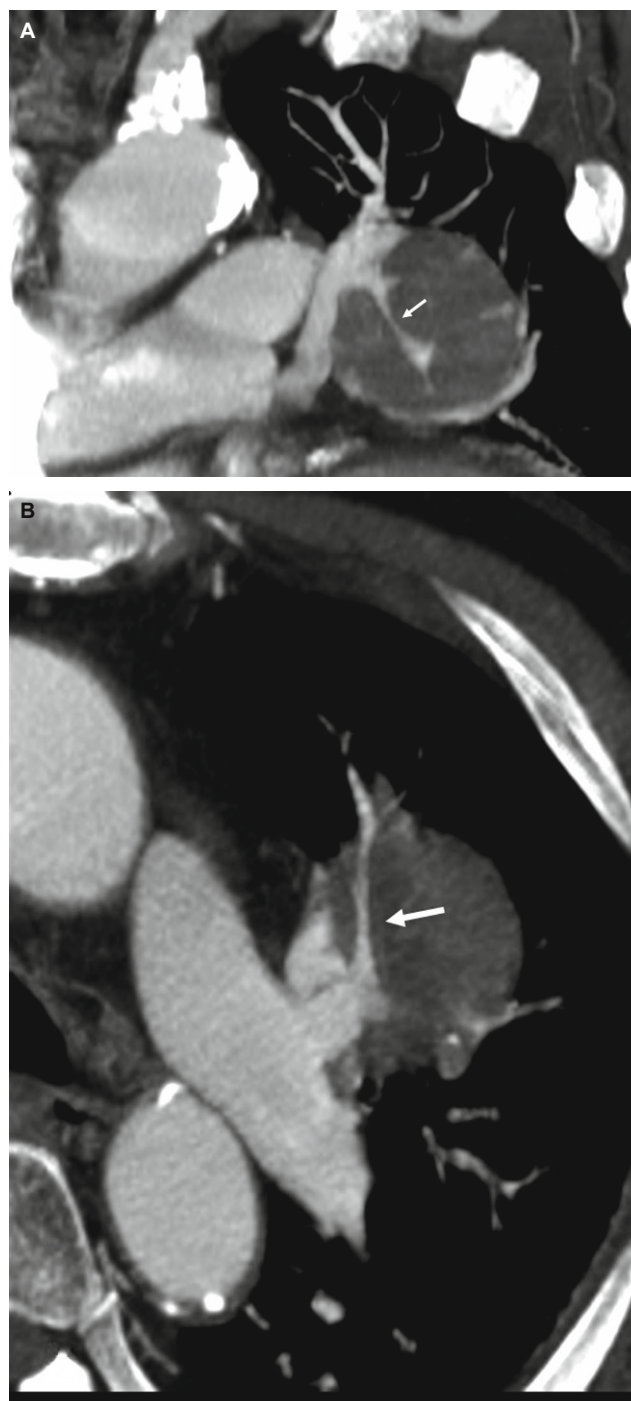


Fig. 1 - Encasement. This is an 82-year-old male with a mass lesion abutting the left hilum. He received bronchoscopic biopsy and pathology revealed small cell lung carcinoma. Coronal (A) and axial (B) section computed tomography (CT) images reveal the main tumor envelops the left segmental pulmonary artery, with decrease in the diameter of this artery (white arrows).

only after the contrast medium injection and the subsequent waiting for the density of aorta to be over 120 Hu was the starting scan used. The region of interest (ROI) was placed in the aortic arch. The scanning parameters were a collimation of 1.25 mm, a

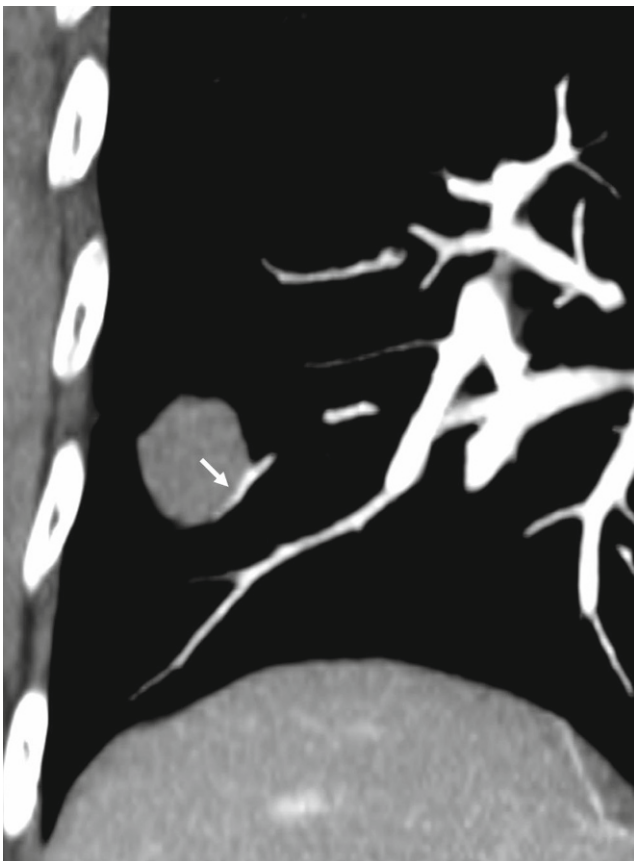


Fig. 2 - Displacement. This is a 68-year-old female with a pulmonary nodule in the right lower lobe. She received right lower lobe lobectomy, and pathology revealed adenocarcinoma. Coronal reformatted CT image reveals the nodule pushing the peripheral right pulmonary artery away from its normal vascular course with a smooth indentation on the pulmonary artery (white arrow).

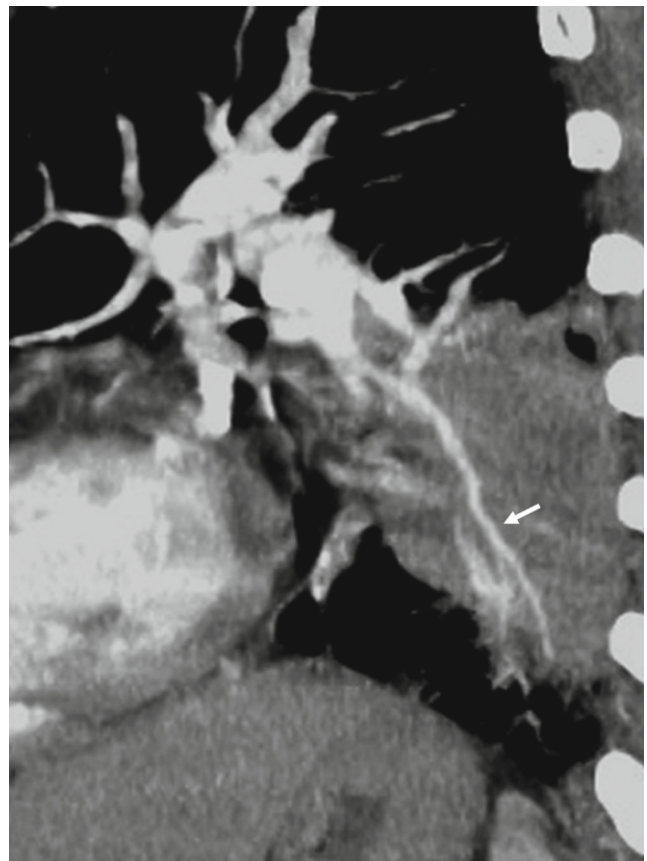


Fig. 3 - Penetration. This is a 64-year-old male with a mass lesion in the left lower lobe. He received ultrasonography-guided biopsy, and pathology revealed adenocarcinoma. Sagittal reformatted CT image reveals the pulmonary artery passes through the lesion without change of the vascular course or caliber of the pulmonary artery (white arrows).

table speed of 34.375 mm/sec and a pitch of 1.375. Axial slices were reconstructed with a slice width of 5.0 mm and a slice interval of 5.0 mm. Then, the 0.625 mm reconstructed raw data of the dynamic CT images were sent to the CT workstation (Advantage Window 4.4).

Two radiologists with 15 years (Observer 1) and 3 years (Observer 2) of experience in chest CT independently reviewed the nearly-isotropic data set consisting of 300-400 reconstructed CT images at the workstation. They were both familiar with the CT workstation techniques and unaware of the final diagnosis of each lung lesion. Several tools were used at the workstation to display data, and, most often, MPR and MIP were used in our study. Rotations around and along any axis in real time were also used. The observers assessed the relationship of the lung lesions and adjacent pulmonary artery with multiple windows and levels simultaneously at CT workstations and recorded the relationships as encasement, displacement, penetration, in the margin, and disconnection.

The definition of encasement is a mass enveloping a pulmonary artery while decreasing the size of a pulmonary artery's caliber (Figure 1). Displacement indicates a mass is causing deviation of a pulmonary artery away from the normal vascular course with/without a notch in the pulmonary artery (Figure 2).

Penetration is when a pulmonary artery passes through the lesion without changing the vascular course or caliber of that pulmonary artery (Figure 3). In the margin is when a pulmonary artery passes across the lesion's margin but without changing its vascular course or its caliber. Disconnection is when there is no pulmonary artery contact with the lesion. More than one type of relationships would be recorded if more than one pulmonary artery was in connection with the lesion. The degree of mass effect in order is encasement, displacement, and then penetration. The mass effect that cannot be clarified as a lesion is the mass effect that involves disconnection or in the margin to/with a pulmonary artery, so these types of lesions were not included in the statistical analyses. Finally, the observers recorded the relationship of each pulmonary artery with the most mass effect of each lesion in the statistical analyses.

As well, two chest radiologists also measured the size of all of the lesions and recorded the location of each lesion as central or peripheral. A central lesion is a lesion that occurs in the hilar bronchus (main, lobar, or segmental bronchus), while a peripheral lesion is one that occurs below the level of the segmental bronchus.

When the result of the same nodule was not the same from the 2 observers, the results were discussed by both observer 1 and 2,

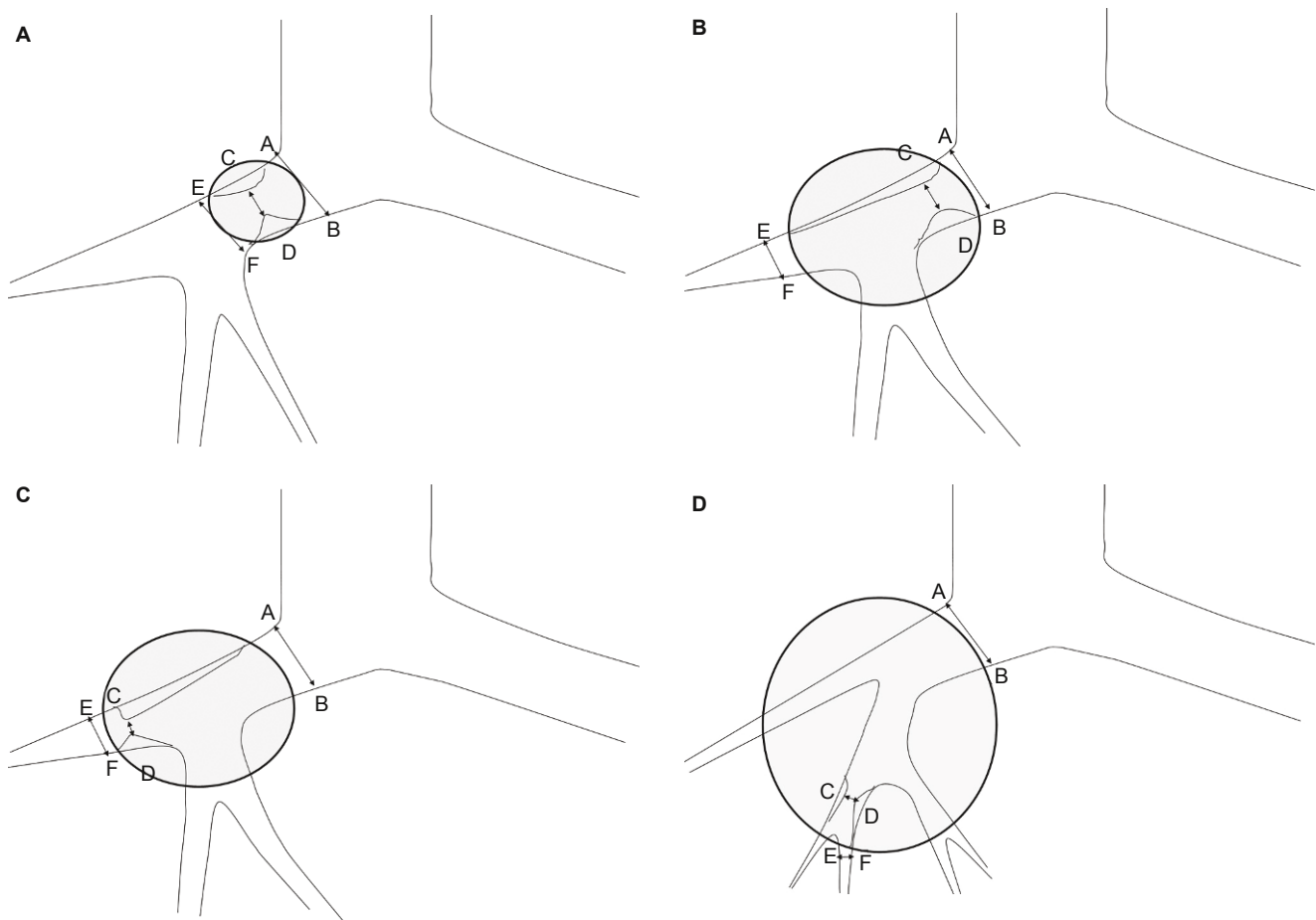


Fig. 4 - (A) A lesion (circle) encases the pulmonary artery, and the encased segment doesn't include a bifurcation. The degree of encasement was determined by the ratio between the luminal diameter at the point of greatest stenosis, CD, and the normal artery beyond the lesion at proximal end, AB. The degree of encasement = $(1-CD/AB)*100\%$; this was labeled as type A encasement. **(B)** A lesion (circle) encases the pulmonary artery, and the encased segment includes a bifurcation, the narrowest segment is proximal to the bifurcation. The degree of encasement = $(1-CD/AB)*100\%$; this was labeled as type B encasement. **(C)** A lesion (circle) encases the pulmonary artery, and the encased segment includes a bifurcation, the narrowest segment is distal to the bifurcation. The degree of encasement = $(1-CD/EF)*100\%$; EF was the normal artery beyond the lesion at distal end. This was labeled as type C encasement. **(D)** A lesion (circle) encases the pulmonary artery and the encased segment includes at least 2 bifurcations. The narrowest point is at the segment between 2 bifurcations. The degree of encasement = $(1-CD/CD')*100\%$, $CD' = EF + EC/EA*(AB-EF)$; CD' was an approximation of an expected normal diameter of the narrowest segment, EC was the distance between the narrowest point to the normal segment beyond the lesion at distal end. EA was the distance of the vessel at normal segments between both ends of the lesion.

and then they reached a consensus.

In addition, as pulmonary arterial encasement was recorded, the degree of encasement was measured by the 2nd observer at the workstation. When there were different degrees of encasement of a pulmonary artery or the lesion was encased by more than one pulmonary artery, he would repeatedly place the tracer in all of the narrowed segments by zooming in on the images, using different thicknesses of the MIP images, checking the tracer in all of the planes, and rotating around the tracer at the workstation. After repeat calculations, he recorded the data showing the most advanced degree of encasement. The degree of encasement was calculated and the methods are listed in Figure 4, categorized by how many pulmonary arterial bifurcations were within the lesion and the location of the narrowest segment of each pulmonary artery. When the vessel was encased, very lightly enhanced, and

barely visualized, it was difficult to measure, so it was recorded as amputation, and the degree of encasement was 100%.

2.3. Statistical analyses

Statistical analyses were performed with SAS software (version 9.13; SAS Institute, Cary, NC). Each patient's gender and the relationship between lung lesion and adjacent pulmonary artery in the benign and malignant groups were analyzed by using Fisher's exact test. Two-independent-sample *T*-test was used to analyze statistically significant difference in patients' ages, and a Wilcoxon rank sum test was used to analyze the degree of pulmonary arterial encasement by each lung lesion in the benign and malignant groups. Odds ratio with its 95% confidence interval (CI) was used to estimate the strength of the association between

Table 2 – The relationships of pulmonary arteries to the lung lesions recorded by 2 observers and the final results.

Observers	Benignancy			Malignancy		
	1	2	Final results	1	2	Final results
Encasement	8	6	8	56	59	58
Displacement	2	1	2	28	25	27
Penetration	10	13	10	4	4	4
In the margin	0	0	0	1	1	1
Disconnection	3	3	3	2	2	2

Table 3 – Basic data compared between benignancy and malignancy.

	Benignancy	Malignancy	<i>P</i> value
Age (years old)	57.2 ± 22	67 ± 11	<i>P</i> = 0.074
Gender (female:male)	6:14	24:50	<i>P</i> = 1
Location (C:P)	9:11	46:28	<i>P</i> = 0.13
Tumor size (mm) (mean ± SD)	51.1 ± 17.4	48.1 ± 21.9	<i>P</i> = 0.578

C = central located, P = peripheral lesion, SD = standard deviation.

Table 4 – The relationships of pulmonary arteries to the lung lesions recorded by 2 observers and the final results.

Observers	Benignancy			Malignancy		
	1	2	Final results	1	2	Final results
Encasement	4	8	8	56	59	58
Displacement	1	2	2	28	25	27
Penetration	15	10	10	4	4	4
In the margin	0	0	0	1	1	1
Disconnection	3	3	3	2	2	2

malignancies and the relationships of the pulmonary arteries to the lung lesions by using the group of those who had lesions with pulmonary artery penetration as the baseline. A *P* value of less than 0.05 was considered to indicate a significant difference.

Inter-observer agreement was assessed by using kappa (κ) statistics, which measures the level of agreement after taking chance agreements into account. Furthermore, the sensitivity and specificity profiles of the degree of pulmonary arterial encasement in the diagnosis of malignancy were determined by plotting an empirical ROC curve.

3. Results

The relationships between pulmonary arteries and lung lesions were recorded by Observer 1 and Observer 2, and the final results are listed in Table 2. Six nodules (3 malignant and 3 benign lesions) were not included in the statistical analyses because in these cases the pulmonary arteries were in the margin or disconnect with the lung lesions. Finally, 74 patients who had bronchogenic carcinomas and 20 patients who had benign lung lesions

were included in the statistical analyses. The final diagnoses of these patients are listed in Table 3. The basic data analyses are shown in Table 4.

There were 15 malignant lesions that had 2 different types of relationship to the pulmonary arteries. The relationship of the pulmonary arteries to the benign lesions and the malignant ones was statistically significantly different (*P* < 0.001). A lesion with a pulmonary arterial encasement had an 18.1 times greater likelihood of being malignant than a lesion with a pulmonary artery penetrating through it (95% CI: 4.6-71.7, *P* < 0.001). A lesion that displaced the pulmonary artery had a 33.7 times greater likelihood of being malignant than a lesion with a pulmonary artery penetrating through it (95% CI: 5.3-213.7, *P* = 0.0002).

Inter-observer agreement was substantial (κ = 0.612; 95% CI: 0.518-0.719).

The lesions with different types of pulmonary arterial encasement that were related to the calculation of the degree of encasement are presented in Table 5. The average degrees of pulmonary arterial encasement in benign and malignant lesions were 52.1% ± 27.3% and 71.8% ± 18.8% (*P* = 0.011), respectively. The empirical ROC curve for the diagnosis of a malignant lung tumor with the

Table 5 – The type of pulmonary artery encasement that related to the calculation of the degree of encasement

Types of encasement	Benignancy (case number)	Malignancy (case number)
Type A	0	0
Type B	0	10
Type C	1	5
Type D	6	32
Amputation	1	11

Type A = The encased segment didn't include any bifurcation, as in Figure 4A; Type B = The encased segment included one bifurcation, and the narrowest point was located proximate to the bifurcation, as in Figure 4B; Type C = The encased segment included one bifurcation, and the narrowest point was located distal to the bifurcation, as in Figure 4C; Type D = The encased segment included more than one bifurcation, as in Figure 4D.

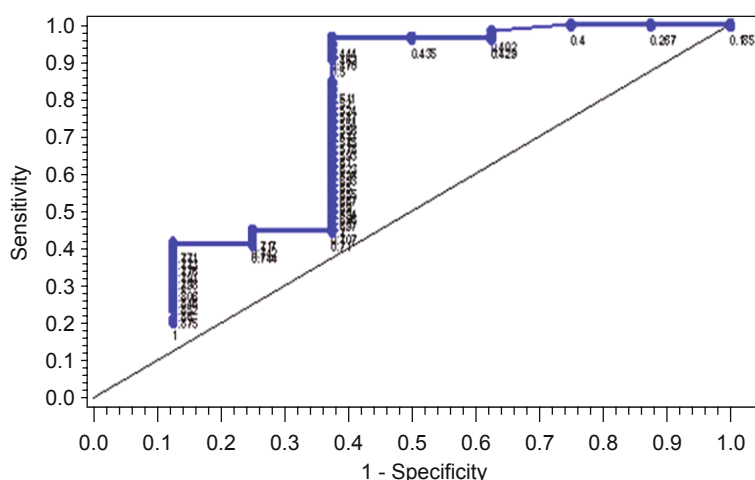


Fig. 5 - The ROC curve for diagnosis of malignancy using the degree of pulmonary arterial encasement. Points labeled in the picture are the values of degree of encasement.

degree of pulmonary arterial encasement showed a moderate discriminating ability in diagnosing lung carcinoma, and the area under the ROC curve was 0.738 (Figure 5). The best cutoff value for the degree of pulmonary arterial encasement in the diagnosis of malignancy was 44.4%. If 44.4% was chosen as the cutoff value for diagnosing malignancy of a lung tumor with said degree of pulmonary arterial encasement, then the sensitivity was 96.6% (56/58), specificity was 62.5% (5/8), positive predictive value was 94.9% (56/59), and negative predictive value was 71.4% (5/7), respectively. The 2 false negative results came from squamous cell carcinoma, and these 2 nodules both had 40% encasement. The 3 false positive results came from 3 tuberculosis (TB) lesions with 71%, 74% and 100% encasement, respectively.

4. Discussion

CT is the most cost-effective image modality for evaluating lung lesions. A benign nodule can be diagnosed by either there being a benign pattern of calcification or the nodule having a doubling time of more than 2 years there being a benign pattern of calcification, by using fat, or by the nodule having a doubling time of more than 2 years [6, 7]. However, if the lesion does not have these features, the radiologist must use the morphologic signs

from CT, like attenuation, margin, contours, cavitation, size, enhanced pattern and clinical information, to judge if the lesion is malignant [1, 2, 4, 5, 7-9]. But, there are several overlaps between benign and malignant lesions.

With the increased use of ultrasonography (US) to evaluate peripheral lung lesions, Hsu *et al.* found that a pulmonary artery vessel signal, a pulsatile flow with vessel signal length ≥ 1 cm demonstrated by color Doppler US, could be a sign for predicting benign lesions (10). However, this finding cannot be applied to CT scans, since the length of the pulmonary arteries within the lesions; both benign and malignant, is always seen in CT as more than 1 cm if the diameter of the lesion is more than 1 cm.

The blood supply for lung cancer is mainly from the bronchial arteries, and Tan *et al.* revealed that 16-slice MDCT demonstrated that fact by showing that bronchial arteries were the blood supply for 94% of lung cancers [3]. According to Muller's report, the largest possible diameter of a bronchial artery supply to the bronchogenic carcinoma depends on tumor size. When the tumor is 1-2 cm, the largest lumen of the feeding bronchial artery is 100 μm , and when the tumor is 2-4 cm, the largest lumen of the feeding bronchial artery is 200-600 μm [11]. The minimal thickness of 16-slice MDCT is 0.625 mm, meaning that it may not be sufficient to demonstrate the whole vascular course of the feeding bronchial artery or for a tumor size of less than 4 cm or even

bigger. The detected rate of blood supply for lung lesions was 42% (41 malignancies and one benign) in our study, which is lower than Tan's report. This may be due to the smaller sizes and marginal locations of the lesions we studied. In addition, some bronchial arteries also supply several non-cancerous lung lesions [12], so we could not always use the feeding bronchial arteries to distinguish between benign and malignant lesions.

At an early stage of tumor development, the bronchial arteries have a regular hilifugal course to supply the tumor, and then a wool ball-like pattern at an advanced stage. When a tumor is larger than 4-6 cm in diameter, it will show regression and the necrotic area of the tumor will be noted. Then it may have a central avascular cavity and increased vascularization in the growth zone at its edges, with bronchial artery-to-pulmonary artery anastomoses [11]. The pulmonary arteries mainly supply the lung parenchyma and several alveolar-originated lesions, but sometimes they are found to supply bronchogenic carcinomas. The histological cell type, tumor grading, tumor size, tumor location, and grade of differentiation of bronchogenic carcinomas have been associated with the possibility of the pulmonary arteries supplying blood to lung carcinomas. Zhang YL *et al.* found that pulmonary arteries had a greater tendency to supply to a big, peripherally located, low-differentiated carcinoma and to supply to squamous cell carcinoma than to adenocarcinoma [13]. This may be due to the rapid growth of these types of tumor and the fact that it receives relatively less blood supply from the bronchial arteries in peripheral lung lesions than in central lung lesions. However, this is rarely evidenced in radiological images, possibly due to poor tissue contrast for bronchogenic carcinoma and lung parenchyma during pulmonary arterial angiography.

Computer-aided detection (CAD) and artificial neural networks have been developed to improve the detection rate and ability in differential diagnosis [4, 5, 9]. Their ability is dependent on the input data, and these systems are at present used as a second opinion to assist radiologists and are not routinely used in daily practice. It is a well-known fact that vascular encasement by a tumor is likely a sign of that tumor's malignancy, such as pancreatic head carcinoma and hepatocellular carcinoma encasing a portal vein. Chen *et al.* used the relationship of the nodule to blood vessels as one of the nine CT signs of the neural network-based CAD scheme in distinguishing a malignant from a benign solitary pulmonary nodule. They classified the relationships into 3 groups: disconnection with blood vessels, connection with blood vessels without notching, and connection with blood vessels with notching [4]. Matsuki *et al.* recorded the vascular involvement of the lung nodule from no involvement (score 0) to the involvements of more than two vessels (score 10). They used this as one of the 16 radiological findings and combined this with 7 clinical parameters to build up a neural network scheme for differentiating benign from malignant pulmonary nodules on HRCT [5]. Both studies suggest that these neural network-based CAD schemes could assist radiologists in improving the overall diagnostic accuracy in differentiating between benign and malignant tumors on HRCT.

With the improvement of the temporal and spatial resolution in MDCT due to dynamic protocol and several useful tools such as MPR, MIP and VR at the workstation, we can clearly trace the pulmonary arteries to the peripheral lung about 2 cm away from pleura. As our study shows, we can use the relationship between the pulmonary arteries and lung lesions to distinguish benignancy from malignancy, since the relationship of the pulmonary arteries to lung lesions has a significant difference between benignancy

and malignancy. In short, we found that malignant lesions had a tendency to encase and displace the pulmonary arteries, and benign lesions had a tendency to be penetrated by the pulmonary arteries. Furthermore, when using 50% pulmonary arterial encasement as the cut-off value, the sensitivity and the specificity in predicting malignancy were 91.4% and 62.5%, respectively. This result is easy to apply in clinics and may further be used as a sign in CAD schemes.

The more desmoplastic reaction of inflammatory lesions, like TB, might show prominent mass effect and different histology cancer cell types, and grades of malignant cell differentiation may also express different degrees of mass effect on adjacent pulmonary arteries. These circumstances may cause some limitations in using the relationship between the vessel and the tumor and the degree of pulmonary artery encasement to differentiate benignancy from malignancy in lung lesions.

The quantification of observer agreement is an essential complement in conventional studies of diagnostic accuracy in the evaluation of a diagnostic test [14]. Agreement between these relationships in our study was also determined, using the κ statistic. The level of agreement was considered poor with $\kappa < 0.20$, fair with $\kappa = 0.21-0.40$, moderate with $\kappa = 0.41-0.60$, substantial with $\kappa = 0.61-0.80$, and very good with $\kappa > 0.80$ [15]. The inter-observer agreement was substantial ($\kappa = 0.639$), which was similar to the agreement found in previous studies of mammography and other CT interpretive tasks [16].

The limitation of this study is the small sample size of benign lesions. This may have led to the sharp slope of the ROC curve, which, as the degree of encasement decreases from 70.8% to 44.4%, inversely increases the sensitivity from 44.8% to 96.6% with a fixed specificity of 62.5%. Also, this study didn't include the lesions of metastasis and bronchoalveolar carcinoma, which were thought to have blood supplies mainly from the bronchial arteries. This suggests the possibility that there may be another story in the relationship of these lesions to the pulmonary arteries. Furthermore, the lack of benign tumors in our benign lesion group was also noted. Further investigation to include more variant origins of benign lesions and different histologic types of malignancy is needed.

Besides, the resolution and enhancement of the pulmonary arteries at 1-2 cm away from the pleura depends on several factors, such as ratio of the amount of contrast medium to patients' body size and contrast medium injection flow rate. Because we have difficulty tracing the pulmonary arteries at this region with confidence, this may cause the routine application of our results to have limitations in evaluating these very peripherally located small lesions.

5. Conclusion

In this study, we have shown that the relationships of the pulmonary arteries to lung lesions and the degree of pulmonary arterial encasement could help in differentiating benignancy from malignancy in lesions, not only for central lung lesions, but also for peripheral lung lesions located below the 2nd-order bronchus to 2 cm away from pleura.

Acknowledgments

There are no acknowledgments.

Ethics committee approval

The Institutional Review Board approved this retrospective study with a waiver of the written informed consent.

Conflict of interest

The authors declare that they have no conflicts of interest.

Open Access This article is distributed under terms of the Creative Commons Attribution License which permits any use, distribution, and reproduction in any medium, provided original author(s) and source are credited.

REFERENCES

- [1] Laurent F, Montaudon M, Corneloup O. CT and MRI of lung cancer. *Respiration* 2006; 73: 133-42.
- [2] Jeong YJ, Lee KS, Jeong SY, Chung MJ, Shim SS, Kim H, *et al.* Solitary pulmonary nodule: characterization with combined wash-in and washout features at dynamic multi-detector row CT. *Radiology* 2005; 237: 675-83.
- [3] Tan LL, Han MJ, Li YB, Jiang JD, Li SX, Zhou SP. Role of 16 slices spiral CT angiography with 3-dimensional CT and CT virtual endoscopy in detecting blood supply of lung carcinoma. *Ai Zheng* 2007; 26: 73-7.
- [4] Chen H, Wang XH, Ma DQ, Ma BR. Neural network-based computer-aided diagnosis in distinguishing malignant from benign solitary pulmonary nodules by computed tomography. *Chin Med J* 2007; 120: 1211-5.
- [5] Matsuki Y, Nakamura K, Watanabe H, Aoki T, Nakata H, Katsuragawa S, *et al.* Usefulness of an artificial neural network for differentiating benign from malignant pulmonary nodules on high-resolution CT: evaluation with receiver operating characteristic analysis. *AJR Am J Roentgenol* 2002; 178: 657-63.
- [6] O'keefe ME Jr, Good CA, McDonald JR. Calcification in solitary nodules of the lungs. *AJR Am J Roentgenol* 1957; 77: 1023-33.
- [7] Nathan MH, Collins VP, Adams RA. Differentiation of benign and malignant pulmonary nodules by growth rate. *Radiology* 1962; 79: 221-31.
- [8] Hartman TE. Radiologic evaluation of the solitary pulmonary. *Semin Thorac Cardiovasc Surg* 2002; 14: 261-7.
- [9] Beigelman-Aubry C, Raffy P, Yang W, Castellino RA, Grenier PA. Computer-aided detection of solid lung nodules on follow-up MDCT screening: evaluation of detection, tracking, and reading time. *AJR Am J Roentgenol* 2007; 189: 948-55.
- [10] Hsu WH, Yu YH, Tu CY, Hsu JY, Chen CY, Chen CL, *et al.* Color Doppler US pulmonary artery vessel signal: a sign for predicting the benign lesions. *Ultrasound Med Biol* 2007; 33: 379-88.
- [11] Müller KM, Meyer-Schwickerath M. Bronchial arteries in various stages of bronchogenic carcinoma. *Pathol Res Pract* 1978; 163: 34-46.
- [12] Carvalho P, Anderson DK, Charan NB. Bronchial arterial imaging using helical computed tomography. *Pulm Pharmacol Ther* 2007; 20: 104-8.
- [13] Zhang YK, Le HB, Chen ZH, Wang C, Zhang B. Study on relationship between blood supply from pulmonary artery and pathological characteristics of patients with primary bronchogenic carcinoma. *Chin J Lung Canc* 2006; 9: 333-6.
- [14] Bossuyt PM, Reitsma JB, Bruns DE, Gatsonis CA, Glasziou PP, Irwig LM, *et al.* Towards complete and accurate reporting of studies of diagnostic accuracy: the STARD initiative. *Clin Radiol* 2003; 58: 575-8.
- [15] Landis JR, Koch GG. The measurement of observer agreement for categorical data. *Biometrics* 1977; 33: 159-74.
- [16] Gierada DS, Pilgram TK, Ford M, Fagerstrom RM, Church TR, Nath H, *et al.* Lung cancer: interobserver agreement on interpretation of pulmonary findings at low-dose CT screening. *Radiology* 2008; 246: 265-72.

Case report

Multifocal osteolytic lesions of the skull: a primary cavernous hemangioma mimicking a neoplastic invasive lesionI-Han Hsiao^a, Der-Yang Cho^{a,b}, Chun-Lin Liu^{a,b,*}^aDepartment of Neurosurgery, China Medical University Hospital, Taichung 404, Taiwan^bMedical Department, China Medical University, Taichung 404, TaiwanReceived 9th of April 2015 Accepted 30th of April 2015

© Author(s) 2015. This article is published with open access by China Medical University

*Keywords:*Cavernous hemangioma;
Langerhans cell
histiocytosis;
Skull;
Osteolytic Lesions;
Intraosseous tumor**ABSTRACT**

Intraosseous cavernous hemangioma is a rare cause of osteolytic lesions of the skull, and its multifocal type is even more infrequent. This tumor is difficult to accurately diagnose by imaging and can be confused with osteolytic Langerhan's cell histiocytosis or other neoplasms. Here we present a case of multifocal intraosseous cavernous hemangioma of the skull treated with surgical intervention in our hospital five years ago. A review of related literatures and case reports is also provided to help clarify the diagnosis and devise treatment regimens. In light of the difficulties of early diagnosis, early en bloc surgical removal is recommended.

1. Introduction

Primary cavernous hemangiomas are rare skeletal tumors accounting for 0.7-1% of all bone neoplasms [4]. These tumors, which arise from the intrinsic vasculature are mostly found in vertebral bodies. Cavernous hemangiomas are usually unifocal, and they represent 0.2% of all benign neoplasms of the skull. The majority of these lesions are asymptomatic, but patients can present with focal pain or palpable mass. A multifocal osteolytic lesion can initially be confused with Langerhan's cell histiocytosis (LCH) or a malignant neoplasm. Here we present a case of multifocal cavernous hemangiomas of the skull bone.

2. Case presentation

A 29-year-old female came to our neurology outpatient clinic because of a painful skull defect found incidentally over the right parietal area. The lesion was soft and with mild dimpling. Intermittent pain had started at least 3 weeks before the initial visit. She denied any history of head injury or systemic disease. Cranial computed tomography (CT) and magnetic resonance imaging (MRI) identified 2 individual osteolytic lesions with contrast enhancement (Figures 1, 2) over the right parietal (10 mm * 9 mm) and frontal (8 mm * 9 mm) areas of the skull. In particular, the CT scan revealed osteolytic lesions with erosion of the skull bone, whereas MRI showed low signals on T1-weighted images, high

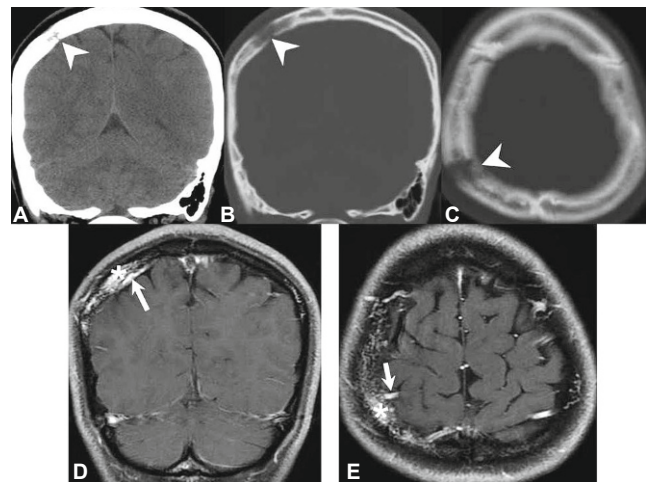


Fig. 1 - (A-C) A parietal osteolytic lesion on brain CT. (D, E) The enhanced lesion (asterisk) with a feeding artery (arrow) revealed by gadolinium-enhanced T1-weighted imaging.

signals on T2-weighted images, and heterogeneous enhancing effects on gadolinium-enhanced T1-weighted images. A neoplastic invasive lesion, such as LCH or malignant metastasis tumor, was initially suspected. A series of tests including: L-spine MRI, bone scintigraphy (Figure 3), and analysis of tumor markers did not

*Corresponding author. Medical Department, China Medical University; Department of Neurosurgery, China Medical University Hospital, No. 2, Yu-Der Road, Taichung 404, Taiwan.
E-mail address: chunlin2539@gmail.com (C.-L. Liu).

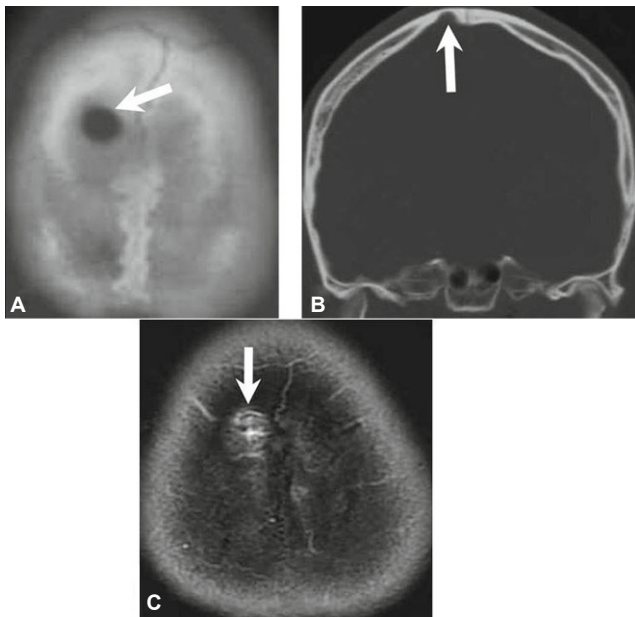


Fig. 2 - (A, B) Another osteolytic lesion at the frontal area on brain CT. (C) The enhanced lesion (arrow) revealed by gadolinium-enhanced T1-weighted imaging.

reveal abnormal results. A large craniectomy was performed for the evacuation of the 2 osteolytic lesions, and cranioplasty with polymethylmethacrylate was carried out for skull reconstruction. The dura was intact, but diffused oozing and central hyperemia were noted during the surgery. The final histological report confirmed the diagnosis of intraosseous cavernous hemangioma. The patient recovered well. She has been followed up for 4 years with no recurrence.

3. Discussion

Primary intraosseous cavernous hemangioma is a rare, benign, and slow-growing tumor formed by blood vessels separating fibrous tissue and accounting for 0.2% of all benign tumors of the skull [4]. In the skull, these tumors are fed by the branches of the external carotid artery, especially the superficial temporal artery, posterior occipital artery, and branches of the middle meningeal artery [5]. Cavernous hemangiomas are usually asymptomatic lesions, but the clinical presentation can include cosmetic changes, increased intracranial pressure caused by parenchymal compression, and the cranial nerve deficits [3]. The peak age of skull hemangiomas is the fourth decade of life, and women are affected 2-4 times more often than men [6]. Some reported treatments include curettage and radiotherapy [2]. Curettage may lead to massive perioperative bleeding and recurrence after the operation. Radiotherapy can only prevent the tumor from growing, but it cannot eradicate the lesions. Additionally, there are reports describing malignant transformation of intraosseous cavernous hemangiomas after radiotherapy.

Differential diagnoses of intraosseous neoplasm include LCH, osteoma, sarcoma, and fibrous dysplasia. LCH is caused by abnormal proliferation of dendritic cells, which often occurs in young patients. It is commonly located in the skull, especially in the parietal and frontal bones [7]. Compared to LCH, the great

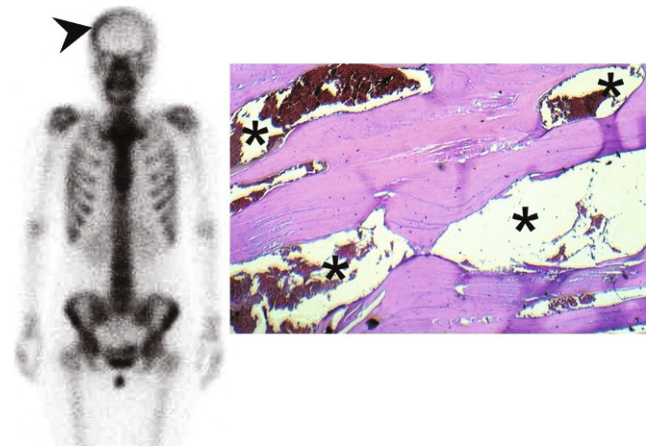


Fig. 3 - Left: A bone scintigraphy image. The arrow-head indicates right skull bone enhancement. Right: The histologic examination showed a cavernous hemangioma (black asterisk) of the diploe with thin-walled, dilated capillary spaces lined by with endothelial cells. No malignancy was observed.

majority of the reported cases of skull hemangiomas are unifocal, although multiple hemangiomas have also been described [6]. Wyke reported that 7 out of 40 reported cases of primary hemangioma of the skull were multifocal [9]. According to the study performed at Mayo Clinic in 1975, only 2 out of 43 patients with hemangiomas had multiple lesions [8].

Our literature search failed to identify an ideal noninvasive method that can differentiate cavernous hemangioma from other diseases such as LCH or malignant cell invasions. Therefore, in the majority of cases, the final diagnosis is established only after surgery. For the above reasons, early en bloc surgical removal of intraosseous tumors is recommended irrespectively of whether the osteolytic lesion is benign or malignant, and unifocal or multifocal. Correction of cosmetic changes and treatment of local pain are other indication for the surgery [3].

Open Access This article is distributed under terms of the Creative Commons Attribution License which permits any use, distribution, and reproduction in any medium, provided original author(s) and source are credited.

REFERENCES

- [1] Chen HC, Shen WC, Chou DY. Langerhans cell histiocytosis of the skull complicated with an epidural hematoma. *AJNR Am J Neuroradiol* 23: 493-495, March 2002.
- [2] Dogan S, Kocaeli H, Sahin S, Korfali E, Saraydaroglu O. Large cavernous hemangioma of the frontal bone, case report. *Neurol Med Chir* 2005; 45: 264-7.
- [3] Heckl S, Aschoff A, Kunze S. Cavernomas of the skull: review of the literature 1975-2000. *Neurosurg Rev* 2002; 25: 56-62.
- [4] Naama O, Gazzaz M, Akhaddar A. Cavernous hemangioma of the skull: 3 case reports. *Surg Neurol* 2008; 70: 654-659.
- [5] Pastore FS, De Caro G, Faiola A, Mauriello A, Giuffre R. Cavernous

hemangioma of the parietal bone. Case report and review of the literature. *Neuro Chirurgie* 1999; 45: 312-5.

- [6] Peterson DL, Murk SE, Story JL. Multifocal cavernous hemangioma of the skull: report of a case and review of the literature. *Neurosurgery* 1992; 8: 778-781. discussion 782.
- [7] Tetsu Yamaki, Yasuaki Kokubo, Yuki Saito. A case of Langerhans cell histiocytosis of the skull in which preoperative methionine positron emission tomography was useful in comprehending the spreading of the lesion. *Surg Neurol Int* 2014; 5: 27.
- [8] Thomas JE, Baker HL. Assessment of roentgenographic lucencies of the skull: a systematic approach. *Neurology* 1975; 25: 99-106.
- [9] Wyke DB. Primary hemangioma of the skull: a rare cranial tumor. *Am J Roentgenol* 1949; 61: 302-16.